

AD-A229 933

REPORT DOCUMENTATION PAGE			Form Approved OMB No 0704-0188
Public reporting burden for this collection of information is estimated to average 1 hour per response, including the time for reviewing instructions, searching existing data sources, gathering and maintaining the data needed, and completing and reviewing the collection of information. Send comments regarding this burden estimate or any other aspect of this collection of information, including suggestions for reducing this burden, to Washington Headquarters Services, Directorate for Information Operations and Reports, 1215 Jefferson Davis Highway, Suite 1204, Arlington, VA 22202-4302, and to the Office of Management and Budget, Paperwork Reduction Project (0704-0188), Washington, DC 20503.			
1. AGENCY USE ONLY (Leave blank)	2. REPORT DATE October 29, 1990	3. REPORT TYPE AND DATES COVERED Annual Interim report for 3/01/89 - 9/30/90	
4. TITLE AND SUBTITLE "Transformation Toughening of Composite Ceramics"		5. FUNDING NUMBERS G AFOSR-89-0300 (2)	
6. AUTHOR(S) Professor Waltraud M. Kriven		AFOSR-TR-	
7. PERFORMING ORGANIZATION NAME(S) AND ADDRESS(ES) Department of Materials Science and Engineering University of Illinois at Urbana-Champaign 105 South Goodwin Avenue Urbana, IL 61801		8. PERFORMING ORGANIZATION REPORT NUMBER UIIU-ENG-90-5017	
9. SPONSORING/MONITORING AGENCY NAME(S) AND ADDRESS(ES) Air Force Office of Scientific Research Dr. Lisolette J. Schioler, Program Manager Electronic and Material Sciences Directorate Bolling Air Force Base, Washington, DC 20332-6600		10. SPONSORING/MONITORING AGENCY REPORT NUMBER 2306/A2	
11. SUPPLEMENTARY NOTES			
12a. DISTRIBUTION/AVAILABILITY STATEMENT Publically Available		12b. DISTRIBUTION CODE S DEC 26 1990 Co D	
13. ABSTRACT (Maximum 200 words) Research is underway into the application of martensitic transformations in ceramics to toughen a variety of ceramic-ceramic composites, i.e., to reduce their brittleness. The toughening agents of interest and their volume changes are dicalcium silicate (Ca ₂ SiO ₄ , 12%), nickel sulfide (NiS, 4%), lanthanide sesquioxides (Ln ₂ O ₃ , 8%) and lutetium borate (LuBO ₃ , 8%). Ceramic processing routes have been developed to fabricate different types of toughened composites, viz., either by using a dispersed second phase microstructure, or as a fine grained, single phase material. Specifically, Ca ₂ SiO ₄ has been dispersed in CaZrO ₃ and the mechanical properties measured by bend tests. The critical importance of matrix toughness and grain size, as well as role of intergranular microcracking has been established. Dense pellets of fine grained, pure β-Ca ₂ SiO ₄ have been sintered and their transformability by grinding established. Their microstructures were examined by TEM and preliminary micromechanical studies made on it, and on Gd ₂ O ₃ by indentation and SEM techniques. NiS inclusions in glass were examined by TEM and EDS and a sol gel processing route to precipitate NiS in glass has been identified. Composites of Dy ₂ O ₃ in SiC and powders of LuBO ₃ in B ₂ O ₃ have been fabricated.			
14. SUBJECT TERMS Transformation toughening of ceramic composites, processing, SEM, TEM, EDS, microstructure, toughness, fracture testing by 4 point bending, Vickers indentations.		15. NUMBER OF PAGES 75	
16. PRICE CODE		17. SECURITY CLASSIFICATION OF REPORT Unclassified	
18. SECURITY CLASSIFICATION OF THIS PAGE Unclassified		19. SECURITY CLASSIFICATION OF ABSTRACT Unclassified	
20. LIMITATION OF ABSTRACT III			

Report AFOSR - 89 - 0300

TRANSFORMATION TOUGHENING OF COMPOSITE CERAMICS

**Professor Waltraud M. Kriven
Department of Materials Science and Engineering,
University of Illinois at Urbana- Champaign
105 South Goodwin Ave.,
Urbana, IL, 61801.**

**Oct 30th 1990
Interim Report for the Period March 1st 1989 to Sept 30th 1990.**

**Prepared for:
Air Force Office of Scientific Research,
Dr. Lisolette J. Schioler, Program Manager.
Electronic and Material Sciences Directorate,
AFOSR/NE
Bolling Air Force Base,
Washington DC 20332-6600**

Section 1 Objectives of the Research Effort

(Professor W.M. Kriven)

The brittleness of monolithic ceramics is a well-known limitation to their use in many applications, both structural and electronic. However, by fabricating composite ceramics in which the matrix is reinforced by minor portions (10 to 15 volume %) of a second phase, the toughness can be improved. This can be a particularly effective mechanism when the second phase undergoes a martensitic transformation which is nucleated in the stress field of a propagating crack tip. The classical example is transformation toughening of zirconia-containing ceramics viz., partially stabilized zirconia (PSZ), zirconia toughened alumina (ZTA) or tetragonal zirconia polycrystals (TZP). The transformation in zirconia is accompanied by a 3 % volume increase on cooling through its transformation temperature at 950°C, or a 4.9 % increase in metastably retained particles cooled to room temperature. Zirconia also experiences a unit cell shape change resulting from the crystal symmetry change from tetragonal to monoclinic. In addition, like any martensitic transformation mechanism, there is a macroscopic shape change (m_1) associated with the transformation. Fracture mechanics theories⁽¹⁾ developed to describe the phenomenon of transformation toughening identify both a dilatational component and a deviatoric shear component which contribute to the toughening mechanism.

More recently, several possible new candidates for transformation toughening have been identified on the basis of the anomalous behavior on cooling, of a positive volume change accompanying potentially martensitic transformations in ceramics or minerals.^(2,3) Some of these are listed in Table 1. The four systems all exhibit quite large positive volume changes on transformation, as well as various crystal symmetry changes and hence unit cell shape changes. The macroscopic shape changes (m_1) have not been determined as insufficient is known about the precise martensitic crystallography as yet.

Table 1. Summary of Possible Transformation Tougheners Alternative to ZrO₂

<u>Compound</u>	<u>Crystal Symmetries</u>	<u>Transformation Temperature (T₀)</u>	<u>Volume Change (ΔV)</u>	<u>Unit Shape Change</u>
ZrO ₂	tetragonal→ monoclinic	950°C	(+) 4.9% (R. T.)	9°
Ln ₂ O ₃	monoclinic→ cubic	600- 2200°	(+)10%	10°
2CaO·SiO ₂	monoclinic→ orthorhombic	490°C	(+)12%	4.6°
NiS	rhombohedral→ hexagonal	379°C	(+)4%	--
LuBO ₃	hexagonal→ rhombohedral	1310°C	(+)8%	--

(--) crystallography is unknown

The aim of our work in this project is to systematically investigate the toughening effects of these compounds in various chemically compatible matrices. The questions which we address in so doing include the following:

1. What are the relative contributions of volume change versus the different types of shape changes to the toughening mechanism(s)?
2. How important are other factors in the design of transformation toughened composites? For example such factors as chemical compatibility, relative elastic modulus, relative thermal expansion coefficients.
3. Can we identify other parameters which enhance or limit the effectiveness of transformation toughening with the candidate tougheners? For example, the brittleness of the matrix, or the relative/grain sizes of matrix and toughener?

4. What are the scientific reasons for the dependence on such factors?
For example:
- (i) effects on the nucleation barrier to transformation
 - (ii) the overall toughness and strength of the composites.

The anticipated yield of this work is a deeper scientific insight into the application of martensitic transformations to toughening of ceramic materials, and the development of systematic ways to design, fabricate and evaluate a variety of composites.

In the following Section 2, the objectives and current status of each toughening system will be presented in detail.

References

1. A.G. Evans and R.M. Cannon, "Toughening of Brittle Solids by Martensitic Transformations," *Acta Metall.*, **34** [5] 761-800 (1986)
2. W.M. Kriven, "Possible Alternative Transformation tougheners to Zirconia: Crystallographic Aspects," *J. Am. Ceram. Soc.*, **71** [2] 1021-1030 (1988)
3. W.M. Kriven, "Martensitic toughening of Ceramics," *Mat. Sci. and Eng.*, **A127** 249-255 (1990)

Section 2.1 Fine-Grained β -Dicalcium Silicate (Dr. Ian Nettleship and Mr. Y. J. Kim)

1. Background

Zirconia is the primary example of the use of a displacive phase transformation to toughen engineering ceramics. Before the late 1970's it was thought the transformable tetragonal phase could only be metastably retained by dispersing it, at low volume fractions in a high modulus matrix (1), or as precipitates developed in cubic zirconia grains during cooling (2). In both these materials transformation toughening had been observed. However, the incorporation of stabilizing oxides such as yttria into solid solution depressed the M_s temperature for the constrained transformation below room temperature and a single phase tetragonal polycrystal (TZP) could be retained at room temperature. (3).

Later the mechanical properties of the TZP materials were shown to be consistent with transformation toughening. The strength and toughness were easily controlled by changing the stabilizer content (4). The most popular material is 3Y-TZP which is tetragonal zirconia polycrystals stabilized with 3mol% Y_2O_3 ; this material has a toughness about $4-6\text{MPam}^{1/2}$ and a strength of 1-1.5 GPa. The main disadvantage of this material is that, like many zirconia ceramics the useful toughening is limited to temperatures below 500°C . Y-TZP materials are also susceptible to chemical corrosion induced surface transformation at about 300°C that can reduce the strength from 1 GPa to 100 MPa(5).

By the mid 1980's a different TZP stabilized with ceria had been developed(6). Although the trends in mechanical properties with grain size and stabilizer content were similar to Y-TZP, the values of the mechanical properties were very different. The toughness was in the range of $15-20\text{MPam}^{1/2}$ but the strength was as low at 500MPa even though the grain size was below $2\mu\text{m}$. This has been attributed to transformation plasticity (7), in which transformation occurs as the material is stressed, leading to pronounced inelasticity and a permanent strain when the stress is removed. It was shown that this is associated with very dramatic microstructural effects, including shear bands around indents and on tensile surfaces. Both of these phenomena are caused by autocatalytic transformation beyond the normal process zone associated with transformation toughening. The shear bands become fracture origins and are responsible for the moderate strengths of these materials. This phenomenon is called transformation controlled fracture (8).

Hence, in terms of their properties Y-TZP and Ce-TZP are at the opposite ends of the spectrum of zirconia based engineering ceramics. Y-TZP exhibits flaw controlled fracture and has high strength (1 to 1.5 GPa) and moderate toughness (4-6 MPam^{1/2}). In contrast Ce-TZP shows transformation controlled fracture and has moderate strength (~500MPa) and high toughness (15-20 MPam^{1/2})

The objective of this work is to fabricate a dicalcium silicate material which is an analogue to TZP zirconia ceramics. This requires the production of a fully dense material in which the β phase is metastably retained at room temperature in a stress transformable state. The β phase is only thermodynamically stable between 675°C and 490°C (9).

Such a material will facilitate the characterization of the $\beta \rightarrow \gamma$ transformation because there has been difficulty with XRD and TEM of composite materials that only contain 10-20 vol% dicalcium silicate. This has inhibited observation and direct proof of the stress induced transformation of the β -phase. The material should also have the potential to show the maximum toughening increment for β -Ca₂SiO₄ because the whole material is composed of the metastable phase which means that whole process zone could be composed of transformable material.

2. Preparation of β -Ca₂SiO₄ Powders

In order to produce dense β -Ca₂SiO₄ polycrystals the powder must have a high surface area and a submicron particle size, so that the material can be densified at low temperature to prevent excessive grain growth. Hence this is the primary goal of the powder preparation route.

Most of the powder preparation routes are devised for cement production because β -Ca₂SiO₄ is an important hydrating phase in hydraulic cements. The methods usually involve a solid state reaction between CaO (from decomposed limestone) and SiO₂ (quartz sand) at temperatures as high as 1450°C. The product is usually a low surface area powder containing large grains of Ca₂SiO₄ which transform to the γ phase on cooling to room temperature. The particle size distribution is also very wide and most unsuitable for the preparation of ceramics. The β phase is usually stabilized at room temperature by the addition of stabilizing oxides before calcination, these include: K₂O, Al₂O₃, Na₂O, B₂O₃, P₂O₅, BaO, etc. (10).

Chemical synthesis of Ca₂SiO₄ has been achieved using silica sol which is gelled or spray dried in the presence of Ca(NO₃)₂ (11). The product was β phase but only the spray dried dicalcium silicate has a suitable surface area of 12 m²/g for

fabricating ceramics, the gelled material only had a surface area of 7.4 m²/g. Unfortunately the authors did not comment on the particle size distribution. In this work a Pechini method (12) was used, but instead of using expensive silica precursors like tetramethylorthosilicate, used in metal-organic decomposition routes for dicalcium silicate (13), this method used silica sol. The Pechini process involves the formation of a chelate between mixed cations (dissolved salts) and a hydroxycarboxylic acid such as citric acid. This is then mixed with a polyhydroxylalcohol such as ethylene glycol. When the mixture is heated there is a condensation reaction with the formation of water. When as all the water is driven off the polyesterification take place and the gel foams and increase its surface area. Finally the expanded gel is dried and calcined to give a fine oxide powder.

2.1 Experimental Procedures

20g batches of Ca₂SiO₄ were prepared from assayed raw materials. First the required amount of Ludox SM silica sol was weighed out and the pH reduced to 1.5 using concentrated nitric acid, in order to change the charge on the SiO₂ particle surface. Then the Ca(NO₃)₂·4H₂O was dissolved in 250 ml of deionized water and added to the silica sol. The fact that the sol remained clear showed that the addition of the nitrate did not adversely effect the size of the colloidal silica. Then a 60/40 wt% resin of citric acid and ethylene glycol was added such that the ratio of the expected weight of oxides to the weight of the resin was 15% oxides. Then the mixture was heated on a hot plate and the water boiled off at approximately 120°C. The resulting dried gel was ground and calcined at temperatures ranging from 800°C to 1500°C. X-ray diffraction (XRD) was used to determine the phase distribution in the powders and surface area and particle size were evaluated using nitrogen adsorption BET and light scattering respectively. DTA was also carried out on the gel during heat at 10°C/min. In order to determine the effect of the resin content on the phase distribution and power characteristics, gels were prepared containing different amounts of citric acid/ethylene glycol resin. This is expressed as:

$$\frac{\text{weight of Ca}_2\text{SiO}_4 \times 100}{\text{weight of citric acid} + \text{ethylene glycol}}$$

and the oxide contents studied were; 0, 7%, 15%, 30% and 50%.

2.2 Results and Discussion

When the mixture is heated, the water is driven off and the condensation/polyesterification reaction takes place, causing the viscosity of the gel to rise. The remaining water vapor foams the resin which can then be dried, solidified and crushed.

Figure 1 shows the DTA curve for the resin during heating at 10°C/min. This shows a very large exotherm at 450°C corresponding the pyrolysis and decomposition of the gel which releases a lot of heat. During this exotherm the precursors decompose and the oxides crystallize.

After calcination of the gel, corresponding to 15% oxides, at 800°C for 1 hour, the resulting oxide powder is white which suggests that most of the carbon produced by the pyrolysis of the gel had been removed. The XRD trace in Figure 2 shows that the powder is fully β -Ca₂SiO₄ and Figure 3 shows the morphology of the powder. This shows that the powder agglomerates are highly porous, consisting of many small crystallites. The fine crystallite size is thought to be responsible for the metastable retention of the β phase at room temperature.

Further examination of Figure 2 shows that the fine crystallite size developed through calcination of this gel give β phase even when the powder is calcined at temperatures above 1100°C. Only powders calcined at temperatures of 1400°C and above show some γ phase which becomes more pronounced as the temperature is increased. Despite this the major phase is still β -Ca₂SiO₄.

Figure 4 shows the effect of resin content and calcination temperature on the surface area of the powders. As expected, the calcination temperatures as a dramatic effect on the surface area of the powder especially below 1000°C. This can be illustrated by the change in surface area from 17m²/g at 800°C to less than 5m²/g at 1000°C and is attributed to sintering and coarsening of the crystallites within the agglomerates.

The resin content also effects the surface area of the powder. In general, materials containing the most resin give powders with the highest surface area. This is in contrast to Pechini methods using mixed salt solutions which generally have an optimum resin content of 30-50% oxides (12). All the powders made by the Pechini method have higher surface areas than that prepared by gelling the silica sol (100% oxides). This is probably due to the high exotherm on pyrolysis of the resin which breaks up the gel such that the powders retain a high surface area. The

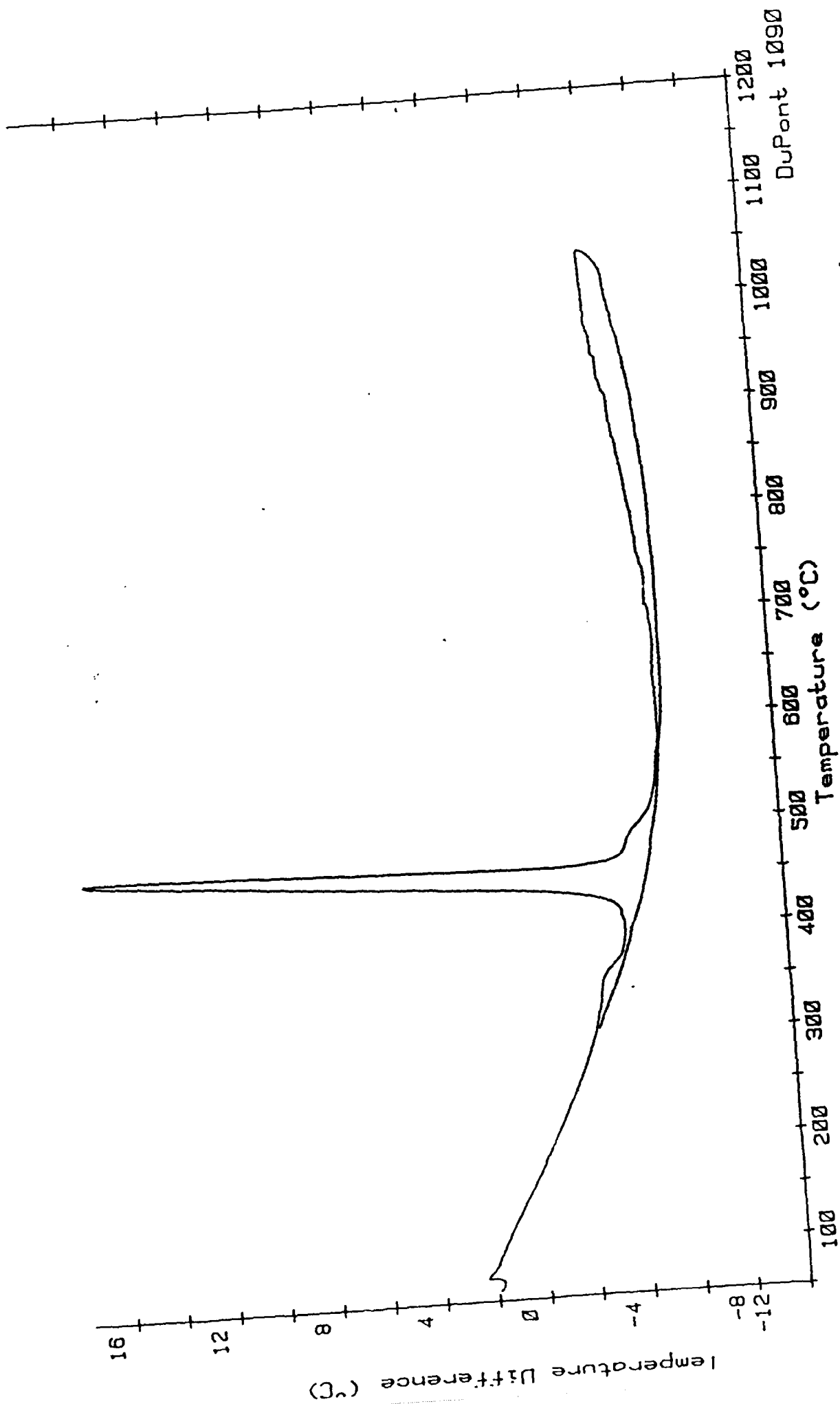


Figure 1: Differential thermal analysis (DTA) plot showing a large exothermic peak corresponding to the pyrolysis of the pechini gel as it is heated at 10°C/min. (courtesy of T.I. Hou).

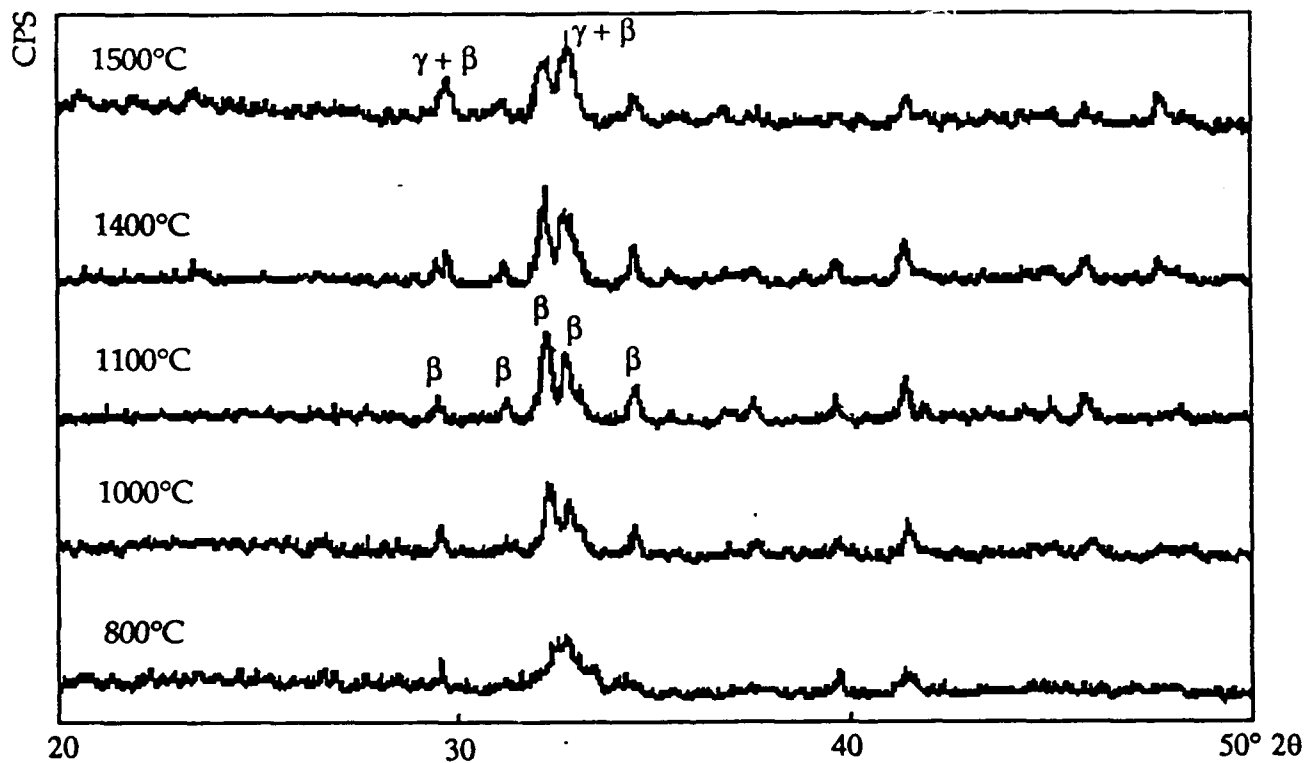


Figure 2: X-ray diffraction (XRD) plots of the 15% oxide gel fired at different temperatures between 800°C and 1500°C for 1 hour.

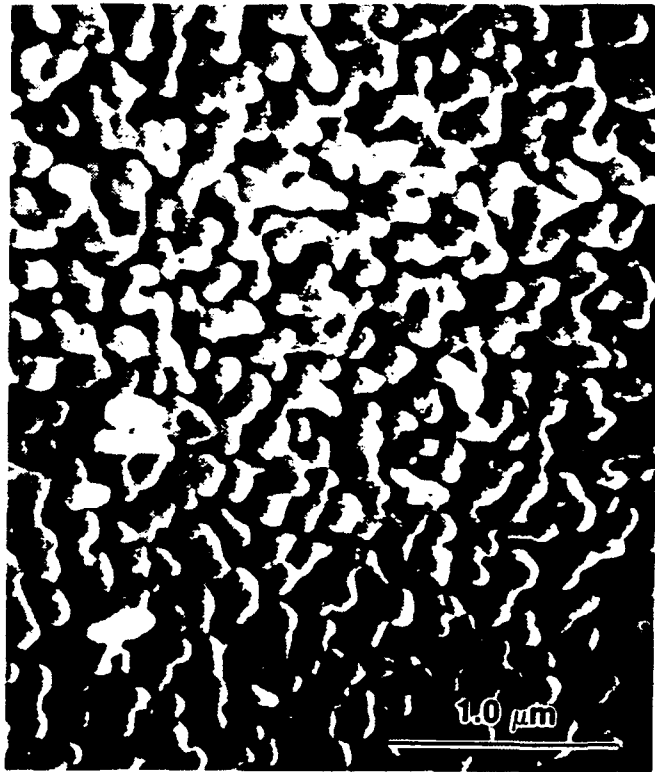


Figure 3: SEM micrograph of Ca_2SiO_4 powders showing the internal structure of the porous agglomerates, typical of powders derived from the pechini process.(courtesy of T. I. Hou).

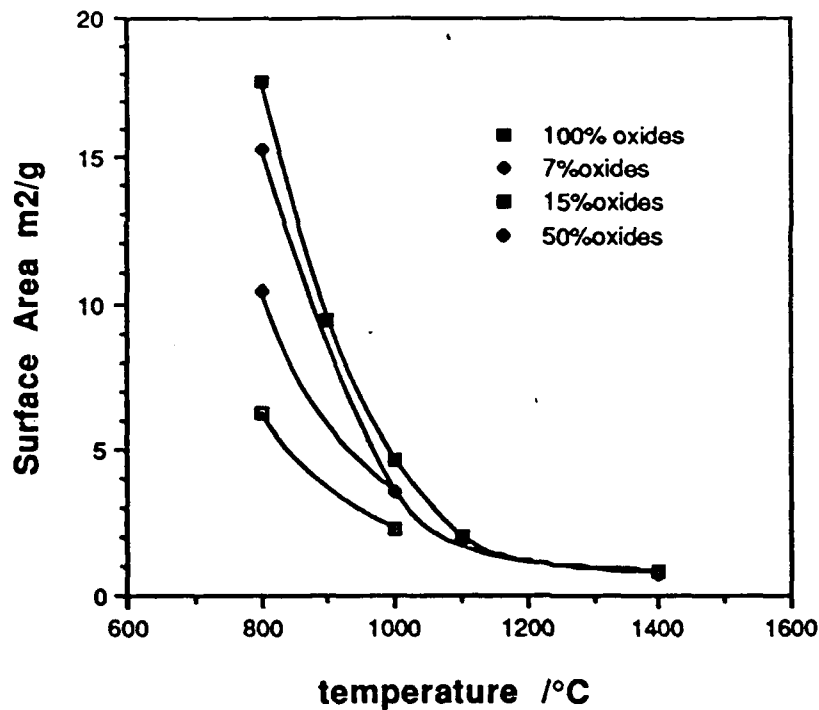


Figure 4: Plot of surface area against calcination temperature for powders prepared from pechini gels with different oxide/resin contents.

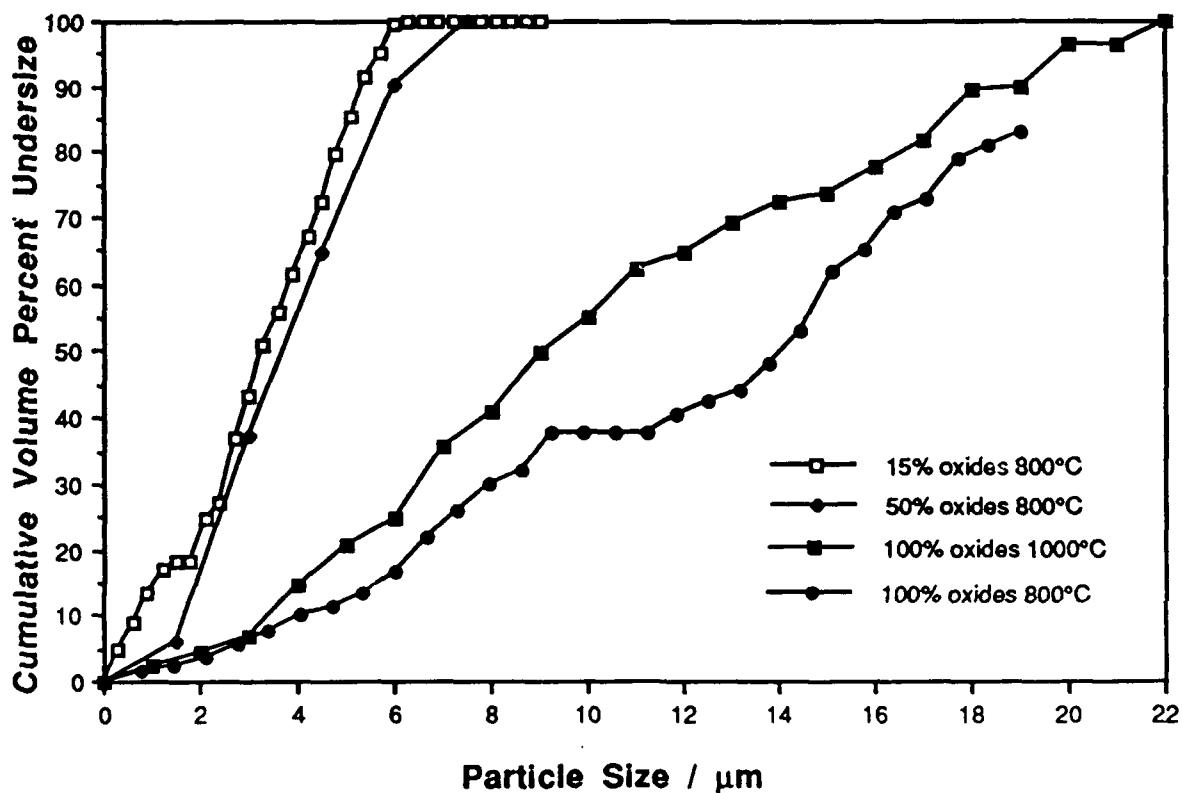


Figure 5: Plot of particle size against calcination temperature for powders derived from pechini gels with different oxide/resin contents.

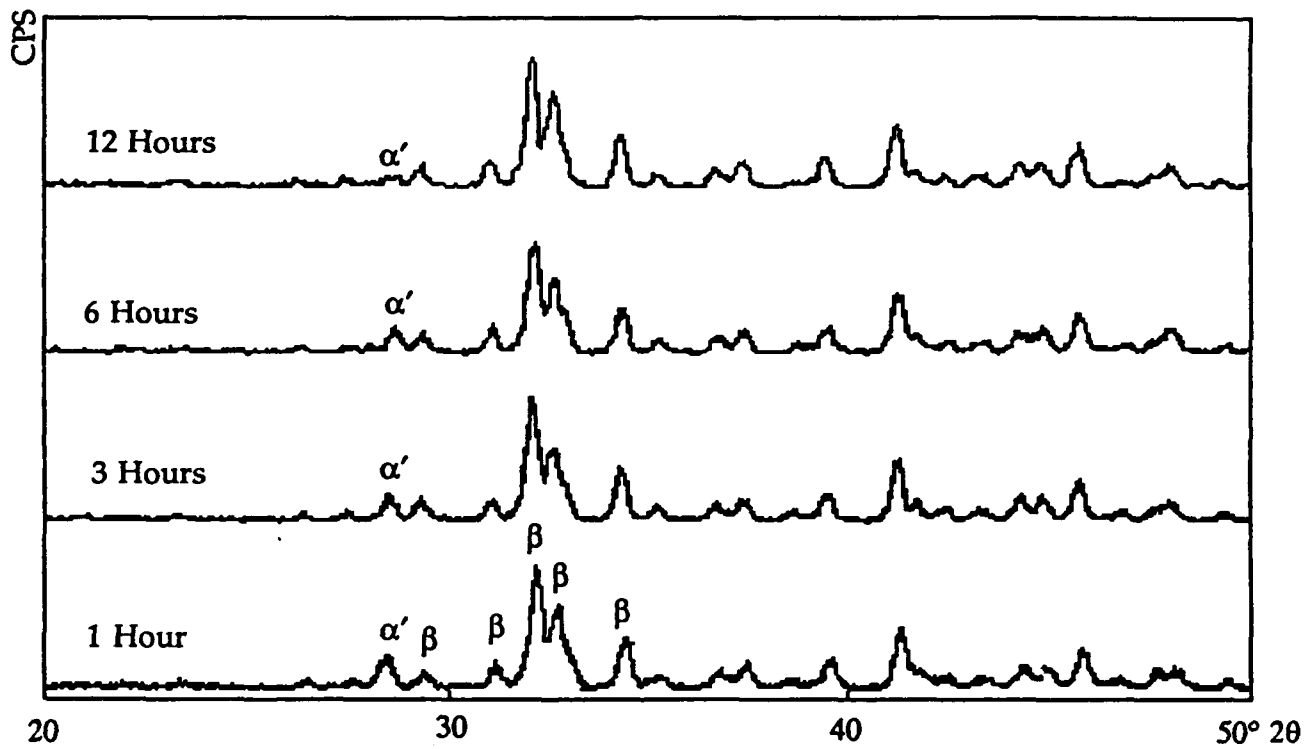


Figure 6: Comparison of the phase distributions on sintered surfaces of polycrystals sintered at 1400°C for different times.

Pechini gel is also thought to prevent the Ludox from gelling as the water is driven off.

Figure 5 shows the particle size distributions of powders calcined at 800°C. Again the powders prepared using the pechini gels have a superior particle size distribution to the materials prepared by gelling silica sol. This is again thought to be due to the expanded gels produced by the Pechini method which breaks up on pyrolysis. The 15%oxide gel has a very narrow particle size distribution (2-6 μ m) in comparison with the powder prepared by gelling colloidal silica (100% oxides).

The optimum powder characteristics of high surface area and small particle size were achieved when the powder made from the 15% oxide gel was calcined at 800°C for 1 hour.

surface area = 17m²/g
particle size = 2-6 μ m
 β -phase retained

3 Preparation of β -Ca₂SiO₄

The β -Ca₂SiO₄ powders were used to develop an analogue to tetragonal zirconia polycrystals TZP. Materials prepared by solid state reaction between CaO and hydrated silica have been prepared by the addition of K₂O and Al₂O₃ additives (14). These materials when sintered at 1450°C for 90 minutes had an unusual microstructure of dense agglomerates of dicalcium silicate surrounded by large amounts of glass that contained some other crystalline phases. The additives did stabilize some β -phase but microanalysis showed that they did not go into solid solution in the dicalcium silicate. The retention of the β -phase was attributed to the mechanical constraint of the glass grain boundary phase.

Although this material was impure and it was difficult to study the metastability of the β -phase, it did establish that it was possible to produce β -phase without incorporating it into another ceramics matrix.

3.1 Experimental Procedures

β -Ca₂SiO₄ powders were prepared as described in section 2. The gel corresponding to 15% oxides was calcined at 800°C for 1 hour. The resulting powder was ball milled in high density polyethene jars with alcohol and high purity ZrO₂-

3mol% Y_2O_3 balls. After milling for 48 hours the Ca_2SiO_4 powder was suspended in alcohol such that the solid content of the colloid was under 3vol%, to prevent interaction of the particles and flocculation. It was then allowed to sediment for either 20 hours or 50 hours. These were the times calculated using the stokes equation to sediment particles larger than $1 \mu m$ and $0.75 \mu m$ respectively, through a distance of 70 mm. The supernatant was then syphoned off and dried. The powder obtained was then redispersed in alcohol containing polyethylene glycol (MW=400) that is used as a binder for the powder. Pellets were then die pressed and isostatically pressed at 180 MPa. Finally the pellets were sintered in air. Table 1 shows an example of a typical firing schedule:

Table1

Temperature interval	Ramp Rate / Dwell Time
20°C → 1400°C	5°C/min
1400°C	1 hour
1400°C → 700°C	5°C/min
700°C	4.5 hours
700°C → 20°C	5°C/min

The annealing step at 700°C was designed to release residual stress developed in cooling of the thermally anisotropic dicalcium silicate. This was found to be important in controlling the metastability of the β -phase in Ca_2SiO_4 - MgO composites(14).

The materials so produced have been studied by XRD and TEM, before and after grinding experiments.

3.2 Results and discussion

Two series of materials were sintered at 1400°C on discovering that materials could be sintered to a relative density of 94% after only 30 minutes at this temperatures. Sintering for 1 hour and 3 hours gave densities of 96% and 98% respectively. The first series was of powders classified to less than $1 \mu m$ and fired for different times including 1 hour, 3 hours, 6 hours, and 12 hours. Figure 6 shows the phase distributions of the sintered surfaces of these materials. This shows that the

material was predominantly β phase with α phase which is metastably retained in material sintered for shorter times.

TEM examination of the materials shows that polycrystalline twinned β phase microstructure with no visible grain boundary phase. Figure 7 shows material sintered for 1 hour at 1400°C. There are no microcracks at the grain boundaries but where twins of adjacent grains impinge there are highly localized stress concentrations at the twin terminations. Selected area diffractions showed that some of the microstructure contains grains of α'_L phase which also appear to be twinned like the β phase. Since these grains have not undergone the $\beta \rightarrow \gamma$ transformation, it is not consistent that these grains are twinned, since the material was sintered in the α'_L region. It is not suspected that the $\alpha'_H \rightarrow \alpha'_L$ transformation ordering reaction would cause twinning, so one explanation could be that the twins were remnant from the $\alpha'_L \rightarrow \beta$ on cooling the powders during calcination. However, this is very unlikely because the twins would be annealed out during sintering. Work by Groves (16) also helps discount this explanation because they directly observed detwinning of Ca_2SiO_4 during the $\beta \rightarrow \alpha'_L$ transformation using hot stage TEM. The origin of the twinning in the α'_L phase remains unclear at this time.

The materials sintered for longer times at 1400°C showed cracks of the order of the facet length (figure 8) which then coalesce into extended cracks at larger grain size when the material was sintered for longer times (figure 9). This cracking is probably due to the twinning on the $\alpha'_L \rightarrow \beta$ transformation on cooling, the stress concentrations at the grain boundaries being large enough to cause fracture at some grain boundaries. It is noticeable that the stress concentrations on these grain boundaries have been relieved by the cracking.

Figure 10 shows a single untwinned grain which was identified as γ phase by selected area diffraction. How this grain has detwinned on the $\beta \rightarrow \gamma$ transformation is a mystery and requires further study. Here we are making the reasonable assumption that the grain went through the $\beta \rightarrow \gamma$ transformation on cooling that the γ phase was not metastably retained at high temperature during in sintering. Such a hypothesis is supported by the wide cracks surrounding the grain which could be due to the large shear involved in the $\beta \rightarrow \gamma$ transformation.

Some of the materials were ground with 30 μm diamond and X-ray analysis of the resulting surface was compared with the sintered surface. This showed that the grinding operation caused some $\beta \rightarrow \gamma$ transformation.

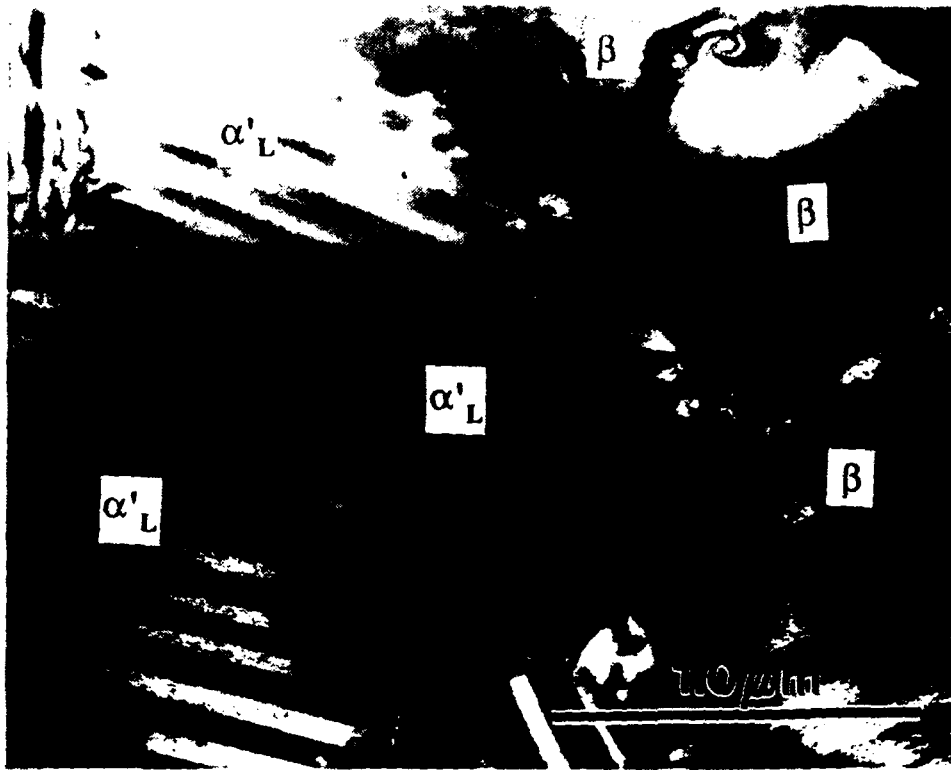


Figure 7: TEM micrograph of polycrystalline Ca_2SiO_4 fired for 1 hour at 1400°C . Note the twinned α'_L and β grains, and the highly localized strain at the grain boundaries.



Figure 8: TEM micrograph of polycrystalline Ca_2SiO_4 fired for 3 hours at 1400°C . Here grain growth has increased the stress at the grain boundaries such that some of the grain boundary facets are microcracked.

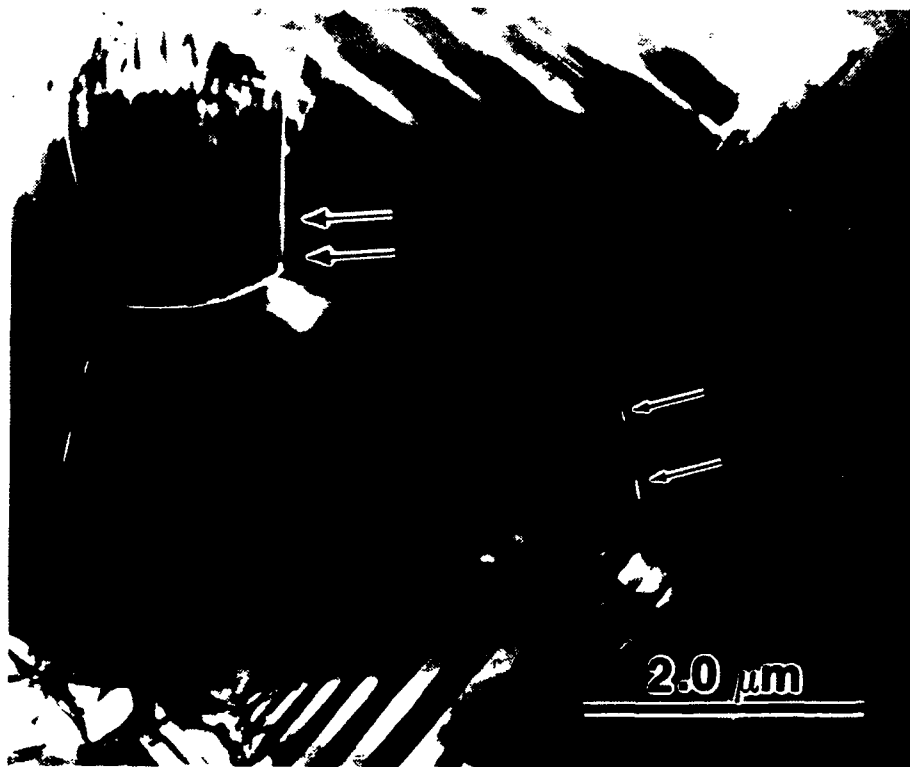


Figure 9: TEM micrograph of polycrystalline Ca_2SiO_4 fired for 6 hours at 1400°C . Further grain growth as has caused the microcracks to extend and coalesce.

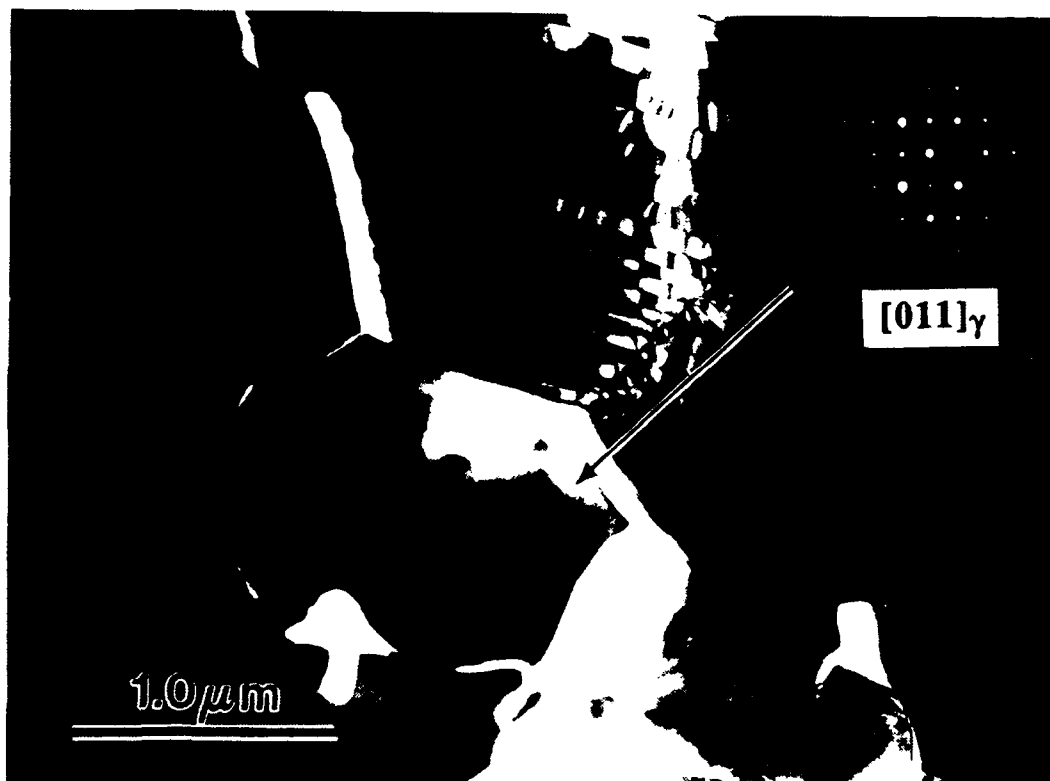


Figure 10: TEM micrograph of polycrystalline Ca_2SiO_4 fired for 3 hours at 1400°C , showing an untwined γ grain. The large cracks surrounding the grain is thought to be due to the large volume increase of the $\beta \rightarrow \gamma$ transformation.

A second series of materials made from powders of less than $0.75\ \mu\text{m}$ in particle size were sintered at 1400°C for times from 30 minutes to 6 hours. X-ray diffraction showed these materials to be completely β phase with no retained α'_L phase. The reason for the different phase distributions of the two series sintered at 1400°C is the subject of further study. It is possible that minor differences of the CaO/SiO_2 ratio may help stabilize different phases.

Grinding one such material has shown that very high grinding loads (9kg) can cause stress induced $\beta \rightarrow \gamma$ transformation which caused the surface of the material to dust. The dusted surface was collected and X-rayed and found to be composed of both β and γ phases, as shown in Figure 11. This is proof that the single phase material undergoes a stress induced transformation to γ phase at room temperature.

Sintering of the materials above the $\alpha \rightarrow \alpha'_L$ transformation (1425°C) at 1450°C caused materials to dust on cooling when sintered for 1 hour. Figure 12 shows the dusted material proved to be completely γ phase. The material sintered for 3 minutes, cracked and fractured over a period of a few days but remained predominantly β phase. It is thought the $\alpha \rightarrow \alpha'_L$ transformation increases the transformability of the β phase and a very strong grain size dependence operates for materials fired at 1450°C . Samples fired below the transformation at 1400°C can be fired for 12 hours and remain predominantly β phase.

4. Stabilization of Ca_2SiO_4 with BaO

Various oxides have been found to stabilize powders of the β -phase of Ca_2SiO_4 at room temperature. These include Na_2O , BaO , P_2O_5 , K_2O , Al_2O_3 (10)

For this study BaO was chosen as the stabilizer. The phase relationships for the Ca_2SiO_4 - Ba_2SiO_4 pseudo-binary system have been studied previously (17)(18), and the phase diagram is shown in figure 13. This additive was shown to stabilize both the β and α'_L phases of Ca_2SiO_4 in portland cements.

4.1 Experimental Procedures

The powder was produced using the same method as outlined in section 2 and all had 15% oxide/resin ratios. The compositions produced are listed in table 2 along with the phases expected from the previous work which used high temperature reaction of mixed oxides (17). The barium was added to the aqueous

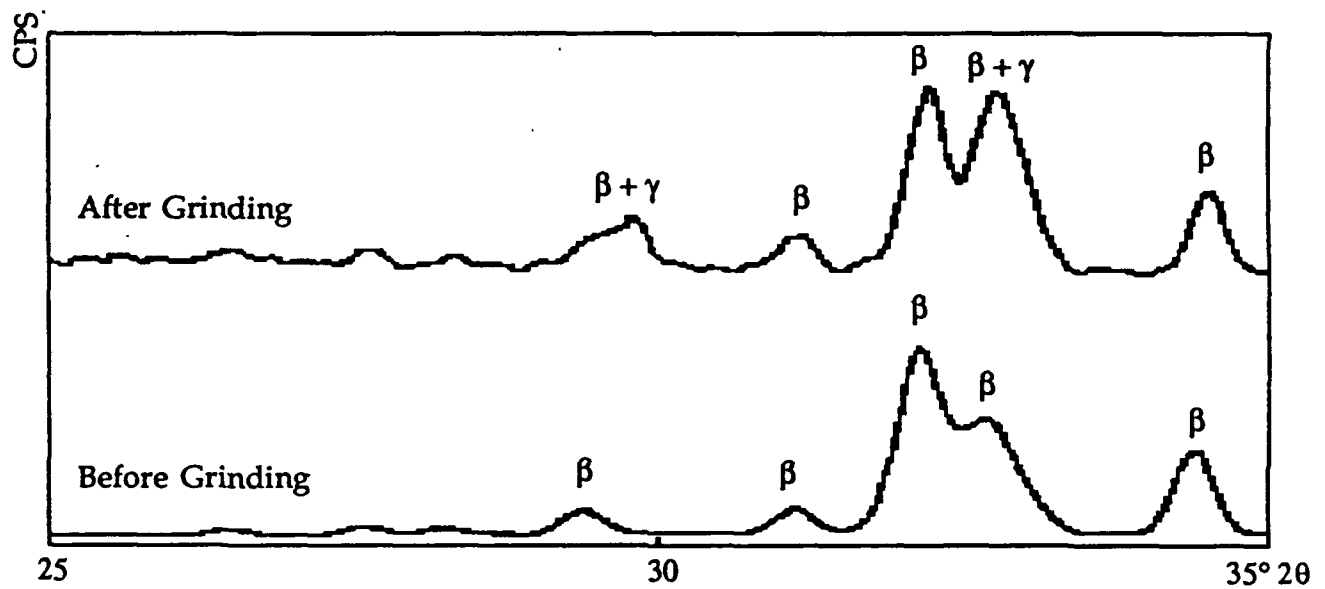


Figure 11: Comparison of XRD plots of a polycrystalline Ca_2SiO_4 sintered at 1400°C for 1 hour and a dusted surface of the sample after grinding under a high load.

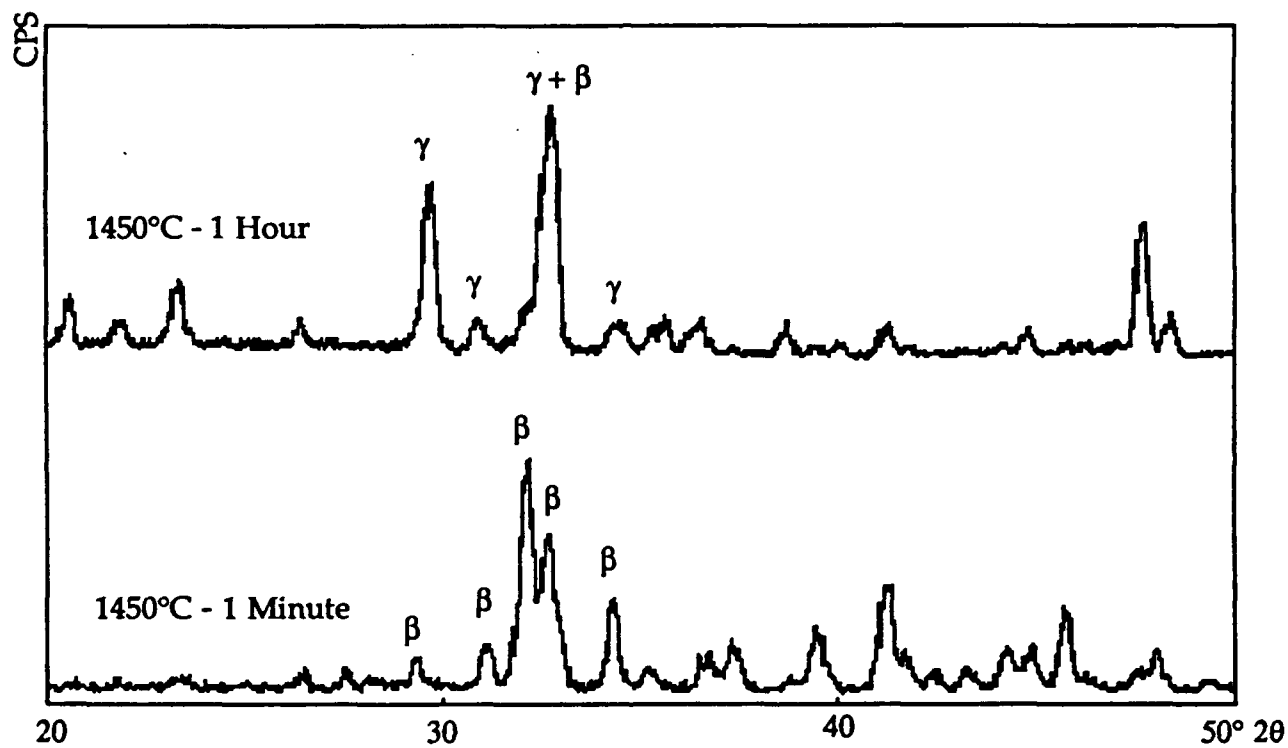


Figure 12: XRD plots of the sintered surface of polycrystalline Ca_2SiO_4 fired at 1450°C for 1 minute and a dusted sample fired at 1450°C for 1 hour.

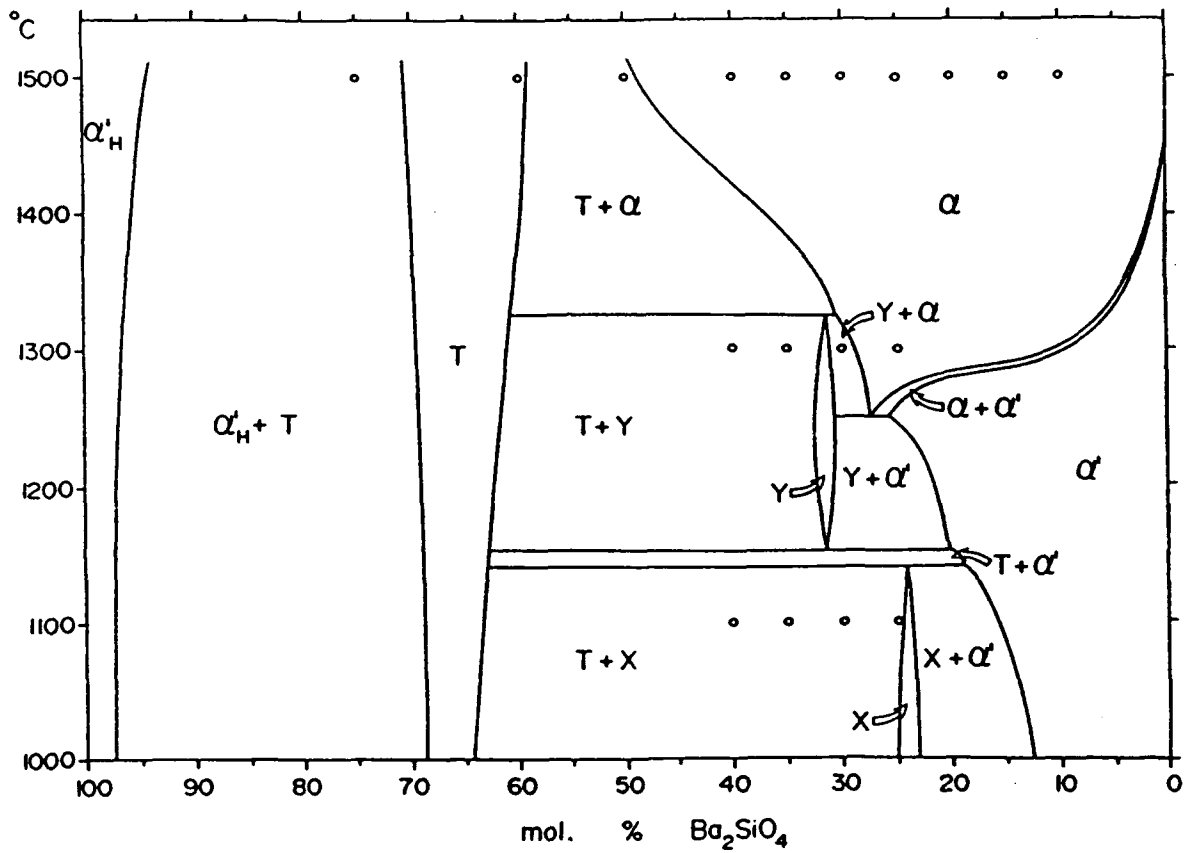


Figure 13: The pseudo-binary phase diagram of the Ca_2SiO_4 - Ba_2SiO_4 system (after Matkovic et al (17)).

solution of $\text{Ca}(\text{NO}_3)_2 \cdot 4\text{H}_2\text{O}$ as barium acetate which is water soluble. The rest of the processing was the same as described in section 2.

Table 2

Composition	Expected Phase
99mol% Ca_2SiO_4 - 1mol% Ba_2SiO_4	$\beta + \gamma$
98mol% Ca_2SiO_4 - 2mol% Ba_2SiO_4	$\beta + \gamma$
97mol% Ca_2SiO_4 - 3mol% Ba_2SiO_4	$\alpha'_L + \beta$
96mol% Ca_2SiO_4 - 4mol% Ba_2SiO_4	$\alpha'_L + \beta$
95mol% Ca_2SiO_4 - 5mol% Ba_2SiO_4	$\alpha'_L + \beta$

The gels were then calcined at 800°C 1300°C and 1400°C and the phase distributions were determined by X-ray analysis.

4.2 Initial Results and Discussion

Figure 14 shows the X-ray analysis of the phase distribution after calcination at 800°C, for 1 mol% Ba_2SiO_4 and 5 mol% Ba_2SiO_4 . Both compositions are β phase dicalcium silicate, similar to the pure Ca_2SiO_4 powder.

Figure 15 shows the phase distribution for all the compositions calcined at 1400°C for 1 hour. From the phase diagram these compositions should begin as α phase at 1400°C and the higher Ba_2SiO_4 contents should be α'_L phase. Table 2 shows the expected phase distributions at room temperature from the work of Matkovic et al (17). The phase distributions in the powder produced at 1400°C in this work appear to be very different, only the 1 mol% Ba_2SiO_4 material appear to be β - Ca_2SiO_4 . the 2 mol% Ba_2SiO_4 contained a lot of γ phase and compositions of 3mol% and above were all γ - Ca_2SiO_4 . This suggests the $\alpha \rightarrow \alpha'_H$ transformation controls the metastability of the β phase because inspection of the phase diagram shows that the 1 and 2 mol% materials are in the α region at 1400°C but those with higher barium contents are in the α'_H region.

This is further reinforced by XRD of materials calcined at 1300°C, as shown in figure 16. For all the barium contents the powders are retained as metastable β phase. At 1300°C all the powders would be in the α'_H region.

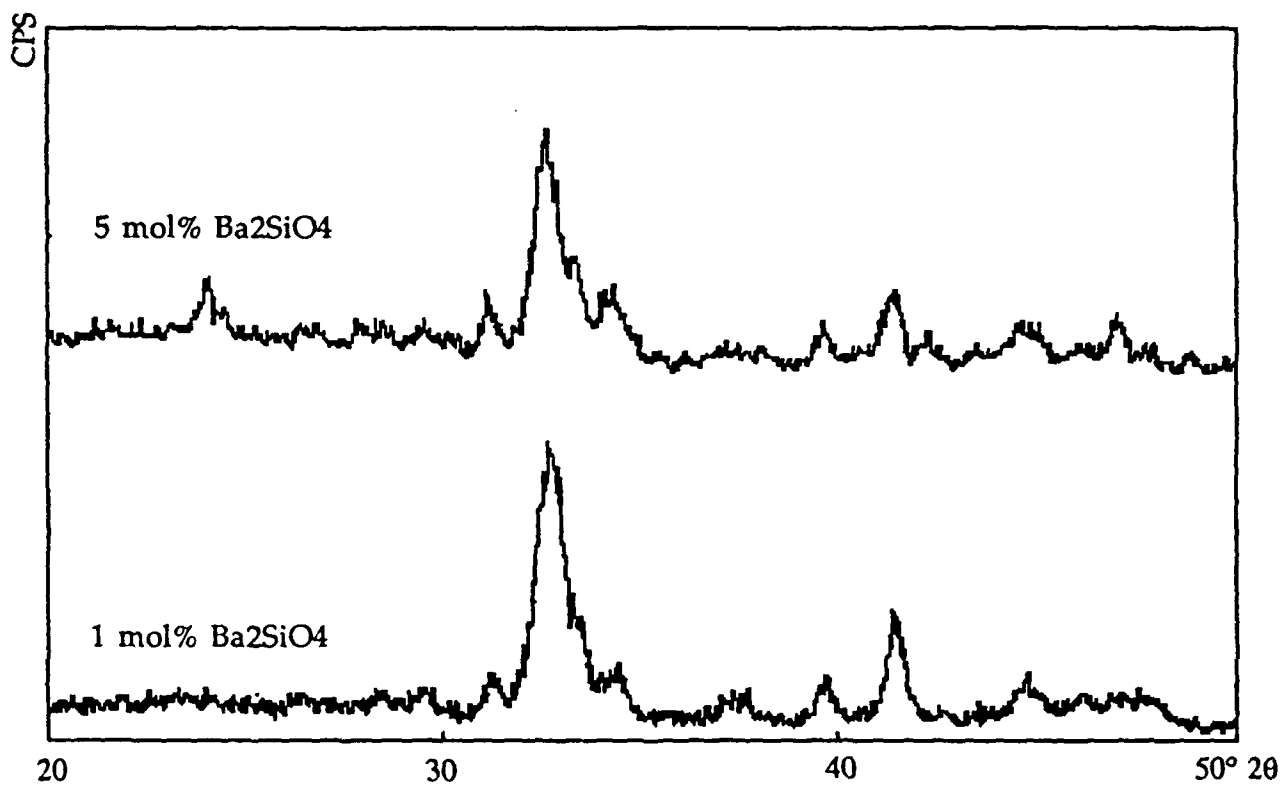


Figure 14: XRD plots of Ca₂SiO₄-Ba₂SiO₄ solid solutions calcined at 800°C for 1 hour.

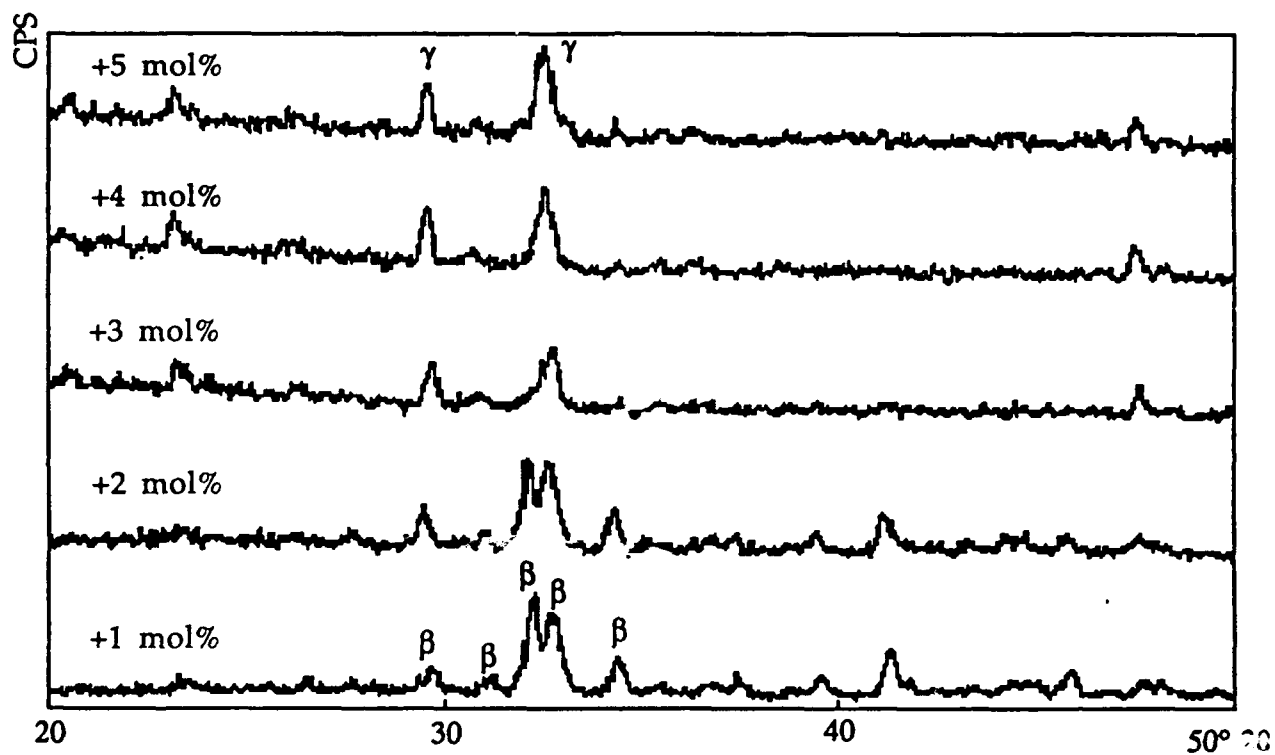


Figure 15: XRD plots of Ca_2SiO_4 - Ba_2SiO_4 solid solutions calcined at 1400°C for 1 hour.

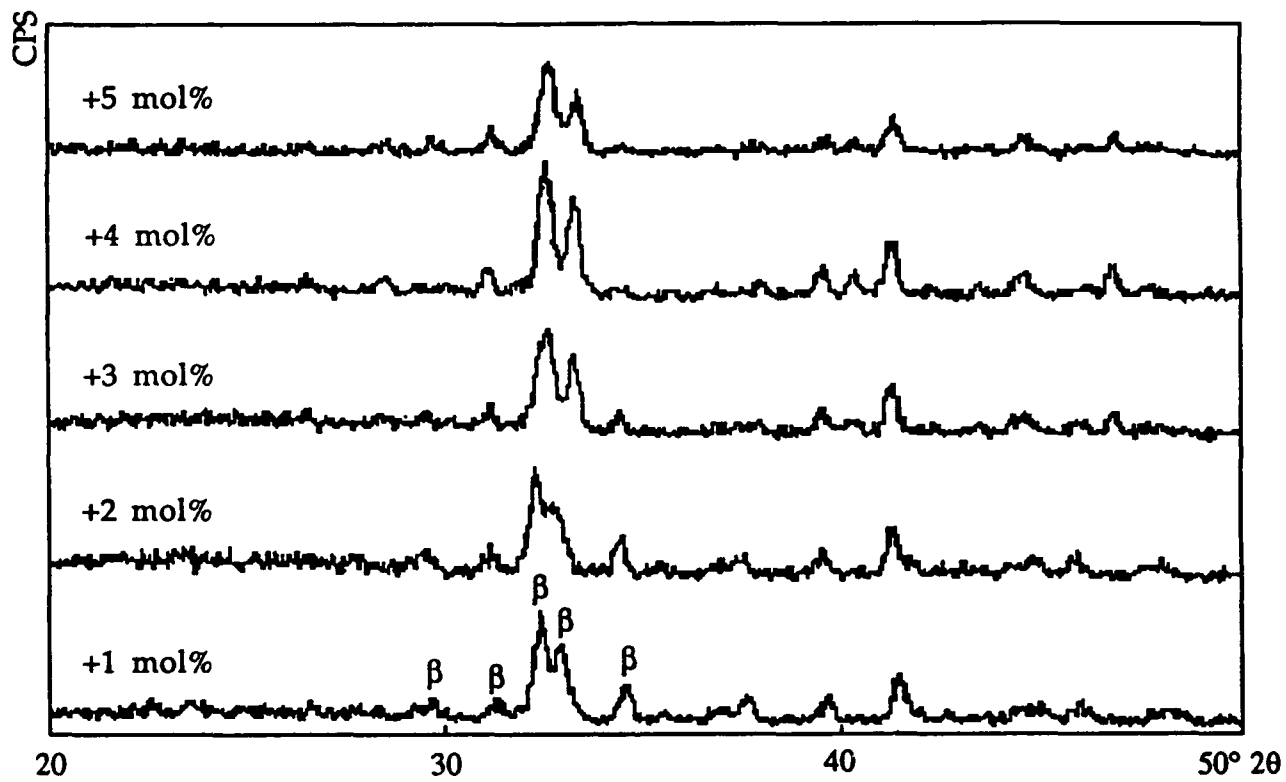


Figure 16: XRD plots of Ca_2SiO_4 - Ba_2SiO_4 solid solutions calcined at 1300°C for 1 hour.

5. Indentation Behavior of β -Ca₂SiO₄ Polycrystals

As a prerequisite to evaluation of the mechanical properties of β -Ca₂SiO₄ polycrystals it was necessary to study the effect of polishing and grinding on the stress induced $\beta \rightarrow \gamma$ transformation. It has already been stated in section 3 that grinding can induce the $\beta \rightarrow \gamma$ transformation and this would be undesirable on the surface of mechanical test bars because it may produce strength controlling flaws. The objective of this study is to see which grinding and polishing treatments can cause the $\beta \rightarrow \gamma$ transformation on the surface of a specimen. It is also important to determine if the damage resulting from such transformation can be polished off.

Preliminary indentation experiments have also been carried out to study the cracking behavior and to establish if evidence of transformation plasticity can be observed around indents.

Experimental Procedure

Specimens of β -Ca₂SiO₄ polycrystal fired at 1400°C for 1 hour were chosen for this study. The sintered surface of one specimen (specimen 1) was ground off with a 30 μ m diamond wheel and then polished with 15 μ m, 6 μ m and 1 μ m diamond. The sintered surface of a second specimen (specimen 2) was then removed with 1 μ m diamond only. In both cases no water was allowed to come in contact with the specimens because β -Ca₂SiO₄ is known to hydrate (19). The phase distributions on the surfaces were analysed by XRD and the specimens were indented with loads of 1 to 2 kg using a Tucon microhardness indenter. Finally the surfaces and the indents were examined using both optical microscopy and SEM.

Preliminary Results and Discussion

Figure 17 shows the surface of specimen 1 which has been ground with 30 μ m diamond and then polished. The surface shows many holes of the order of a few grain diameters in size. Detailed examination of the holes show that the grains in them are faceted and so the holes must have been created after sintering. This indicates that the holes are pullout produced by the grinding process. X-ray analysis

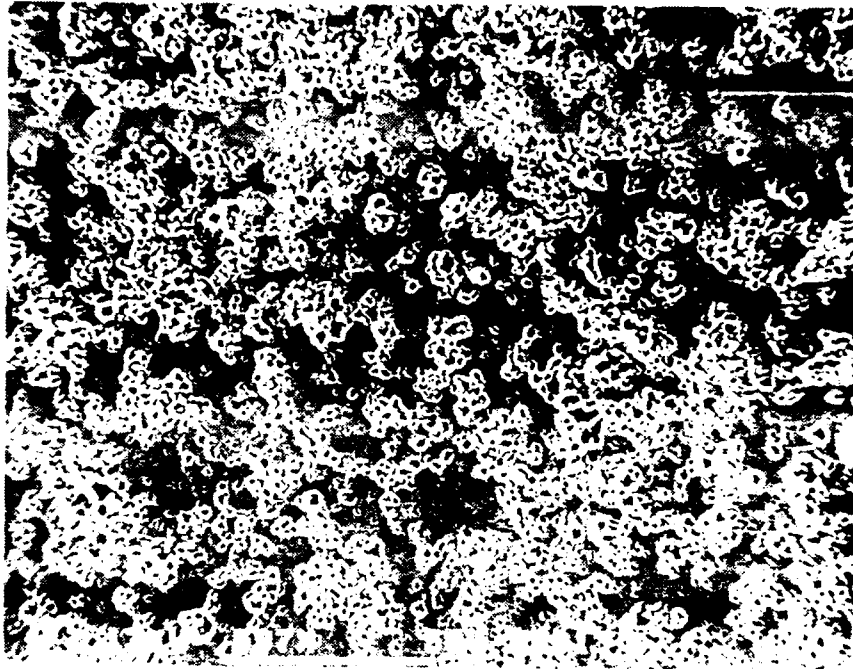


Figure 17: SEM micrograph of the surface of specimen 1 after grinding with 30 μ m diamond and polishing to 1 μ m diamond.

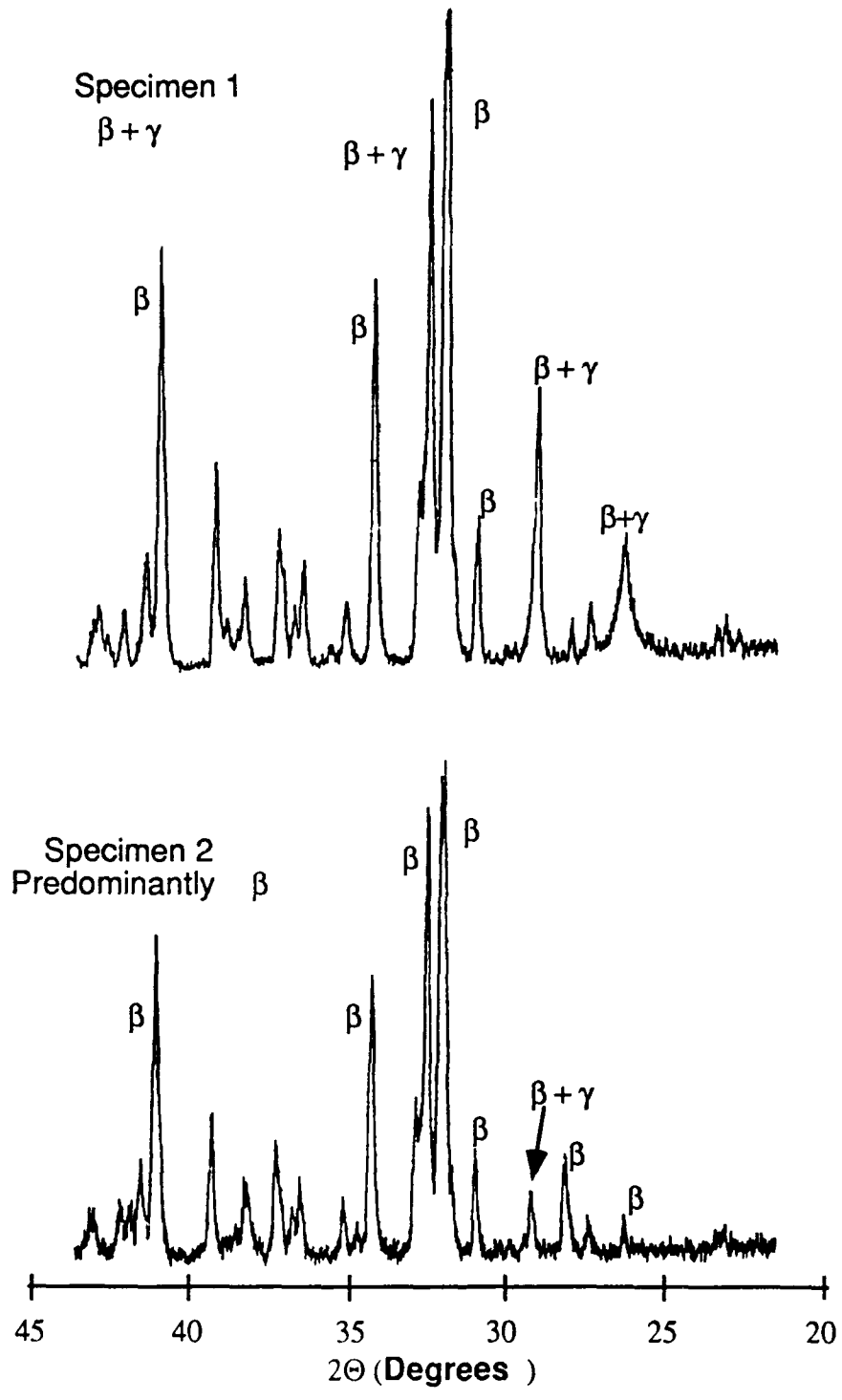


Figure 18: XRD analysis of the surfaces of both specimen 1 and specimen 2 after polishing.

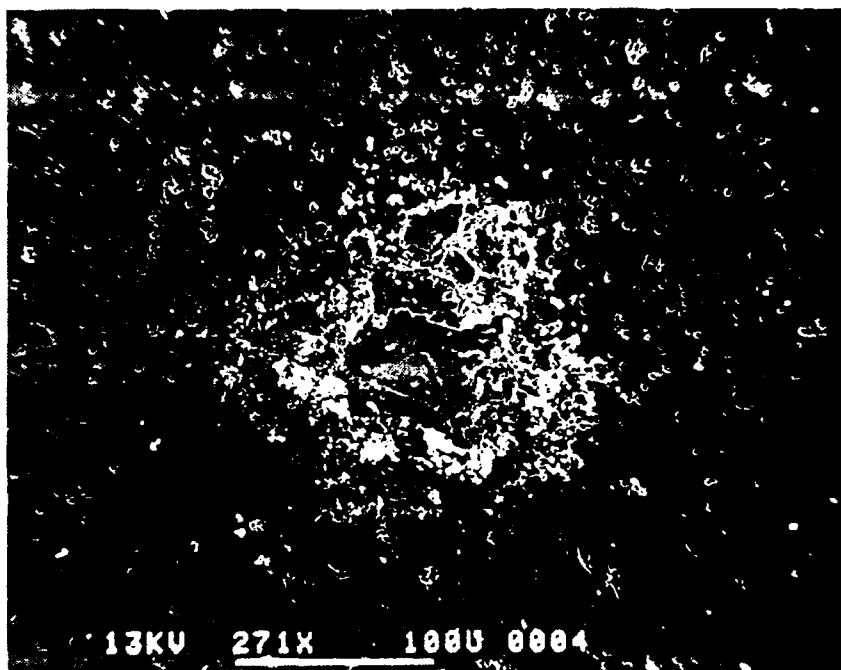


Figure 19: SEM micrograph of indent on specimen 1.

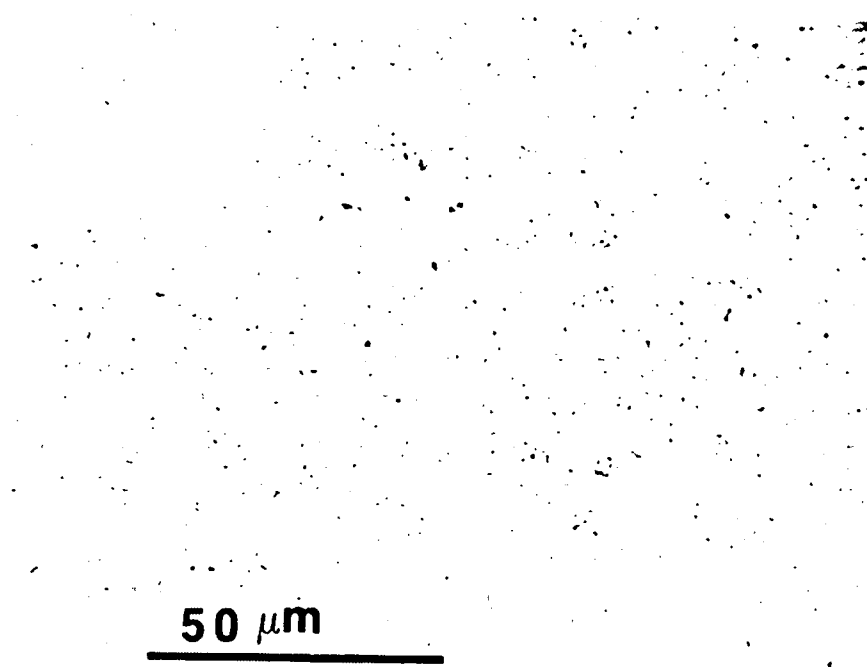


Figure 20: SEM micrograph of specimen 2 after the sintered surface had been removed by polishing with 1μm diamond. Note the reduced level of pullout.



Figure 21: SEM micrograph of indent on specimen 2.

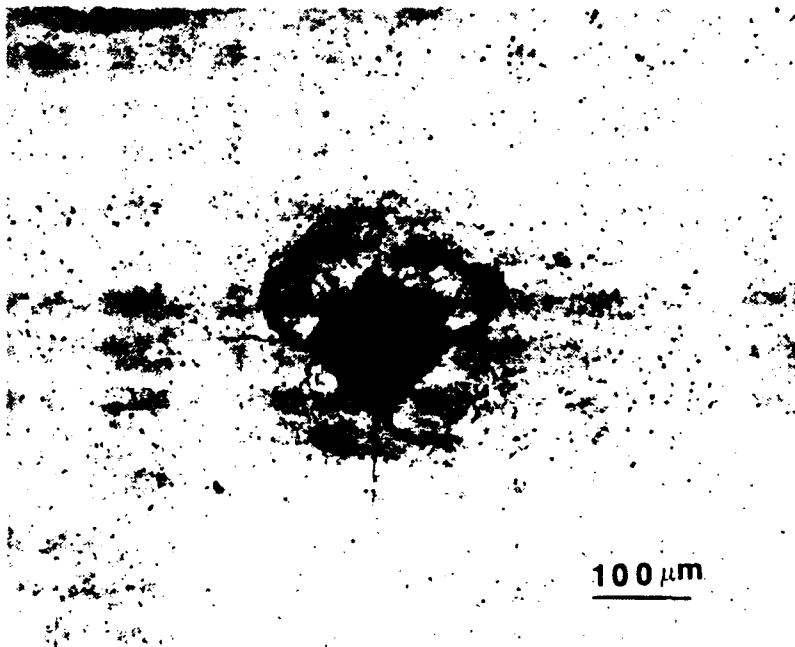


Figure 22: Optical micrograph of indent on specimen 2 showing the "lobe shaped features" on the sides of the indents, indicating lateral cracking.

of the surface shown in figure 18 reveals that both β and γ phases are present. This is in contrast to the sintered surface discussed in section 3 which only contained β phase. We believe that the stress induced $\beta \rightarrow \gamma$ transformation occurred during grinding and was responsible for the large amount of pullout damage. Such surfaces would be unsuitable for mechanical testing and figure 19 shows how the indents put into this surface are destroyed.

Figure 20 shows the surface of specimen 2 after the sintered surface had been removed using only $1\mu\text{m}$ diamond. There is much less pullout and XRD analysis shown in figure 18 indicates that the surface is still predominantly β phase. Hence a suitable surface finish can be obtained if the stress induced $\beta \rightarrow \gamma$ transformation can be controlled during grinding and polishing.

Figure 21 shows classical indentation behavior on the surface of sample 2. This includes clearly defined indents with no major spalling and cracks emanating from the corners. Closer examination of these indents using optical microscopy (figure 22) revealed "lobe shaped features" corresponding to sub-surface lateral cracks (21). Like many ceramics $\beta\text{-Ca}_2\text{SiO}_4$ does not exhibit classical "penny - shaped" cracks and hence the toughness cannot be estimated by indentation. Single edge notched beam (SENB) will be used to study the toughness of these materials as a function of grain size.

6 Summary

Fully dense $\beta\text{-Ca}_2\text{SiO}_4$ have been fabricated using chemically prepared $\beta\text{-Ca}_2\text{SiO}_4$ powders with a high surface area and small particle size. Grinding experiments have shown that this material can undergo the stress induced $\beta \rightarrow \gamma$ transformation. The stability of the β phase seems to be dependent on sintering temperature. Materials sintered above the $\alpha \rightarrow \alpha'_H$ transformation temperature for short times exhibit the $\beta \rightarrow \gamma$ transformation on cooling and the samples fracture or dust. In contrast, materials sintered below the $\alpha \rightarrow \alpha'_H$ transformation remain stable even after firing for 12 hour at 1400°C . The materials sintered for 1 hour at 1400°C show highly localized stress concentrations were twin terminations in adjacent grains impinge at the grain boundaries. Sintering for longer times causes microcracking at these grain boundaries due to grain growth.

7 Future Work

1. Evaluate the mechanical properties of polycrystalline β -Ca₂SiO₄ as a function of grain size for materials fired at 1400°C.
2. Use the β -Ca₂SiO₄ polycrystals to characterize the stress induced $\beta \rightarrow \gamma$ transformation.
3. Study the effect of barium doping on the metastability of β -Ca₂SiO₄.

8 References

- (1) N. Claussen, "Fracture Toughness of Al₂O₃ with an Unstabilized ZrO₂ Dispersed Phase", *J Am Ceram Soc* 59 49-51 (1976)
- (2) R.C. Garvie, R.H.J. Hannink, R.T. Pascoe, "Ceramic Steel ?" *Nature* (London) 258 703-704 (1975)
- (3) T.K. Gupta, J.H. Bechold, R.C. Kuznicki, L.H. Cadoff, B.R. Rossing "Stabilization of Tetragonal Phase in Polycrystalline Zirconia", *J Mat Sci* 12 2421 (1977)
- (4) K. Tsukuma, Y. Kubota, T. Tsukidate, "Thermal and Mechanical Properties of Y₂O₃-Stabilized Tetragonal Zirconia Polycrystal", p 352 in *Advances in Ceramics* 12 edited by N. Claussen, M Rühle, A.H. Heuer. (1984).
- (5) T. Masaki, "Mechanical Properties of Y-PSZ after Aging at Low Temperature", *Int J High Tech Ceramics* 2 85 (1986).
- (6) K. Tsukuma, M. Shimada, "Strength, Fracture Toughness and Vickers Hardness of CeO₂-Stabilized Tetragonal Zirconia Polycrystals (Ce-TZP)", *J Mat Sci* 20 1178 (1985).
- (7) P.E. Reyes-Morel, I-Wei Chen, "Transformation Plasticity of CeO₂-Stabilized Tetragonal Zirconia Polycrystals: I Stress Assistance and Autocatalysis", *J Am Ceram Soc* 71 343 (1988).

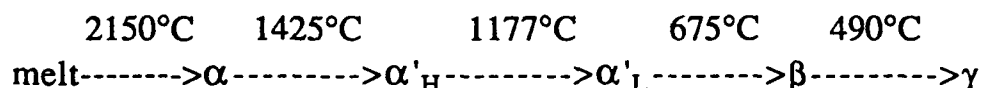
- (8) M.V. Swain, L.R.F. Rose, "Strength Limitations of Transformation- Toughened Zirconia Alloys" *J Am Ceram Soc* 69 511-518 (1986).
- (9) W.M. Kriven, "Possible Alternative Transformation Toughners to Zirconia: Crystallographic Aspects" *J Am Ceram Soc* 71 1021 (1988).
- (10) I.M. Pritts, K.E. Daugherty, "The Effects of Stabilizing Agents on the Hydration Rate of β -C₂S.", *Cement and Concrete Research* 6 783-796 (1976).
- (11) D.M. Roy, S.O. Oyesfesobi, "Preparation of Very Reactive Ca₂SiO₄ Powder" *J Am Ceram Soc* 60 Discussion and Notes 178 (1977).
- (12) P.A. Lessing, "Mixed-Cation Oxide Powders via Polymeric Precursors", *Ceram Bull* 68 1002 (1989).
- (13) J.H. Adair, "Processing and Properties of Chemically-Derived Calcium Silicate Cements" presented at AFOSR Review, Dayton OH April (1990).
- (14) C.J. Chan, W. M. Kriven, J. F. Young, "Analytical Electron Microscopic Studies of Doped Dicalcium Silicate" *J Am Ceram Soc* 71 713 (1989).
- (15) E.S. Mast, MS Thesis, UIUC, Urbana, IL, Oct 1990
- (16) G. W. Groves, "Phase Transformations in Dicalcium Silicate" *J Mat. Sci* 18 1615 (1983).
- (17) M. Matkovic, S. Popovic, B. Grzeta, R. Halle, "Phases in the System Ba₂SiO₄-Ca₂SiO₄" *J. Am. Cer. Soc.* 69 132 (1986).
- (18) J. G. Thompson, R. L. Withers, B. G. Hyde. "Further Consideration of Phases in the System Ba₂SiO₄-Ca₂SiO₄" *J. Am. Cer. Soc.* 70 C-383 (1987).
- (19) S.N. Ghosh, P.B. Rao, A.K. Paul, K. Raina, "Review : The Chemistry of Dicalcium Silicate Mineral" *J Mat Sci* 14 1554 - 1566 (1979).

(20) R.F. Cook, G.M. Pharr, "Direct Observation and Analysis of indentation Cracks in Glasses and Ceramics" *J Am Ceram Soc* 73 787-817 (1990)

Section 2.2 Preparation, Properties, and Microstructures of Dicalcium Silicate-Calcium Zirconate Composites

1. Introduction

Dicalcium silicate, $2\text{CaO}\cdot\text{SiO}_2$, (C_2S) is an important compound in cement. It has five polymorphic transformations at atmospheric pressure, i.e.



Of most interest is the transformation from β to γ because of the large volume increase accompanied by the transformation. It is similar to the transformation of ZrO_2 from tetragonal to monoclinic. However, the volume change is two and a half times that of ZrO_2 . Table 1⁽¹⁾ shows some important characteristics of the β to γ transformation compared with ZrO_2 .

Table 1. Comparison of the Ca_2SiO_4 β to γ transformation with the ZrO_2

Compound	ZrO_2	Ca_2SiO_4
Transformation Temperature	950°C	490°C
Volume Change	+5%	+12%
Unit Cell Shape Change ($\Delta\beta$)	9°	4.6°
Transformation Induced by Grinding	yes	yes
Structure Change	Tet.->Mono.	Mono->Ortho

ZrO_2 has been successfully added to some matrices, and the mechanical properties such as toughness and thermal shock resistance⁽²⁻⁷⁾ were significantly improved. The tetragonal to monoclinic transformation induced by the stress field at a crack tip retarded crack propagation, thereby, increasing the toughness. The mechanical behavior and microstructure have already been studied. Kriven⁽¹⁾ has reviewed several possible transformation tougheners alternative to ZrO_2 . Ca_2SiO_4 , with a much larger volume increase than ZrO_2 , is one of the potential candidates⁽⁸⁾. In addition to the different volume increase percent there are other differences between Ca_2SiO_4

and ZrO_2 . Firstly, the transformation of Ca_2SiO_4 occurs from the twinned β structure to the untwinned γ structure. The reverse is true of ZrO_2 . Secondly, unlike ZrO_2 , the transformation is irreversible. Upon heating under normal pressure, the γ phase must be heated up and transformed to α'_L at $850^\circ C$, rather than to β .

The objective of this research is to investigate the toughening effect of C_2S as a toughener of a $CaZrO_3$ matrix. For example, how does the large volume change due to phase transformation play a role in the phase transformation toughening? All the characterization results will be correlated with one another, in order to have a deeper insight about the toughening effect. The results of this research, compared with those of ZrO_2 -toughened materials, will help to understand the fundamentals of phase transformation toughening and, in the future, help to choose ceramic tougheners and matrices to obtain high toughness increases through the application of martensitic phase transformations.

2. Experimental Procedures

In order to understand the toughening effect of C_2S on the C_2S -containing composites, three steps were taken:

- (i) preparation of C_2S powders
- (ii) preparation of C_2S -containing composites
- (iii) characterization of composites, including mechanical property and microstructure relationships.

2.1. Preparation of C_2S powders

Roy and Oyefesobi⁽⁹⁾ prepared the β - C_2S powder by an inorganic gel and spray drying method with $Ca(NO_3)_2$ and colloidal silica as a starting material. A modified Pechini method (Fig. 1) using the same starting materials was investigated. The modification was that one of the components (SiO_2) existed in a colloidal form. It is hoped that the C_2S powder produced by this method can be used to make a pure β phase pellet which is similar to TZP, and which will be used for future studies on the intrinsic properties of C_2S . The

C₂S Preparation (Pechini method)

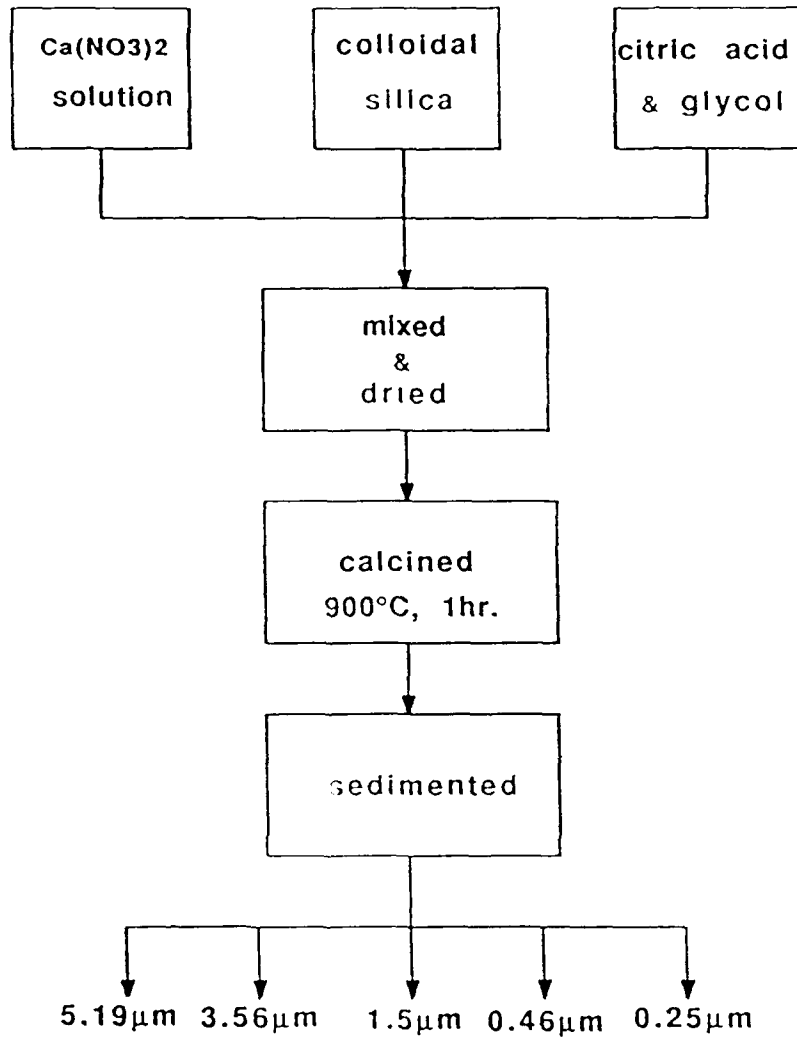


Fig. 1. Flow chart of C₂S powder preparation

sedimentation method was used to obtain different sizes of C_2S and at the same time to narrow the C_2S particle size distribution.

2.2. Preparation of C_2S -containing composites

$CaZrO_3$ was chosen as the matrix. Different sizes of C_2S was mixed with $CaZrO_3$ in isopropyl alcohol, dried, die pressed, isostatically cold pressed and then sintered to high density. Fig. 2 showed the flow chart of sample preparation by sintering. Hot-pressing was also used to reach full density and to obtain smaller grain size, avoiding the matrix microcracking due to itself. Samples was prepared as pellets and mechanical test bars. For comparison, the same procedure was taken for the pure matrix.

2.3. Characterization of composites

2.3.1 X-ray Diffractometry

The phases was analyzed using the X-ray diffraction method. For pellets of C_2S - $CaZrO_3$ composites, a standard polishing procedure, from 9 μm to 1 μm diamond paste finish was taken to eliminate possible surface transformation. The phases which are of most concern are β and γ .

2.3.2. Mechanical Property Characterization

The strength of the pure matrix and composites was measured using the 4-point bending method. Surfaces was polished and the edges of the tensile surface was bevelled. The toughness was measured by the single-edge, notched-beam method in a 3-point loading. The sizes of test bars were about 2.5 x 3.5 x 15 mm with span length 12.7 mm.

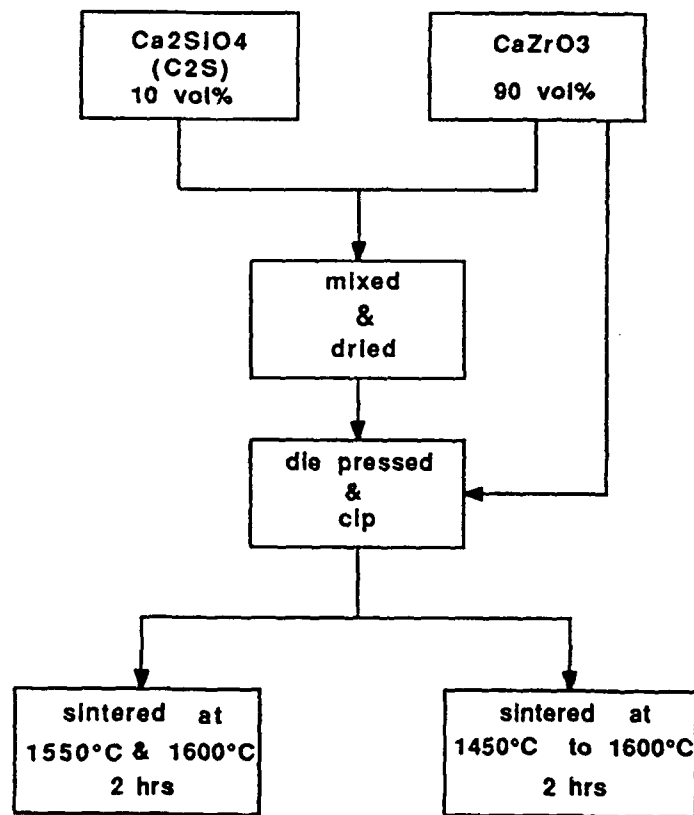


Fig. 2. Flow chart of sample preparation by sintering

2.3.3 Microstructure Characterization

The general microstructure was studied by SEM and TEM. In the SEM, the average grain size of matrix and particle size of C_2S in composites was determined by the linear intercept method. The morphology of C_2S was also noted. TEM was used to examine the microstructure on a finer scale. TEM samples were prepared by standard procedures: polishing, dimpling, and ion-milling. However, special care needed to be taken to remove the damaged zone produced by the previous polishing steps, due to the large transformation zone.

3. Results and Discussion

3.1 C_2S Powders

The result of X-ray diffraction showed the presence of β phase in the monoclinic structure. The shape of the C_2S particle was irregular, with each C_2S being made up of many fine spherical particles, about $0.1 \mu m$ in size. Five sizes of C_2S were obtained after sedimentation, i.e., $5.2 \mu m$, $3.6 \mu m$, $1.5 \mu m$, $0.5 \mu m$, and $0.25 \mu m$.

3.2 Mechanical properties of matrix and composite

3.2.1 Toughness

Fig. 3 shows how the toughness of the pure matrix which had an orthorhombic structure depends on its grain size. The smaller the grain size, the higher the toughness. This phenomenon is common in non-cubic materials such as Al_2O_3 ⁽¹⁰⁾.

Fig. 3(a) shows the toughness for pure matrix prepared by sintering. Fig. 3(b) was the preliminary data of toughness for as-hot-pressed and annealed pure matrix. The grain size for as-hot-pressed specimen was about $1.8 \mu m$. TEM observation showed no microcracking and therefore it was believed that at and below this grain size the toughness was an intrinsic property.

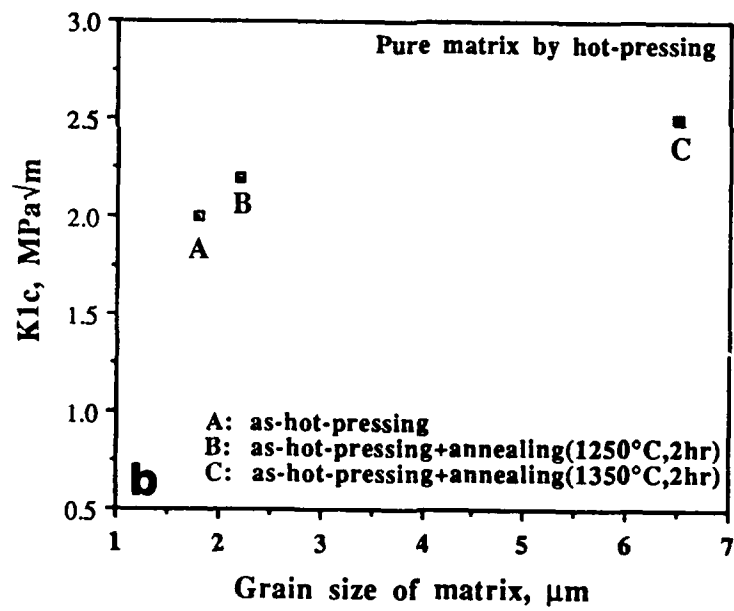
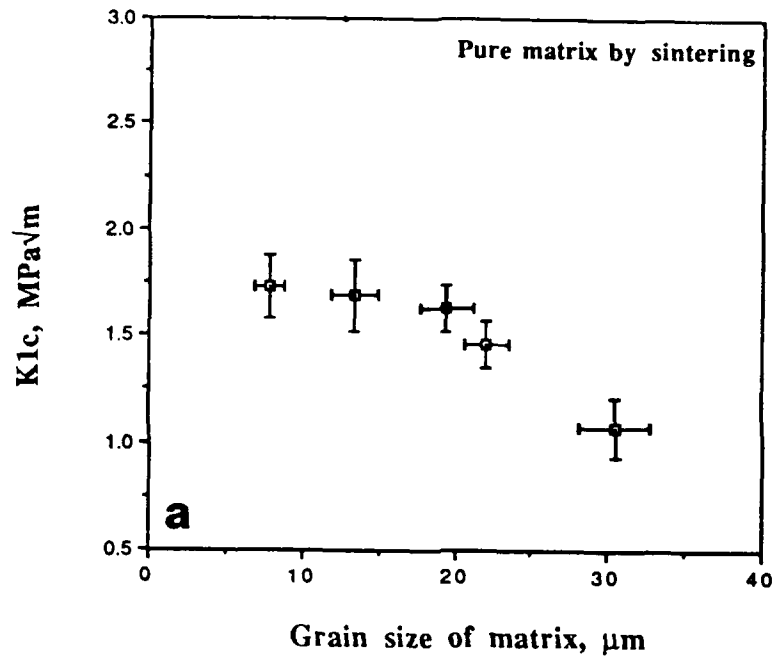


Fig. 3. Change of toughness of the pure matrix as a function of grain size. Samples were prepared by (a) sintering and (b) hot-pressing

Fig. 4(a) and (b) show the results of the toughness measurements of the composites fired at 1550°C and 1600°C, respectively. The toughness of the pure matrix is also shown in the figures. Since the grain size of the matrix affects the toughness, it is plotted against the grain size of matrix for comparison. For the composite fired at 1550°C, the toughness increased from about 2.0 to about 2.6 MPa-m^{1/2}. For the composite fired at 1600°C, the toughness did not vary too much ranging from 1.8 to 2.0 MPa-m^{1/2}. In general, the toughness of the composites was higher than that of the pure matrix.

3.2.2 Strength

Fig. 5(a) and (b) showed plots of strength v.s. grain size of matrix for composites fired at 1550°C and 1600°C respectively. The strength of the pure matrix is also shown in the figure. Generally speaking, the strength of the composites was higher than that of the pure matrix.

3.2.3 Microstructure

Fig. 6(a) is an SEM micrograph showing the general microstructure of the composite fired at 1550°C with the smallest initial C₂S particle size. The darker, irregular-shaped, second phase was C₂S which was about 3 μm in size. There was still about 4% porosity. Fig. 6(b) is a higher magnification of the previous one, showing that in a large C₂S particles a lath structure was sometimes found, and was usually associated with cracks. However, in small C₂S particles, no such feature was found.

Fig. 7 was TEM micrographs for the composite with smallest C₂S particles fired at 1550°C. Microcracking along the grain boundary of matrix and between β-C₂S and matrix was observed as shown in Fig. 8 (a) and (b). In fig. 9 strong strain contrast was associated with the particles. Two radial microcracks were found. One of the radial microcracks occurred along the grain boundary of matrix. The other

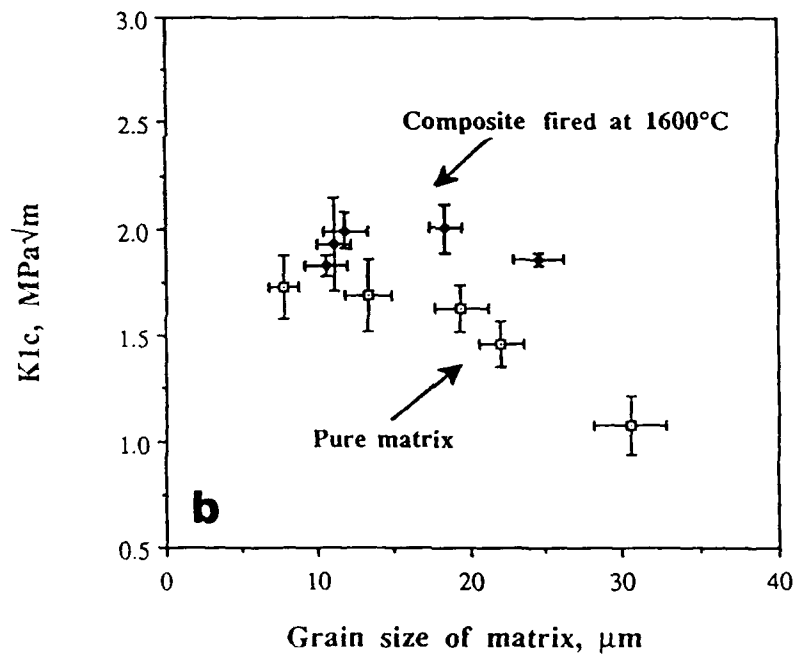
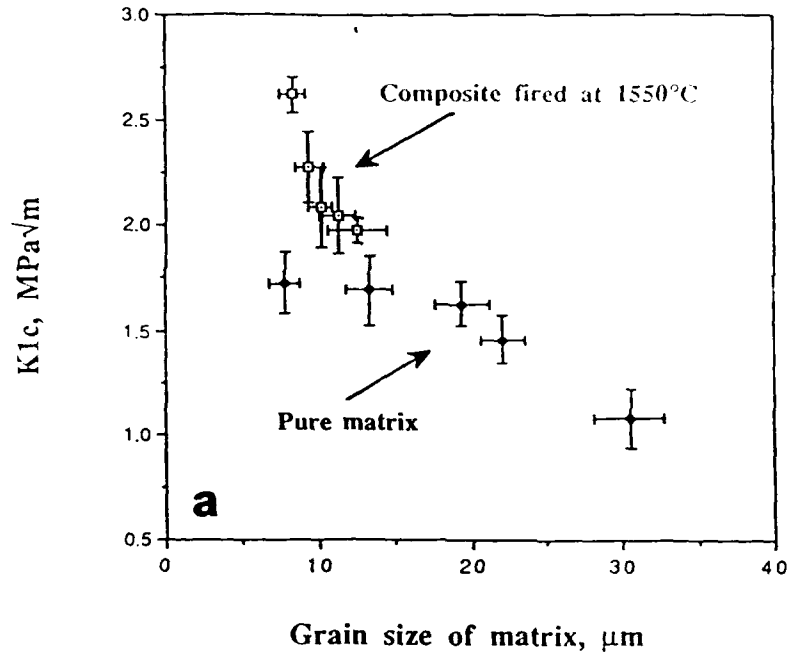


Fig. 4. Toughness of composites fired at (a) 1550°C and (b) 1600°C is plotted against corresponding grain size of matrix. The toughness of the pure matrix is also shown for comparison.

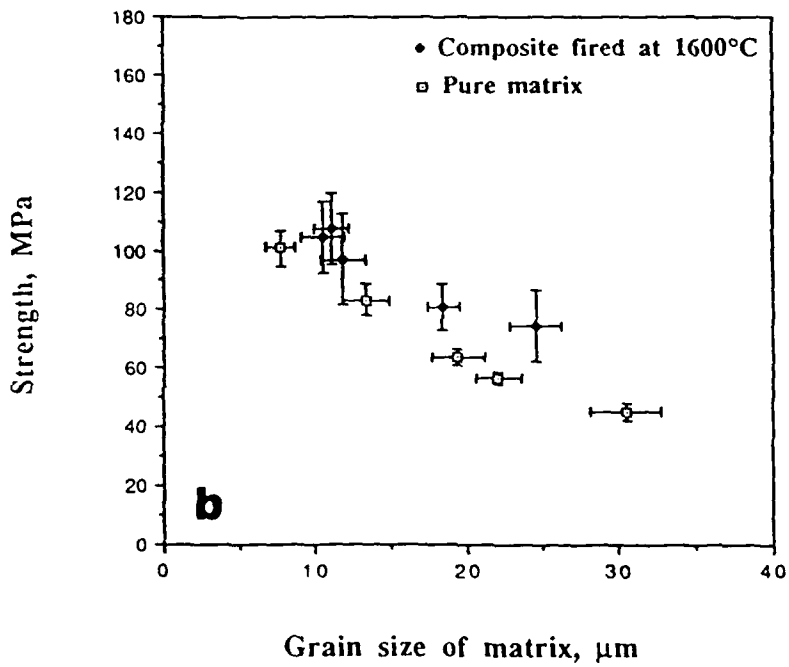
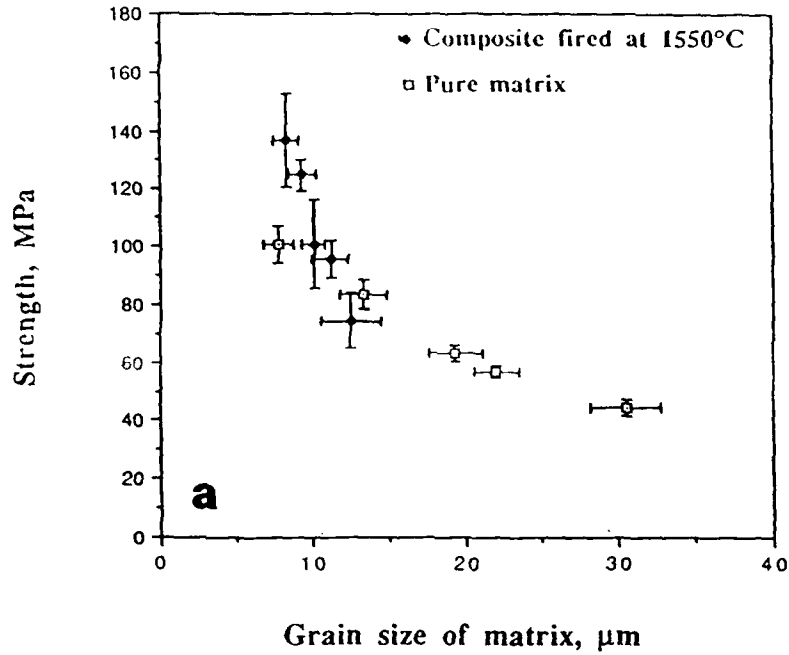


Fig. 5. Strength of composites fired at (a) 1550°C and (b) 1600°C is plotted against corresponding grain size of matrix. Strength of the pure matrix is also shown for comparison.

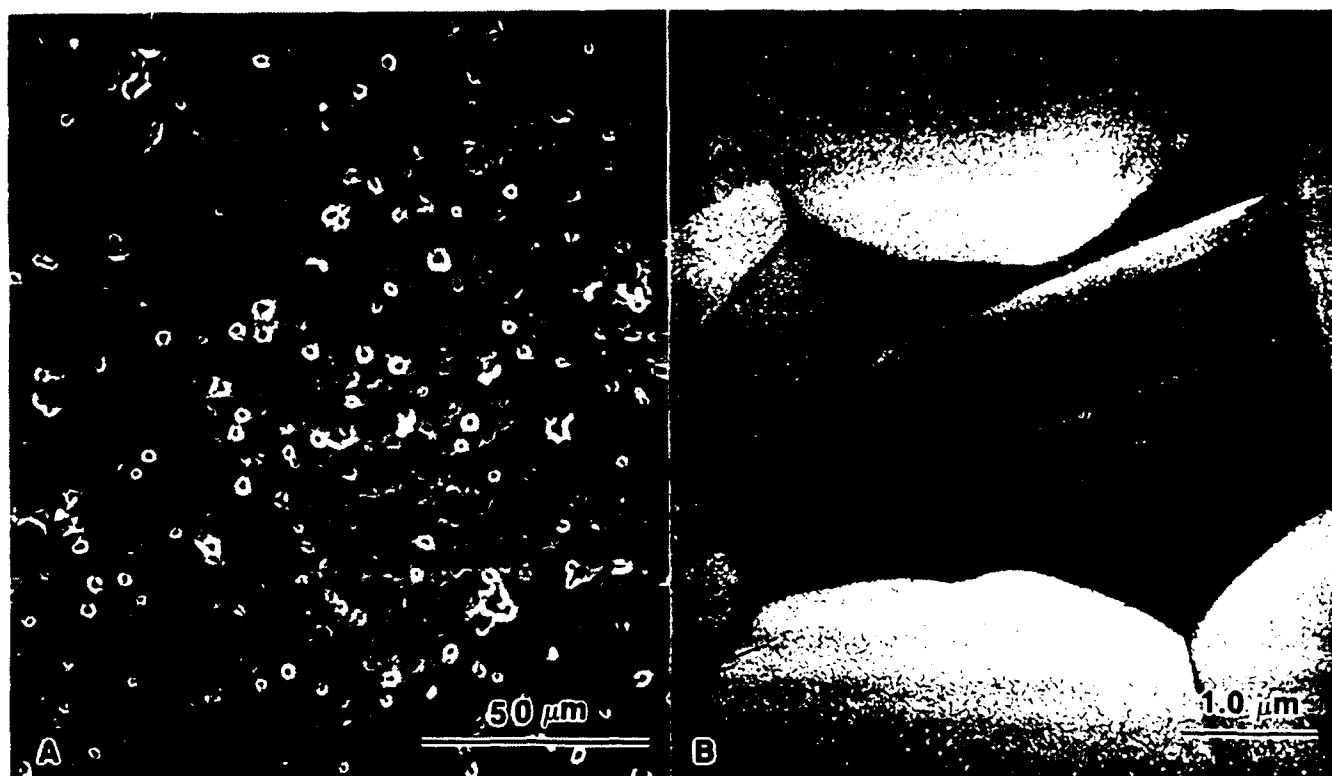


Fig. 6. SEM micrographs of the composite (initial C_2S particle size, $0.25 \mu m$) fired at $1550^\circ C$, showing (a) general microstructures in which the darker, irregular-shaped phase was C_2S and (b) a lath structure associated with cracks in large C_2S .

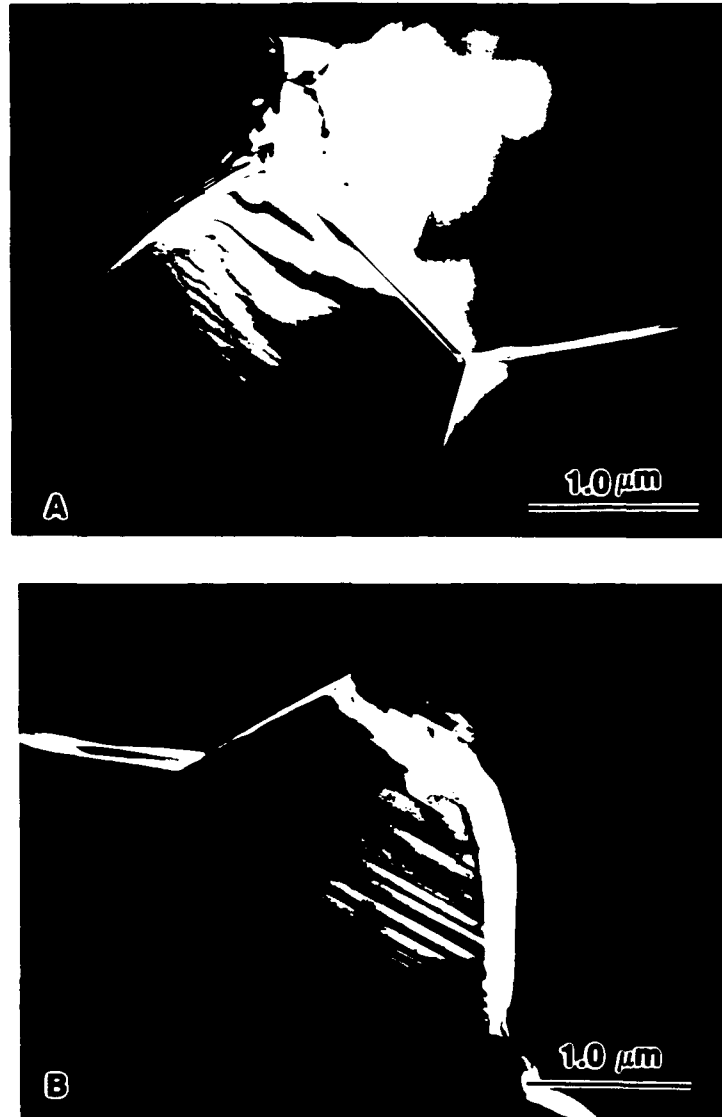


Fig. 7. TEM micrographs of the composite (initial C_2S particle size, $0.25 \mu m$) fired at $1550^\circ C$, showing (a) microcracks along grain boundaries of the matrix and (b) at the interface between twinned $\beta-C_2S$ and matrix.



Fig. 8. TEM micrograph of the composite (initial C_2S particle size, $0.25 \mu\text{m}$) fired at 1550°C , showing radial microcracking emanating from particles (possibly $\gamma\text{-}C_2S$) and extending along grain boundaries of the matrix. Grain boundary sliding (as arrow indicated) is also observed.

propagated into the grain. This microcracking phenomenon is the same as that having been observed in $\text{ZrO}_2\text{-Al}_2\text{O}_3$.

It was believed that the particle has been transformed to the γ phase due to loss of matrix constraint. The matrix was under large tension stress when the transformation took place. Therefore radial microcracking from the particles occurred. Grain boundary sliding associated with the microcracking was also observed as by the arrow shown. This strongly indicated that a stress was produced which was large enough to result not only in microcracking, but also grain sliding.

4. Summary

1. The fracture toughness of pure matrix depends on its grain size. The smaller the grain size the higher the toughness.
2. The strength of pure matrix increases quickly with smaller grain size due to higher toughness and smaller grain size (flaw size).
3. By hot-pressing full density and small grain size ($1.8 \mu\text{m}$) of pure matrix were obtained. The toughness ($2.0 \text{ MPa}\cdot\text{m}^{1/2}$) at this grain size was believed to be close to the intrinsic value.
4. The toughness increase is about $1 \text{ MPa}\cdot\text{m}^{1/2}$ ($2.6 \text{ MPa}\cdot\text{m}^{1/2}$ for composites v.s. $1.6 \text{ MPa}\cdot\text{m}^{1/2}$ for pure matrix, (compared at same grain size of matrix).
5. Radial microcracking emanates from transformed C_2S particles, extending along grain boundaries.

References

1. W. M. Kriven, "Possible Alternative Transformation Tougheners to Zirconia: Crystallographic Aspects," *J. Am. Ceram. Soc.*, **71** [12] 1021-30 (1988)
2. P. F. Becher, "Transient Thermal Stress Behavior in ZrO₂-Toughened Al₂O₃," *J. Am. Ceram. Soc.*, **64** [1] 37-39 (1981)
3. N. Claussen, "Fracture Toughness of Al₂O₃ with an unstabilized ZrO₂ Dispersed phase" *J. Am. Ceram. Soc.*, **59**, [1-2] 49-51 (1976)
4. N. Claussen and J. Jahn, "Mechanical Properties of Sintered In- Situ-Reacted Mullite-Zirconia Composite," *J. Am. Ceram. Soc.*, **63** [3-4] 228-229 (1980)
5. N. Claussen and J. Jahn, "Mechanical Properties of Sintered and Hot-Pressed Si₃N₄-ZrO₂ Composites," *J. Am. Ceram. Soc.*, **61** [1-2] 94-95 (1978)
6. J. Lorenz, L. J. Gauckler, and G. Pezow, "Improved Fracture Toughness of SiC-Based Ceramics," for abstract, see *Am. Ceram. Soc. Bull.*, **58** [3] 338 (1979)
7. D. J. Green and M. G. Metcalf, "Properties of Slip-Cast Transformation-Toughened b"-Al₂O₃/ ZrO₂ Composites," *J. Am. Ceram. Soc. Bull.*, **63** [6] 803-807 (1984)
8. W. M. Kriven, C. J. Chan and E. A. Barinek, "The Particle Size Effect of Dicalcium Silicate in a Calcium Zirconate Matrix," *Advances in Ceramics 24 part A*, 145-155 (1988)
9. D. M. Roy and S. O. Oyefesobi, "Preparation of Very Reactive Ca₂SiO₄ Powder," *J. Am. Ceram. Soc.*, **60** [3-4] 178-180 (1977)
10. R.W. Rice, S. W. Freiman, and P.F. Becher, "Grain-Size Dependence of Fracture Energy in Ceramics: I, Experiment," *J. Amer. Ceram. Soc.* **64** [6]346-350(1981)

Section 2.3 Processing and Microstructure of Dicalcium Silicate in Magnesia

(Mr. Eric Mast)

Introduction

The goal of this research is to obtain a composite of β - Ca_2SiO_4 in magnesia metastably stabilized by matrix constraint. It is recognized in zirconia systems, such as zirconia toughened alumina (ZTA), that toughness can increase when the transformation of metastably stabilized tetragonal zirconia transforms to monoclinic zirconia in the presence of the stress field of an approaching crack. The ultimate goal is the formation of a ZTA analog.

Background

This report is the culmination of three years of work on the $\text{MgO} - \text{Ca}_2\text{SiO}_4$ system. This system was chosen because of three things;

- i) MgO was the only simple oxide which showed no intermediate phase formation between itself and Ca_2SiO_4 on which phase equilibria information was available.
- ii) MgO is a relative soft cubic oxide which compliments the research done on the $\text{CaZrO}_3 - \text{Ca}_2\text{SiO}_4$ system.

The first phase of the research was to determine the feasibility of the system chosen. This means determining the chemical compatibility and stability of the two oxides with respect to one another. The formation of non-equilibrium phases would probably precluded any further research in this system. No additional phases were found upon firing, this was previously verified by X-ray diffraction (XRD) and energy dispersive spectroscopy (EDS) in the TEM.

The next step in the research was to determine the transformability of the Ca_2SiO_4 in a magnesia matrix. Stoichiometric dicalcium silicate (verified by XRD) was prepared by the mixed oxide approach starting with CaCO_3 and $\text{SiO}_2 \cdot x\text{H}_2\text{O}$. The resultant dusted Ca_2SiO_4 was attritor milled for short periods of time and added to a submicron magnesia powder in solution. Here, dusting refers to the self disintegration of a coherent body by the $\beta \rightarrow \gamma$ transformation of dicalcium silicate. The resultant pellets dusted after firing which gave proof to the ability of dicalcium to transform while contained in a magnesia matrix.

The third phase involved the densification of the magnesia matrix. This was performed without additions of dicalcium silicate. Using ceramic powder

processing techniques an ultimate density of $\geq 95\%$ was consistently obtained at firing temperatures of 1600°C . Density results were measured to determine acceptability limits. Four different additives which were able to modify the surface characteristics of the sub-micron magnesia particles were tried. These additives were an acid, weak nitric acid, a base, weak ammonium hydroxide, and two different polymers, a polyvinyl butyral and a polyacrylic resin. The acrylic resin was determined to be the best single additive. These results compare well to the best results reported in the literature for pressureless sintering.

The fourth step was the attainment of a composite of metastably stabilized dicalcium silicate. All composites were formulated to contain 15 volume percent dicalcium silicate in magnesia. It was in this step that a very narrow particle size distribution of the dicalcium silicate was necessary before adding it to the magnesia. At the upper limits of retainably coherent specimens the transformation was unpredictable. A certain percent of pellets would transform while others would remain intact. Three different methods of particle size control or classification have been tried. With the last report made three methods had been tried with limited success. These methods are listed here;

- i) attrition milling
- ii) sieving, and
- iii) air classification

Attrition milling gave the widest particle size distributions of Ca_2SiO_4 . Sieving gave very clean distributions but were all too large to be successfully stabilized by the matrix. The air classification method could give very narrow distributions, but contamination by the classification system, poor yields, and other problems with the equipment made it desirable to look for yet another method of particle size classification.

Current Work

Sedimentation was the final method of classification used for both the dicalcium silicate and the magnesia matrix powders. A standard curve was prepared for the dicalcium silicate first. This calibration curve is shown below in Fig. 2. The method followed flow chart in Fig. 1;

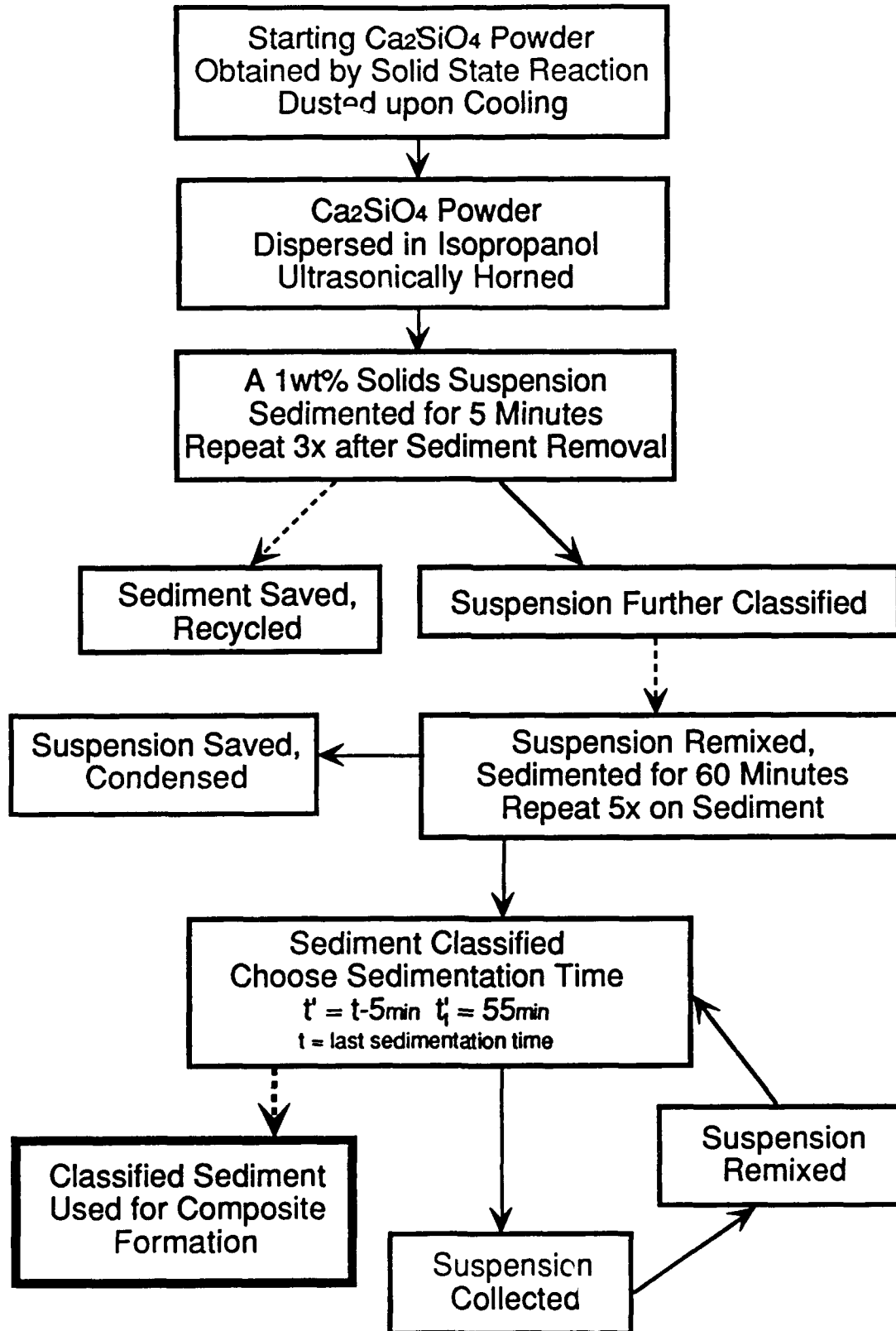
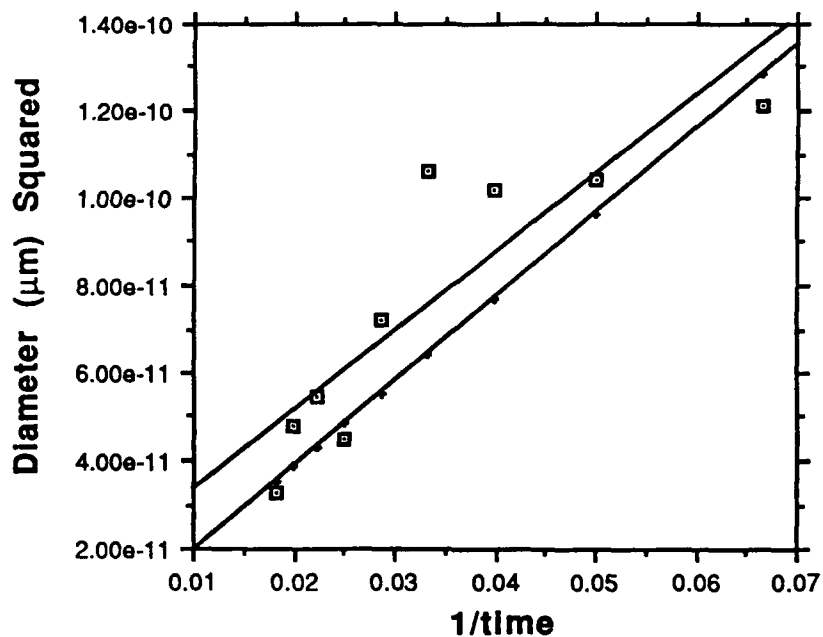


Figure 1. Sedimentation classification flow chart for the classification of dicalcium silicate.



Degree of fit for the experimental (squares) and theoretical (dots) respectively.

$$y = 1.55 \times 10^{-11} + (1.80 \times 10^{-9})x \quad R^2 = 0.77$$

$$y = 3.16 \times 10^{-15} + (1.93 \times 10^{-9})x \quad R^2 = 1.00$$

Figure 2. Comparison between experimental calibration curve and Stoke's Law for sedimentation of dicalcium silicate in isopropyl alcohol.

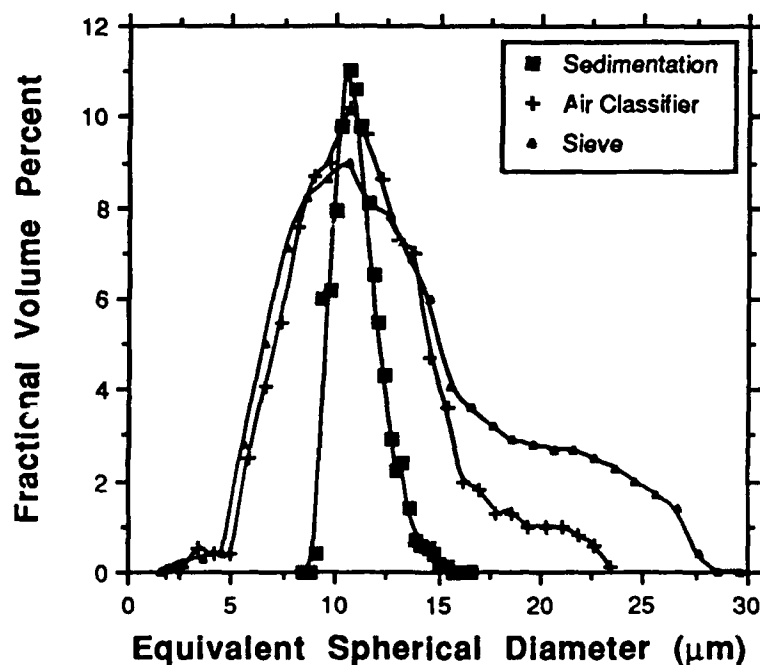


Figure 3. Comparison of particle size distributions of dicalcium silicate achieved by sieving, air classification and sedimentation. Sedimentation and sieve distributions were shifted by $+4.4\mu\text{m}$ and $-2.4\mu\text{m}$ respectively.

A comparison of the relative widths of the last three particle size classification methods is given in Fig. 3.

The powders were analyzed for particle size on the Horiba particle size analyzer. Visible light ($\approx 560\text{nm}$) is passed through a cell containing a suspension of the powder to be analyzed. Isopropanol was the suspending liquid, with no additional suspending aids. This should give the most accurate results since this is the same fluid used throughout the rest of the powder and composite processing. Stoke's Law, given below;

$$D^2 = 18\eta L / (\rho - \rho_0)gt$$

was assumed and constants of $\rho_0 = 0.783 \text{ g/cc}$ and $\eta = 1.76 \text{ centipoise}$ for the isopropanol at 20°C and $\rho = 3.15\text{g/cc}$ for the dicalcium silicate were used. In this equation L is the suspension height (7cm), η the viscosity, g the gravitation constant and t the time for settling of a given particle size. Comparison between data obtained by experimentation and that calculated by Stoke's Law is shown in Fig. 2 above. The final particle size distributions obtained by this method are shown in Fig. 4.

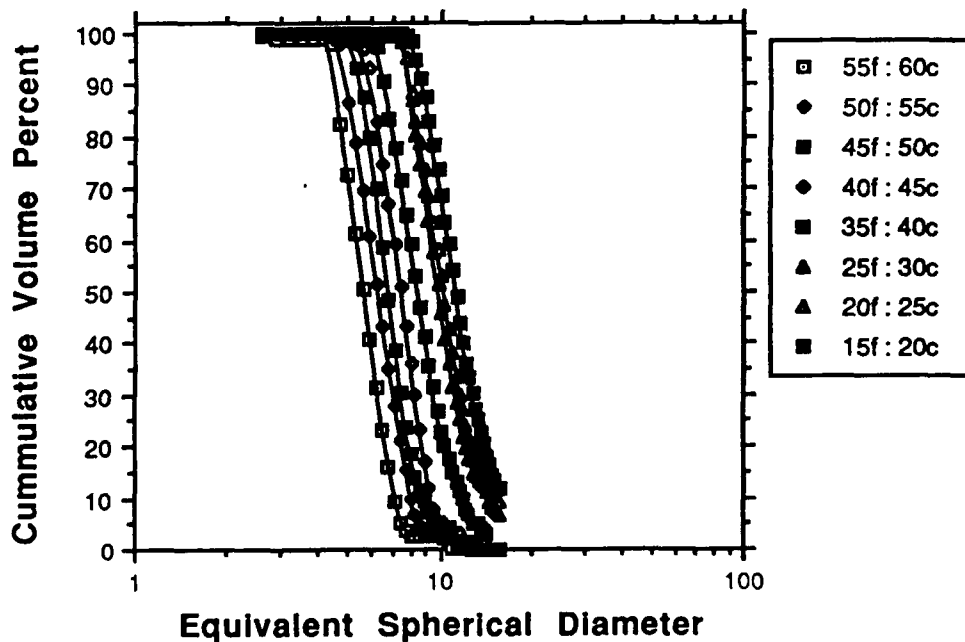


Figure 4. Particle size distributions of dicalcium silicate achieved by sedimentation

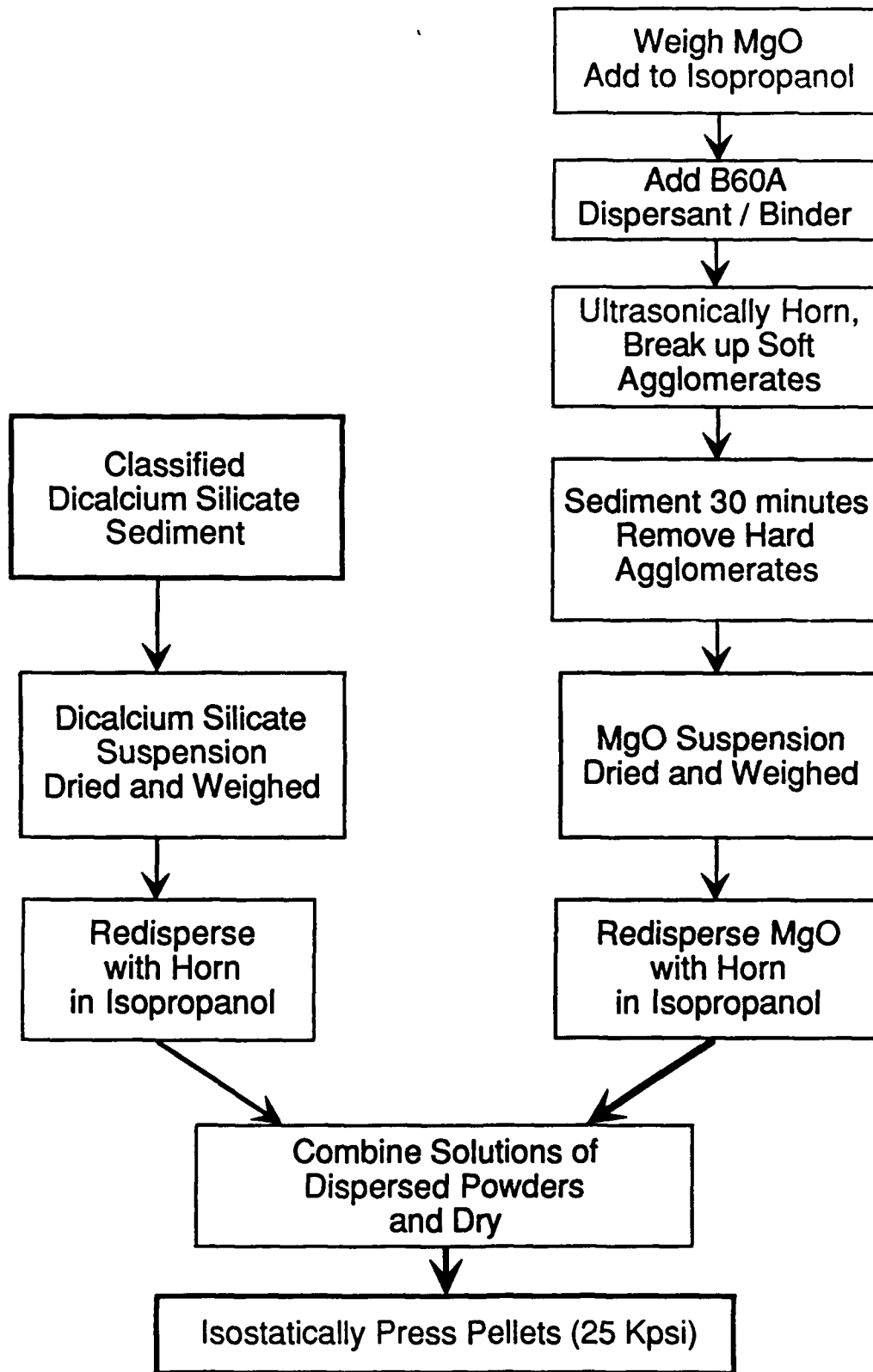


Figure 5. Composite fabrication flow chart using 15 volume % classified dicalcium silicate.

The fabrication of the composites followed the flow chart in Fig. 5. The classified dicalcium-silicate was dried and the amount required to form a 15 volume percent composite was weighed out following the calculations in Table 1.

15 vol% Sedimented Dicalcium-silicate Composites				
Ca ₂ SiO ₄ cut time	Yield (g) C ₂ S	mol C ₂ S	vol% C ₂ S	(g) MgO
55f 60c	1.585	9.20e-03	0.15	9.8032
50f 55c	1.631	9.47e-03	0.15	10.0877
45f 50c	1.374	7.98e-03	0.15	8.4981
40f 45c	1.202	6.98e-03	0.15	7.4343
35f 40c	1.094	6.35e-03	0.15	6.7663
30f 35c	1.067	6.19e-03	0.15	6.5994
25f 30c	0.675	3.92e-03	0.15	4.1748
20f 25c	1.293	7.51E-03	0.15	7.9972
15f 20c	1.76	1.02E-02	0.15	10.8855

Table 1. Table calculating grams of MgO required for forming 15 vol % pellets from sedimented dicalcium silicate powders.

The powders were dried so that they could be weighed out to determine the amount needed to form the 15 volume percent composites. The dried and weighed powders were redispersed in isopropanol and the two suspensions of matrix and second phase were mixed. This mixture was then dried on a hot plate whilst stirring and 1/2" diameter pellets were pressed in a uniaxial hydraulic press. These pellets were re-pressed at 25,000 psi in an isostatic press.

The pellets were fired at temperatures ranging from 1500°C to 1650°C in air to study microstructure development. The electric furnace for air firing was specially designed and manufactured. The final firing schedule which developed through the various stages of this project is shown in Fig. 6. The two major steps of critical importance in the control of the transformation known to date were the 5°C/minute cooling rate through the $\alpha \rightarrow \alpha'_L$ transformation at 1425°C and the thermal stress relief anneal. Two different thermal stress relief annealing temperatures were tried, one at 700°C and one at 650°C, above and below the $\alpha'_L \rightarrow \beta$ transformation temperature respectively. Both anneals lasted 4 1/2 hours. Platinum was used to surround the pellets to minimize any interactions with the furnace atmosphere.

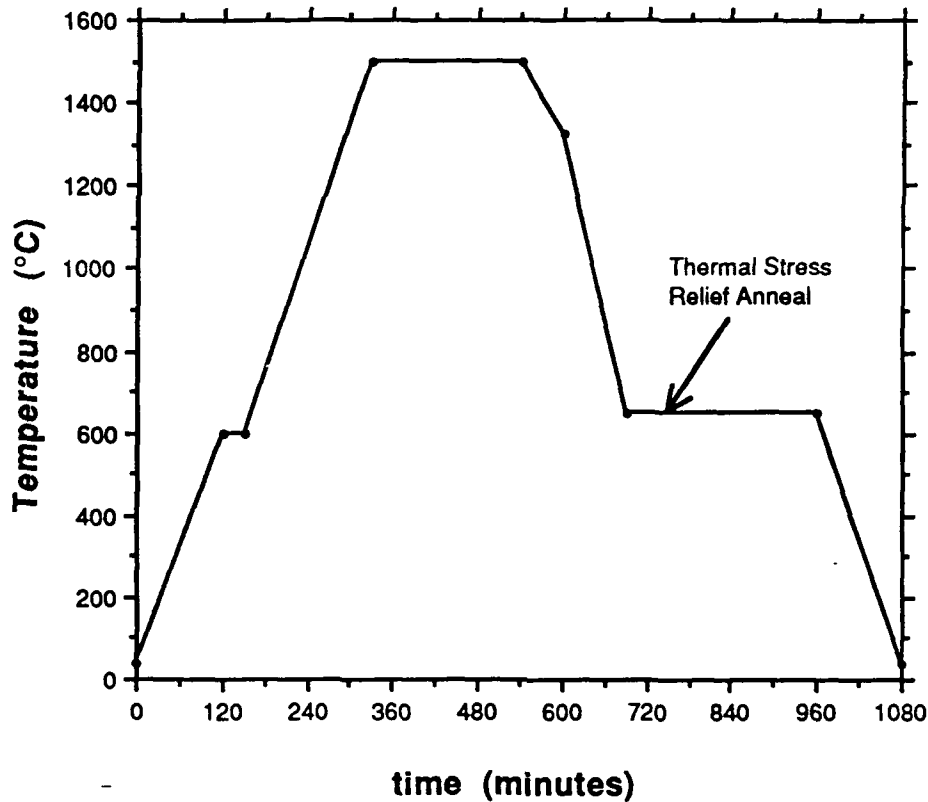


Figure 6. Firing schedule for mixed oxide composites, firing temperatures of 1500°C, 1550°C or 1600°C.

To obtain a composite with the best physical properties it is desirable to minimize the grain size. Grain growth is a function of temperature and therefore the firing temperature should be minimized without sacrificing density. This was the final stage of research before mechanical properties testing of the composite. The decrease in firing temperature to 1500°C from 1600°C was originally accompanied by a decrease in density to less than 90% theoretical. This necessitated an improvement in the processing of the magnesia powder which formed the matrix. The dicalcium silicate powder could not be altered further to increase composite density.

It was known from SEM that the magnesia had some hard agglomerations present which were densifying differentially to the matrix. The processing of the matrix needed to include a step for the elimination of these agglomerations. The solution was as follows;

- i) ultrasonically horn the matrix suspension to break up all soft agglomerates present in powder

- ii) the same method used for the preparation of particle size distributions of dicalcium silicate by sedimentation was used to settle out the hard agglomerates
- iii) hard agglomerates were removed by siphoning off the suspension after large agglomerates settled out from solution
- iv) powder dried, weighed, for volume percent calculation of composite, and resuspended in isopropanol before addition of dicalcium silicate solution.

Two micrographs are included which show the current state of the microstructure. The top TEM micrograph of the dicalcium silicate-magnesia interface shows that there is no interaction between the two phases. The lower SEM micrograph shows the dense fine grain (average $4\mu\text{m}$ particle size) matrix and the well dispersed dicalcium silicate (average $10\mu\text{m}$ particle size) in the matrix.

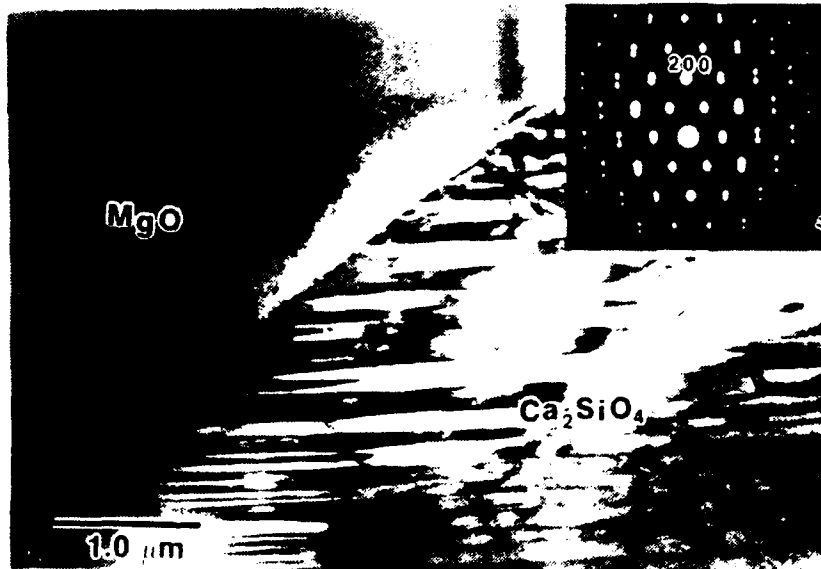


Figure 7. TEM micrograph of dicalcium silicate and magnesia interface. No intermediate phases were present at the interface. Diffraction pattern was of monoclinic b-dicalcium silicate twin structure.

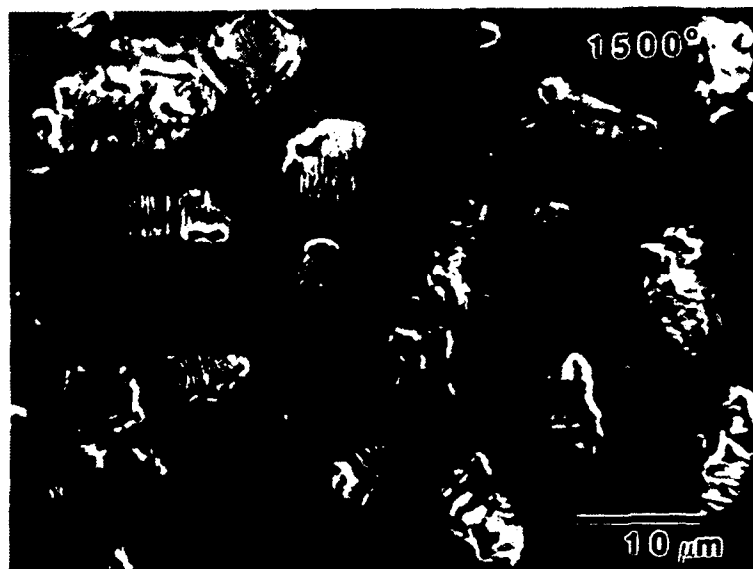


Figure 8 SEM micrograph of composite (sedimented 55f-60c Ca_2SiO_4), fired at 1500°C and thermally etched and annealed at 650°C . Grain growth was decreased with no loss in density and porosity was maintained as intragranular in the magnesia. Note transformation and partial fall out of dicalcium silicate at the surface, especially at points of high curvature.

Conclusions

The conclusions which can currently be derived from this work are;

For the mixed oxide processing method:

- i) A pure magnesia matrix (without the addition of a second phase) was processed and fired to a density of 95% and greater at 1500°C. This is as good as the literature values and applicable references were cited previously.
- ii) Narrow particle size distributions in the range of $10\mu\text{m} \pm 2\mu\text{m}$ of dicalcium silicate were prepared by sedimentation. The three other methods tried proved inadequate for producing the narrow particle size distributions required for this work.
- iii) Composites of high density ($\geq 95\%$) with a well dispersed second phase of dicalcium silicate were formed at firing temperatures as low as 1500°C.
- iv) β -dicalcium silicate was metastably retained at room temperature in a magnesia matrix.
- v) Particle size control and colloidal chemistry techniques were used to control the powder processing, and correct firing and cooling schedules were experimentally determined for the composites. The grain size of the magnesia in the composite was kept to an average of $\leq 4\mu\text{m}$ while the β -dicalcium silicate maintained its grain size at $10\mu\text{m}$. This particle size is the same as that of the powder. Therefore no grain growth or coalescence occurred, showing that control of the initial particle size distribution control led grain size at the above firing temperature of 1500°C.
- vi) Finally, there was no reaction phase formation between dicalcium silicate and the magnesia matrix.

For the in situ liquid phase formation method:

- i) It was shown that dicalcium silicate could be formed in magnesia in situ from merwinite ($3\text{CaO}\cdot\text{MgO}\cdot 2\text{SiO}_2$) and calcia. The merwinite liquid phase aided in the formation of solid dicalcium silicate.
- ii) Densities $\geq 95\%$ were obtained at firing temperatures $\geq 1750^\circ\text{C}$.
- iii) The final β -dicalcium silicate particle size in the composite was controlled by merwinite's initial particle size. The dicalcium silicate particles tended to be located at the triple points of the magnesia grains.
- iv) β -dicalcium silicate was metastably retained at room temperature in the magnesia matrix.
- v) At such high firing temperatures exaggerated magnesia grain growth occurred. This would limit the possible effect of toughening since the matrix grains were several times larger than the toughening phase.
- vi) It was difficult obtaining complete reaction between the merwinite and the calcia.

Future Work

Firstly the toughness needs to be determined. First attempts by Vicker's indentation have all failed to induce measurable results. The toughness results will be useful to compare to the results obtained by Barinek for Ca_2SiO_4 in calcium zirconate (CaZrO_3). Calcium zirconate is a hard matrix compared to magnesia. Bend bars will be used to measure toughness and R-curve behavior. A transformation zone needs be looked for around the cracks initiated by the indenter using SEM.

TEM could be used to look at the Ca_2SiO_4 grain interfaces to study the effect and method of constraint on both phases. In situ straining experiments in the TEM will be made in order to observe a transformation zone.

Acoustic emission can be used to help understand the transformation in situ. The properties of the transformation can be analyzed while the particles of Ca_2SiO_4 are completely constrained by the matrix and a crack is induced.

Many parameters such as higher temperature transformations (those above the $\beta \rightarrow \gamma$ transformation), twin size, residual thermal stresses and the effect of thermal cycling through the changing lattice correspondences affect control of the $\beta \rightarrow \gamma$ transformation in Ca_2SiO_4 .

Section 2.4 Processing and Microstructures of Nickel Sulphide Composites. (Ms. Jemima J. Cooper)

1. Introduction

Interest in nickel sulphide, NiS, as a possible transformation toughening phase (1, 2) arose because of observations of spontaneous fracture of plate glass which contained small nickel sulphide stones (3). Ballantyne identified nickel sulphide stones at the origin of each fracture, and by X-ray diffraction found that these stones were α -NiS and β -NiS. Bradt (4) found them to be composed of nickel and sulphur using SEM X-ray EDS, and noted that it was probable that the stones were polycrystalline and not single phase. A study of sulphide inclusions in plate glass by EPMA (5) identified sulphide stones of various compositions, including Ni_3S_2 and Ni_{1-x}S . Hsiao (6) examined a small stone from a fracture surface and identified both α -NiS and β -NiS by X-ray diffraction.

Two alternative explanations for the fracture-initiating behaviour of the nickel sulphide stones have been proposed. Many workers believe that the phase transformation of α to β -NiS, which is accompanied by a volume increase, is responsible for the fracture of the thermally tempered plate glass (3, 4, 6, 7). A study of the glass with additions of nickel sulphide impurities (8) concluded that the fracture-initiating stones were not necessarily the NiS compound, and that the cause of fracture was the thermal expansion mismatch between the nickel sulphide phases and the glass matrix. For example, it is known (9) that pentlandite, $(\text{Fe,Ni})_9\text{S}_8$, a naturally occurring mineral, has an unusually large coefficient of thermal expansion.

2. Background to Our Work

In order to determine the potential of NiS as a transformation toughening phase it is necessary to characterize the α to β transformation more precisely, with respect to variables such as stoichiometry and temperature. If the transformation is strain induced, then a particle size effect may also be significant (10). Thus the nature of the transformation requires some study, particularly its kinetics and its crystallography, and how it is affected by stress. Experience with zirconia and other transformation toughening phases (11) has shown that the behaviour of the material in bulk is different to the behaviour of the dispersed phase. A transformation

toughening phase is best studied in the context of a matrix which it might reasonably be expected to toughen.

Our work has therefore developed in three directions. Study of the transformation commenced with an analysis of the nickel sulphide stones associated with the fracture of plate glass, since these stones were suspected of having undergone the transformation. The second focus of study was the characterization of the NiS phases and the transformation itself. The third was the development of a suitable matrix and the fabrication of a NiS-containing composite.

3. The Nickel Sulphide Phase Transformation

Current understanding of the nickel sulphur system and the α to β -NiS phase transformation is based on the phase diagram developed by Kullerud and Yund in 1962 (12). (Diagram 1.) Their work has established that the compound NiS has two stable phases at atmospheric pressure. The room temperature phase, β -NiS, occurs naturally as a mineral, millerite, in association with other sulphides. On heating, stoichiometric β -NiS inverts to the α NiS form at $379^\circ \text{C} \pm 3^\circ \text{C}$. The reverse inversion takes place at a lower temperature on cooling. The α -NiS crystal form can accommodate several weight % of nickel deficiency, and the composition is best expressed as Ni_{1-x}S , where $x \leq 0.034$. The α - β inversion temperature is composition dependent. The inversion temperature for the most nickel deficient compound, $\text{Ni}_{0.966}\text{S}$, is $282^\circ \pm 3^\circ \text{C}$. A positive volume change of between 2.15 and 3.69% accompanies the transformation from α to β phase.

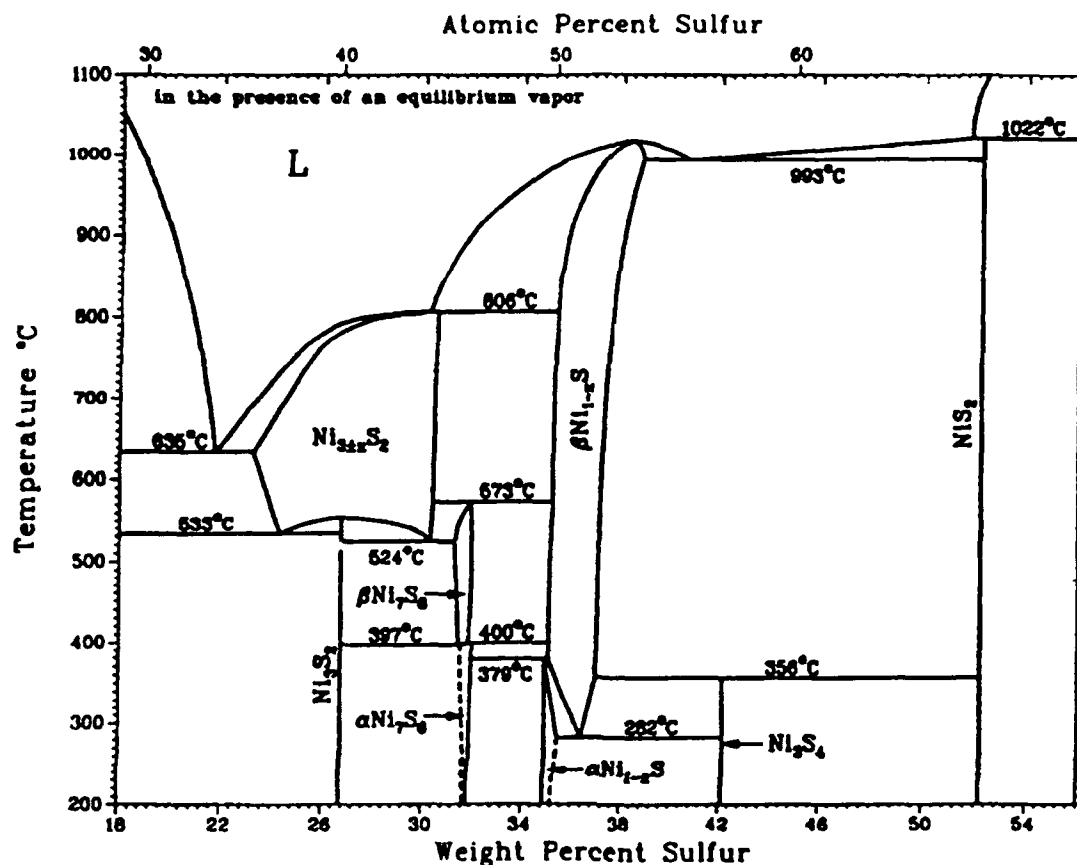


Diagram 1. Nickel-Sulphur Phase Diagram (after Kullerud and Yund, 1962)

Table 1. Crystal Structure Data for Alpha and Beta Phase NiS.

	α -NiS	β -NiS
Mineral name	'Niccolite'	Millerite
Crystal Symmetry	Hexagonal	Rhombohedral
Space Group	6/m 2/m 2/m	R3m
Unit Cell Contents (Z)	2 (4 atoms)	3 (6 atoms)
a axis dimension (Å)	3.4392	5.655
c axis dimension (Å)	5.3484	
α angle		116° 36'
Unit Cell Volume Å ³	54.89	84.1
JCPDS Card No.	2-1280	12-41

β -NiS is rhombohedral, space group R3m (13). α -NiS is hexagonal, space group 6/m 2/m 2/m, and is isomorphous with niccolite, NiAs (14). Crystal structure data for both phases are summarized in Table 1 (13).

Several authors have noted that synthetic Millerite, when kept at room temperature, may invert to α -NiS after a period of time (13). This strange behaviour may be due to the existence of a third phase, γ -NiS, which is stable below about -8°C , and has a crystal form very similar to that of α -NiS (15, 16, 17).

From Trahan et al:

	<u>T ($^{\circ}\text{K}$)</u>	<u>Lattice Parameters (\AA)</u>	
		a	c
α -NiS	300	3.4395	5.3514
γ -NiS	77	3.4456	5.405

(Transformation occurs at about 267°K)

The kinetics of the α to β transformation are of interest from the point of view of transformation toughening. Kullerud and Yund found, by TGA, that the NiS transformation becomes progressively more sluggish as the composition is made more off-stoichiometric. The α phase is more easily retained in its metastable state, at lower temperatures, as the structure becomes more nickel-deficient. However, even the α phase of the stoichiometric composition may be easily retained to room temperature by rapid quenching from temperatures above 379°C . (This allows the α to γ transition to take place at about -8°C .) In fact, commercially obtainable NiS powder (Alpha Chemicals) is in the α phase. The transformation is evidently dependent on cooling rate.

The α phase may also be stabilized by the substitution of sulphur by arsenic or selenium (18). The α phase shows complete iron-nickel solid solubility above 300°C (19), whereas the naturally occurring β phase may contain only small amounts of iron, and also cobalt (20). The effects of these substitutional atoms on the α to β phase transformation are not known. Other factors which may be important in determining the rate of the transformation are pressure and the partial pressure of sulphur. In addition, the transformation may be stress-assisted, if the rate is nucleation controlled.

Section 4 Investigation of Stones from Fractured Glass

Theoretical calculations indicate that stones with a diameter greater than 57 microns can cause spontaneous fracture of glass (7). The tiny spherical stones, 80 to 250 microns in diameter, posed a challenge for electron microscopy sample preparation. A novel technique using ultramicrotomy was developed. There have been a number of semiquantitative (mostly EPMA and X-ray) studies of these stones, however a detailed account of their internal microstructure and microchemistry has yet to be presented.

4.1. Experimental

Two types of sample were available for study (provided by M. Swain, Australia). The first were stones recovered from fractured plate glass. These stones were therefore known to be fracture origins. The second were stones in bulk unfractured glass.

In the fracture surface of the broken plate-glass, the fracture-causing stones were observed to adhere well to the glass. These stones, just visible to the naked eye, were examined by optical microscopy, under polarized light, and then by SEM, after first being coated with carbon. The stones were then removed from the glass by carefully crushing the glass and recovering the stone with tweezers.

A $\sim 40 \text{ cm}^3$ bulk glass sample was found to contain 5 or 6 small stones. The stones were golden brown in color and had metallic lustre. By optical microscopy it was determined that they were almost perfectly spherical, and had a rough surface. A stone was removed from the bulk glass by first using a diamond saw and then gently breaking off the thin glass and recovering the stone, which was also broken in the process.

To prepare samples for TEM, the stones were embedded in an epoxy. A suitable epoxy must be chemically compatible with the stones and must wet their surfaces to give good adherence of the embedding matrix. Eponate 12 (Ted Pella Inc.) epoxy resin was used. The embedding mixture formulation included 5.0 ml Eponate 12, 1.0 ml dodecanyl succinic anhydride, 4.0 ml nadic methyl anhydride and 0.2 ml tri-[dimethyl amino ethyl] phenol. Embedding the samples was accomplished by first polymerizing shallow blanks of the mixture in a silicon mold, then placing the stone on the blank, filling the mold with the mixture and repolymerizing for 48 hours. The blank was cut into shape for ultramicrotome using a razor blade. Using a diamond knife, tiny

wafers $\sim 900\text{\AA}$ thick were cut from the embedded stone. These were recovered onto copper TEM grids, air-dried and coated with a thin film of vacuum-evaporated carbon in readiness for TEM. Transmission electron microscopy was performed using a Philips EM 420 instrument at 120 keV, in conjunction with a SiLi X-ray analysis unit.

4.2. Results

Optical microscopy of the stone in bulk unfractured glass under polarized light showed the presence of a strain field around the stone (Figure 1). Figure 2, a SEM micrograph, shows the stone adhering to the glass fracture surface. TEM images of the stones (Figure 3.) indicate that they sustained mechanical damage during ultramicrotomy. Much of the microstructure consisted of small 'leaves', all of approximately the same size, shape and orientation, lying in parallel rows.

4.2.1. Nickel Sulphide Stone from Bulk Glass Sample

Twenty EDS analyses of different areas of the sample gave a range of compositions, from $\text{Ni}_{55}\text{S}_{44}$ to $\text{Ni}_{81}\text{S}_{18}$ (atomic %), with the distribution being bimodal about $\text{Ni}_{60}\text{S}_{40}$ (Graph 1) and $\text{Ni}_{75}\text{S}_{25}$ (Graph 2). No $\text{Ni}_{50}\text{S}_{50}$ was found. A small (~ 0.5 at%) amount of iron was detected in each analysis. The sample was possibly beam sensitive, with a slight (1.5%) loss of sulphur occurring after prolonged exposure to the beam. The sample also responded to the beam by undergoing twinning (Figure 4.), thought to be an indication of transformation.

4.2.2. Nickel Sulphide Stone from Fracture Surface

Repeated EDS analyses gave a range of compositions from $\text{Ni}_{50}\text{S}_{50}$ to $\text{Ni}_{63}\text{S}_{37}$, with the majority of the regions analyzed having a composition close to $\text{Ni}_{60}\text{S}_{40}$. Very little $\text{Ni}_{50}\text{S}_{50}$ was found (Graph 3.). The microstructure of the region analyzed as NiS, shown in Figure 5, consists of twinned lamellae. No iron was detected in most of the analyses, although one analysis of an amorphous region showed a considerable amount of iron. An attempt to induce sulphur loss by prolonged beam irradiation showed no difference in sulphur content before and after irradiation.

The very small amounts of $\text{Ni}_{50}\text{S}_{50}$ found in the fracture-causing stone would seem to indicate that the α - β phase transformation of NiS is not a likely cause of fracture in this glass. This is supported by the analyses of other nickel sulphide-



Figure 1. Optical Micrograph of Nickel Sulphide Stone in Bulk Glass.
Polarized Light. X250.

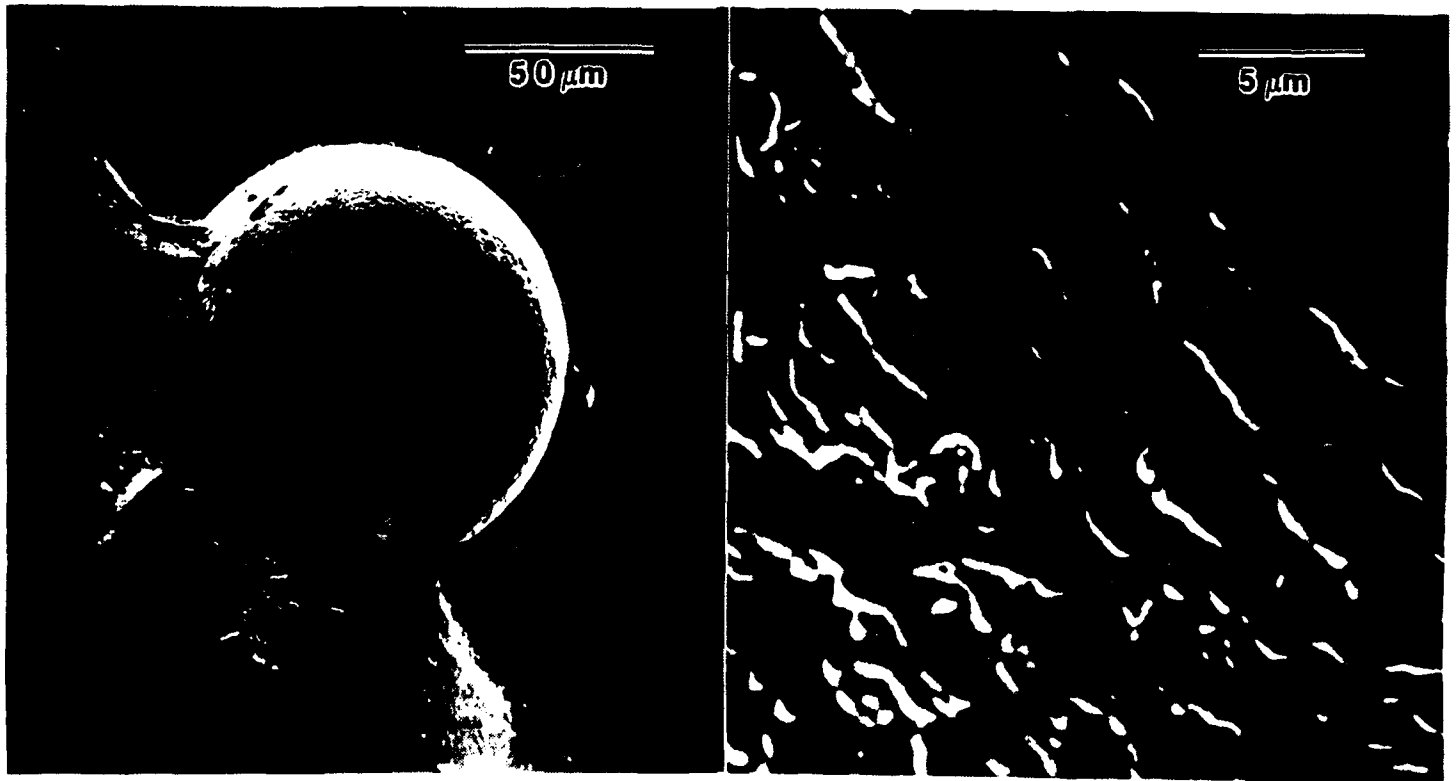


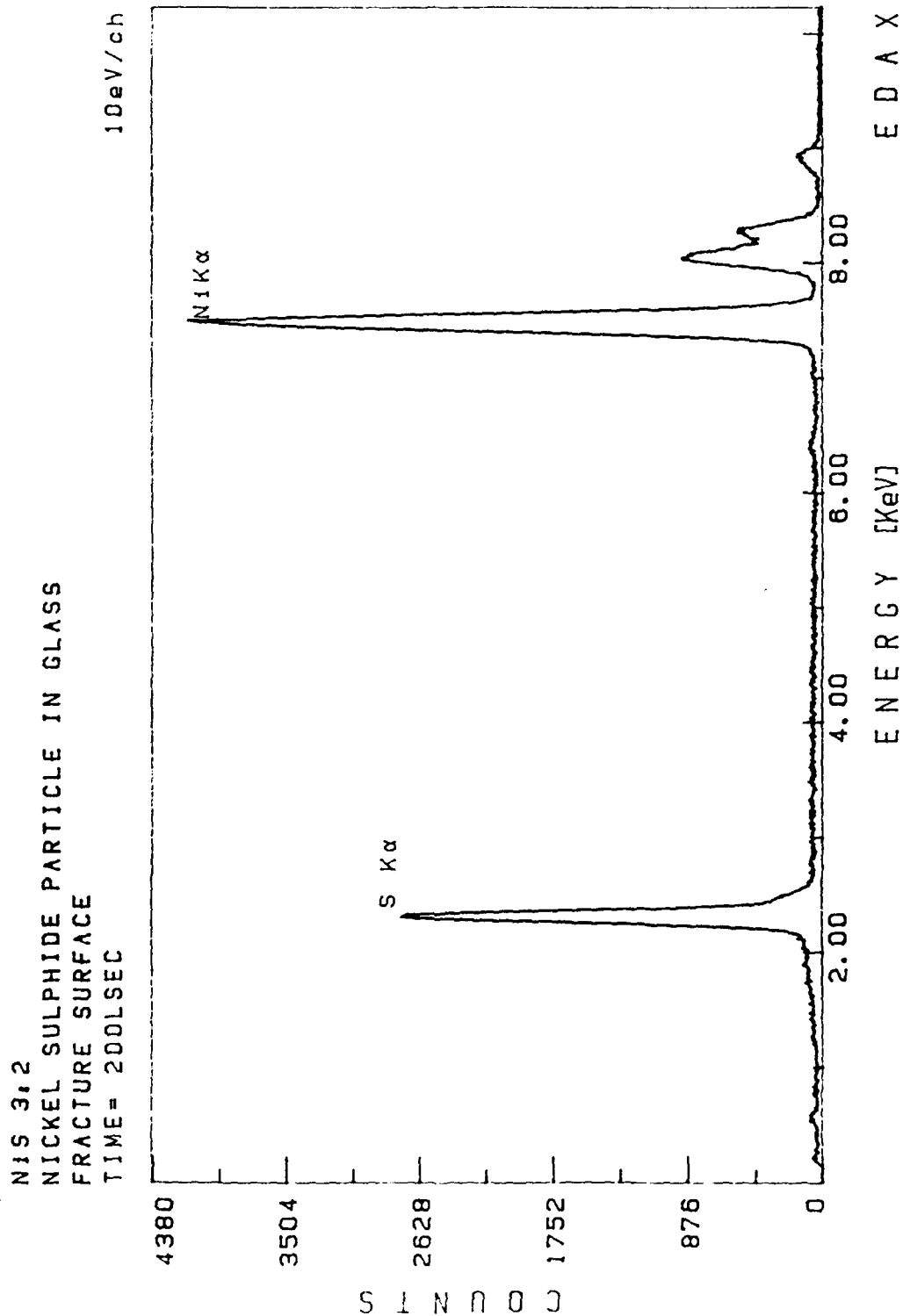
Figure 2. Nickel Sulphide Stone in the Fracture Surface of Broken Glass.
a). Stone adhering to glass. b). Rough surface of stone.



Figure 3. TEM micrograph showing ultramicrotomy damaged structure of cut stone.

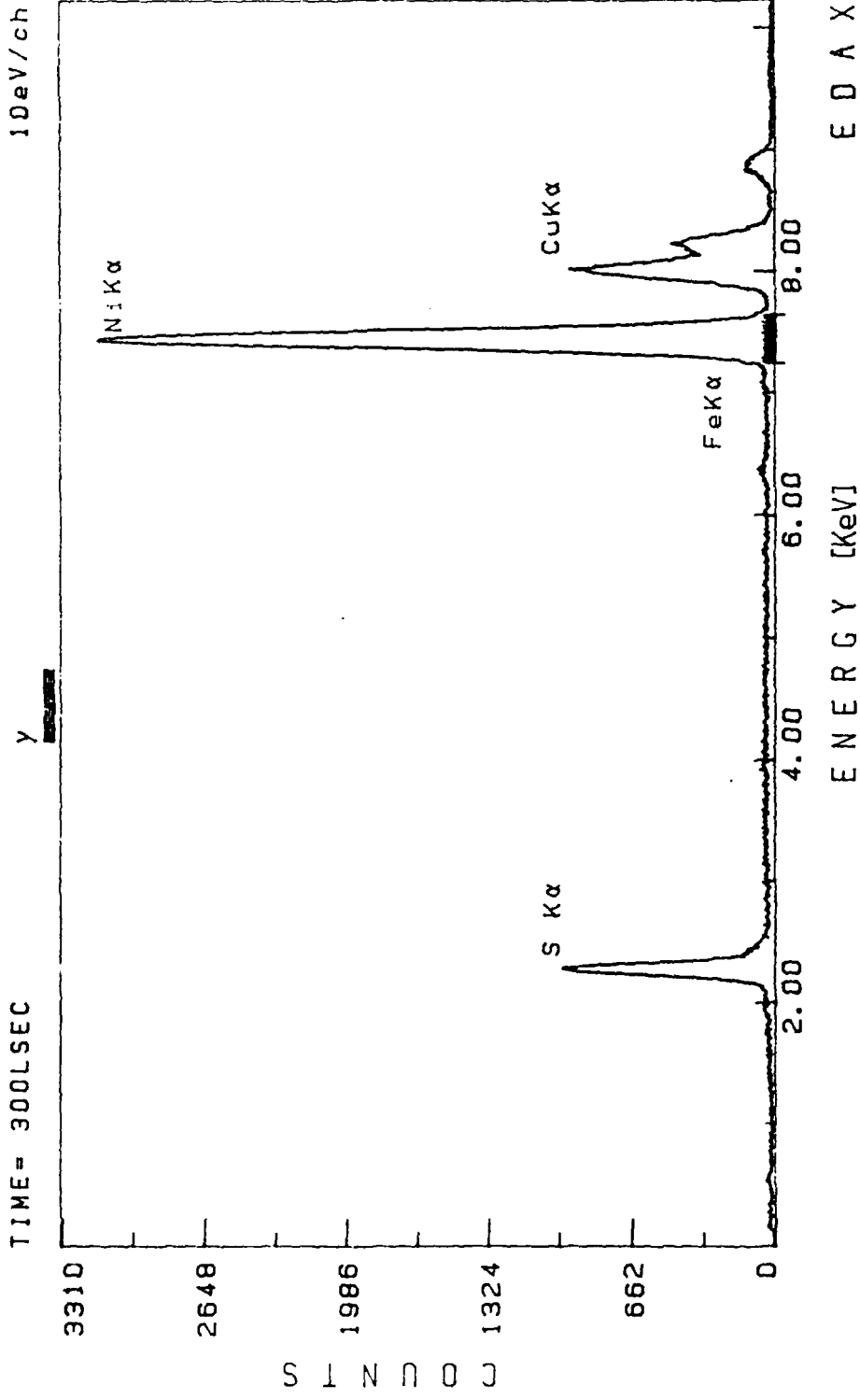


Figure 4. Twinned Nickel Sulphide



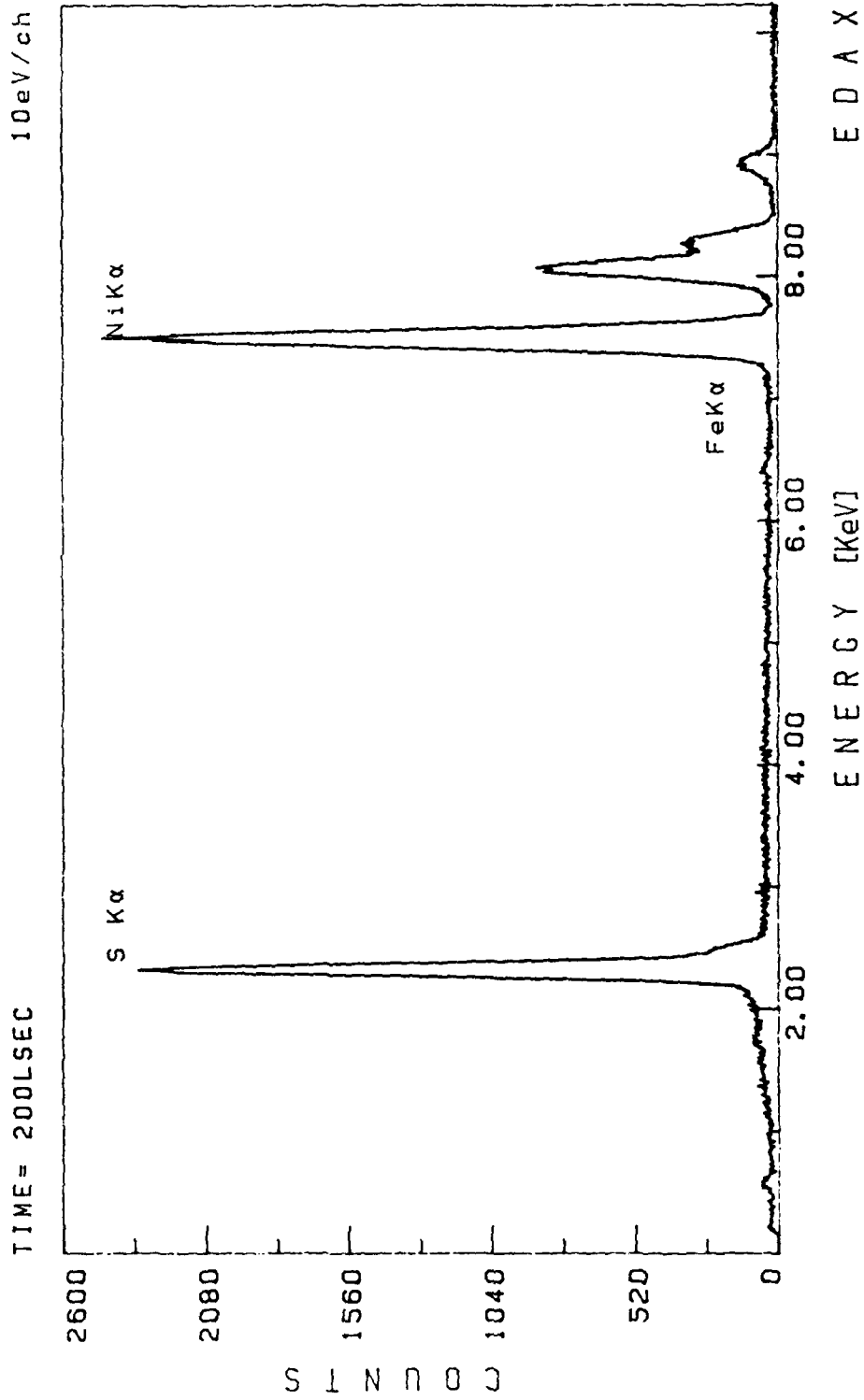
Graph 1. Energy Dispersive X-Ray Spectrum. Composition Ni₃S₂.

NiS 3:1
NICKEL SULPHIDE PARTICLE IN GLASS
UNFRACTURED SURFACE
TIME = 300LSEC



Graph 2. Energy Dispersive X-Ray Spectrum. Composition Ni₃S.

NIS 1.1
NICKEL SULPHIDE PARTICLE IN GLASS



Graph 3. Energy Dispersive X-Ray Spectrum. Composition NiS.



Figure 5. Fine Lamellae in NiS

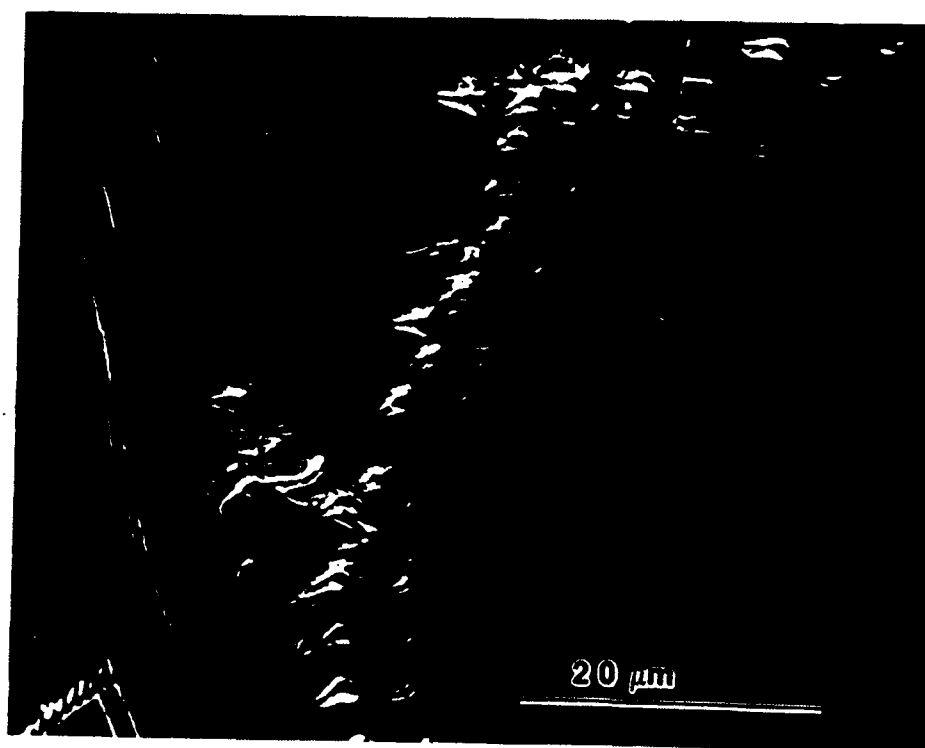


Figure 6. SEM micrograph of Polished Surface of α -NiS.

containing stones which are not found to contain NiS at all (5). The small regions of NiS in the stone may undergo the α to β transformation, however we might expect that the 4% volume increase would be accommodated by the relatively ductile sulphide phases that comprise the matrix of the polycrystalline stone. Our findings support the conclusion that the mechanism of fracture of glasses containing nickel sulphide stones is the thermal expansion mismatch between nickel sulphide and glass. This was the mechanism favoured by workers at St. Gobain, who studied the relative expansions of the two materials by dilatometry and found nickel sulphide phases to have larger thermal expansion coefficients than glass. This would lead to the glass being in a state of tension around the stone, after cooling from the temperature of fabrication to room temperature. However, we do not observe circumferential cracks around the stones; the glass adheres well to the stone. The only cracks observed were small radial cracks, in one instance. Optical microscope observations of the bulk glass sample under polarized light showed that the glass surrounding the stone was under stress.

Our results are in agreement with the findings of the St. Gobain report (8), which found that stones from the fracture surfaces of glass were nickel-rich in comparison to the stoichiometric NiS compound.

5. Pure NiS

5.1. Experimental

Samples of both α -NiS and β -NiS were prepared by solid state reaction of the elements under vacuum at 600°C. Nickel powder (Aldrich Chemicals, 99.7%) was mixed with 35.33 % by weight sulphur powder and placed in a quartz glass ampoule and sealed under primary vacuum. The sample was fired horizontally in a tube furnace at 600° C for 85 hours. The heating rate was 140° C/hr. Two different cooling treatments were used. A water quench from 600°C was employed to retain the α phase in the first case. For the second sample, a furnace cool over 5 hours (~65°C/hr cooling rate to 270° C) was used to allow the α to β transformation to take place. The samples were analyzed by X-ray diffraction using a Rigaku instrument with CuK α radiation at 40 keV and 40mA. A scanning rate of 2°/min through a 2 θ region of 15 to 65° was used.

The samples were prepared for electron microscopy by first cutting thin slices with a diamond saw. For scanning electron microscopy, the sample surfaces were ground with diamond paste and polished to 0.5μ with alumina powder, then given a light carbon coating. SEM was done using an ISI DS 130 instrument at 8 keV.

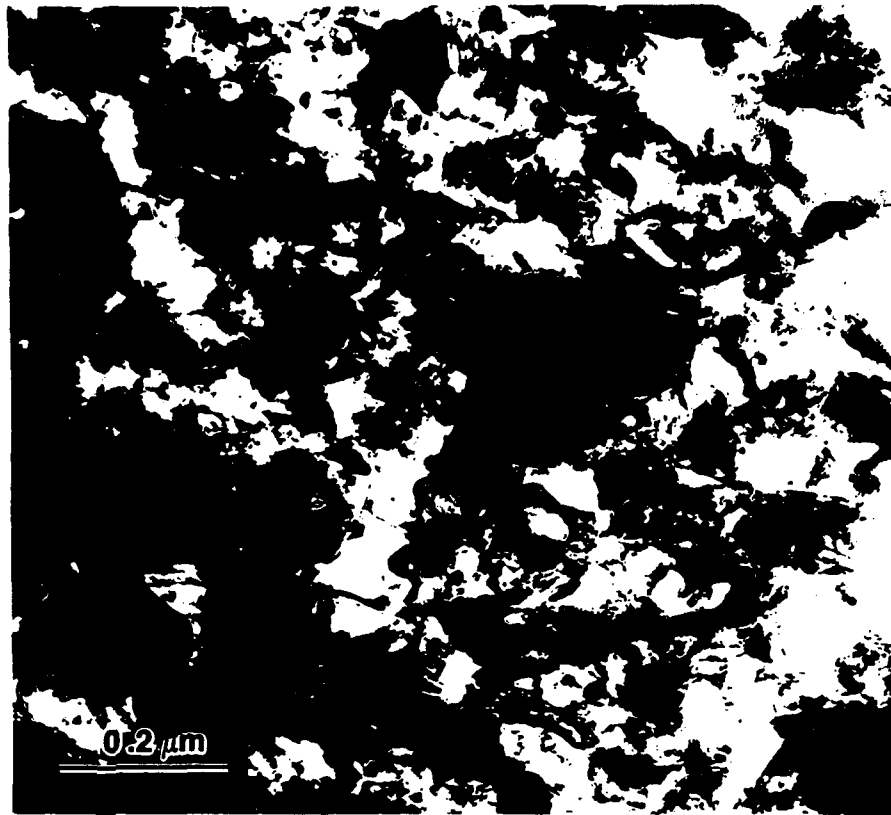
Transmission electron microscopy samples were ground using SiC paper to a thickness of less than 150μ . Surfaces were then ground with 15μ diamond paste and polished with 6, 1 and 0.25μ diamond paste to a mirror-like finish. 3mm or smaller pieces were dimpled to a nominal thickness of $15-20\mu$ using $\sim 3\mu$ diamond paste, then polished on the dimpler with 0.25μ paste. The specimens were then ion milled on a cold stage Gatan miller at 5V and 1mA for about 8 hours at an angle of 10° . No carbon coating was applied before TEM which was carried out on a Philips 400 instrument at 120 keV.

5.2. Results

The material was in the form of a loosely sintered powder, with quite large pores visible to the eye. The samples were indistinguishable in appearance. Both were grey and metallic in lustre. Both materials were found to be good electrical conductors. XRD showed them to be phase pure α and β -NiS, respectively. (Graphs 4 and 5). SEM of the unetched surfaces showed little surface detail. Grain boundaries could not be identified (Figure 6). TEM of these samples showed evidence of considerable strain, and a variable grain size (Figure 7).

6. Matrix Studies

When studying a displacive transformation there are several advantages of studying the transforming material as a second phase inside a matrix. If the transformation is accompanied by a significant volume change then the matrix will serve to contain the transformation and prevent loss of the sample. This is a particularly useful function if the transformation is to be studied by electron microscopy, where extremely thin fragile specimens are required. In addition, the conditions under which the displacive transformation can take place may vary with the size of the transforming region. A two-phase composite allows some control over the size of the transformable particles so that a systematic study can be developed.



a) α -NiS

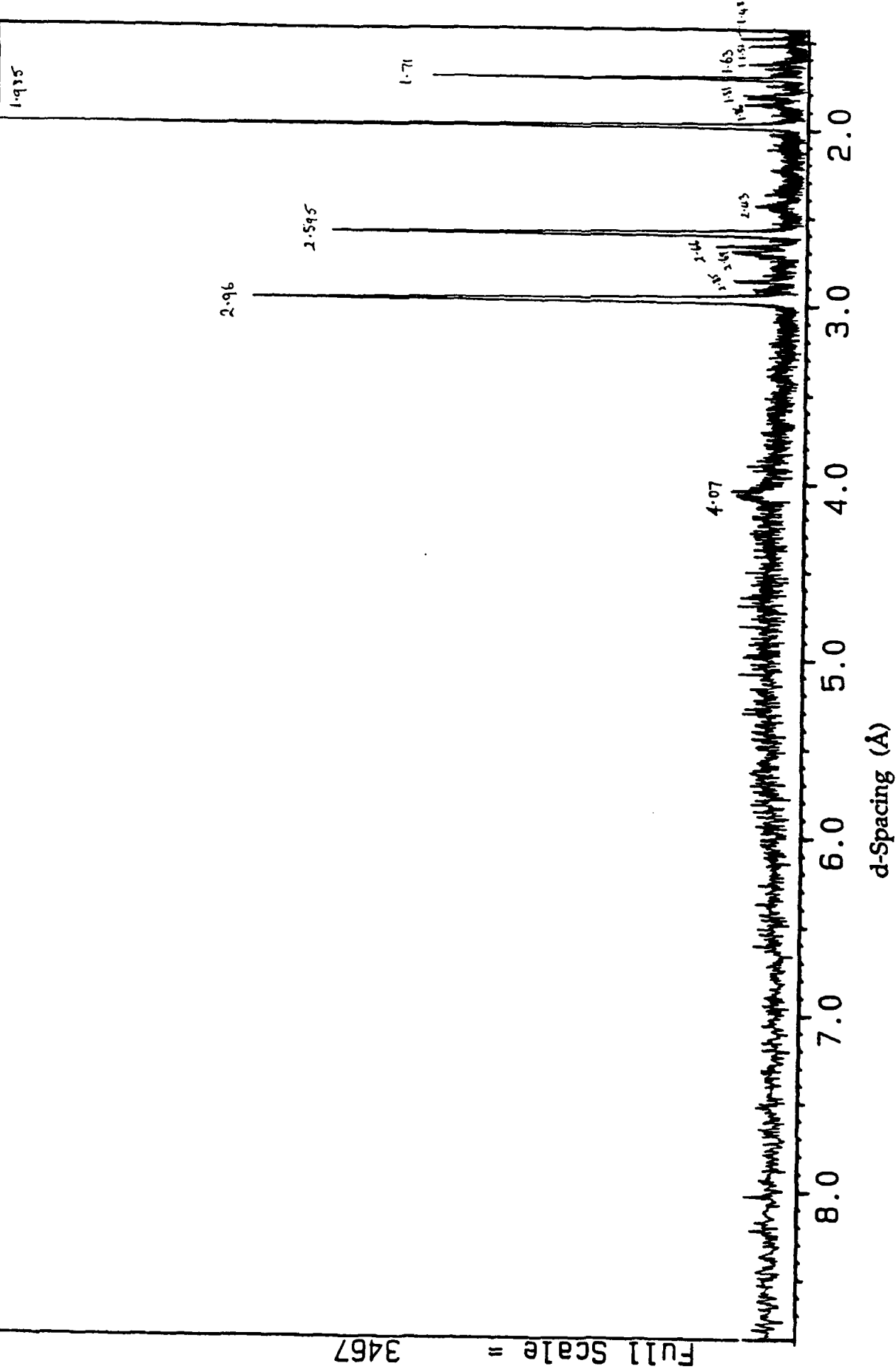


b) β -NiS

Figure 7. TEM Micrographs of Synthetic NiS.

FILE: Z00004.RAW

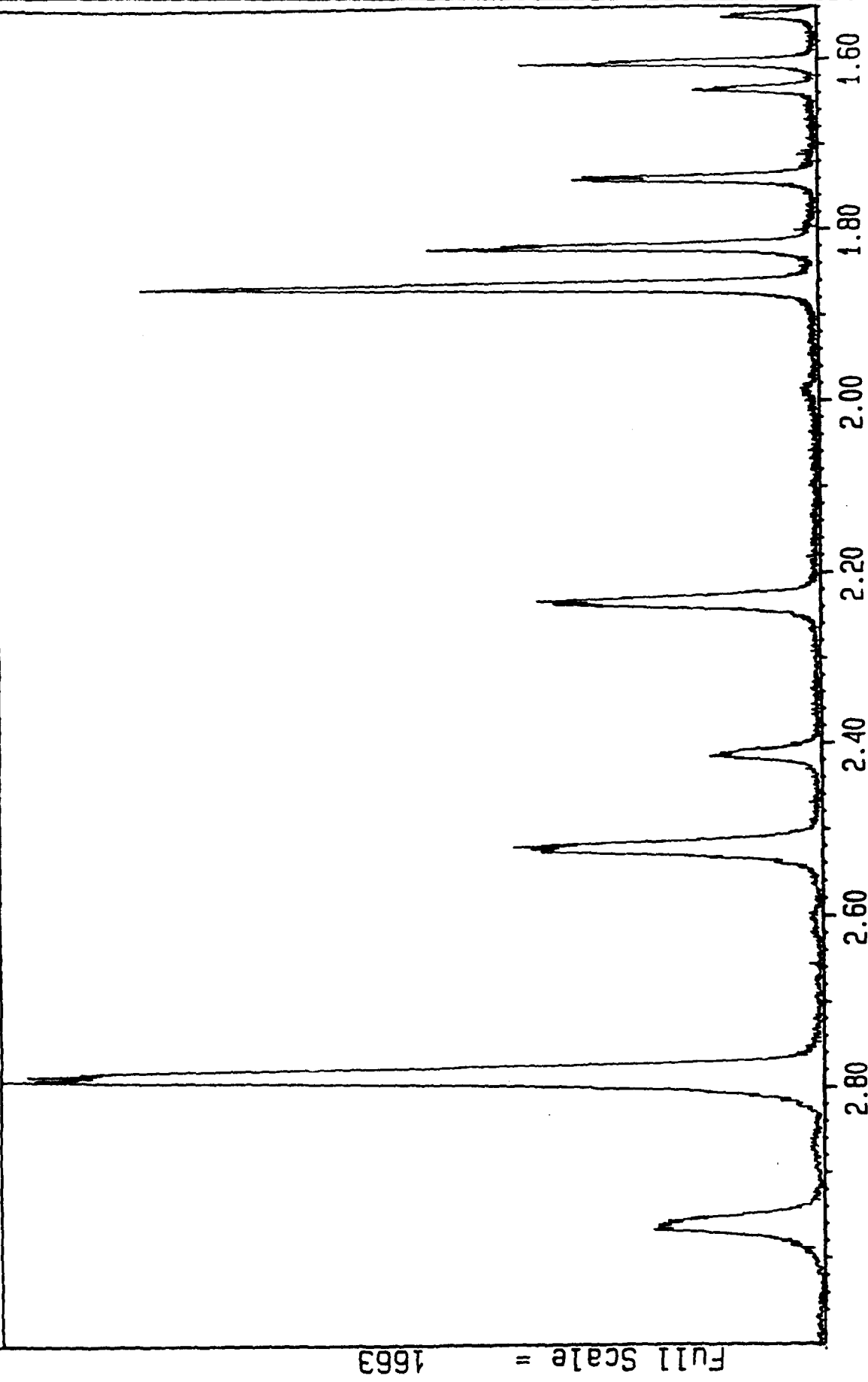
NIS 7/20/90 MADE BY CARLOS



Graph 4. X-Ray Diffraction Trace for α -NiS.

FILE: Z00030.RAW

JEMIMA NIS BATCH 2 SLOW COOL



d-spacing (Å)

Graph 5. X-Ray Diffraction Trace for β -NiS.

A further reason for studying the characteristics of the NiS transformation in the context of a confining matrix is the desire to investigate and exploit the toughening effect of the transformation upon the matrix. For this reason the choice of a matrix is of more than academic interest. Many materials would be useful for containing a sample for study, however these materials would not be suitable for toughening studies. A number of materials have been considered as possible matrix phases.

To obtain any benefit from potential transformation toughening by NiS, the matrix phase would be a fairly brittle material. Further requirements are chemical compatibility with NiS and ease of fabrication of the composite system. It would also be of more utility to work with a material which was an established engineering material with well characterized properties. Materials which have been considered as matrix candidates include: glass, specifically cordierite and silica glass, and zinc sulphide, and possibly other sulphides.

6.1. ZnS Matrix

Zinc sulphide is of interest because it is an engineering material which finds application as an infrared window material. However, its mechanical properties are relatively poor and the incorporation of some sort of toughening agent would be an advantage, if the optical properties were not compromised. The normal fabrication of ZnS is a hot-press powder route (21), which may possibly be modified to produce composites from NiS and ZnS powders, or a chemical vapour deposition method (22).

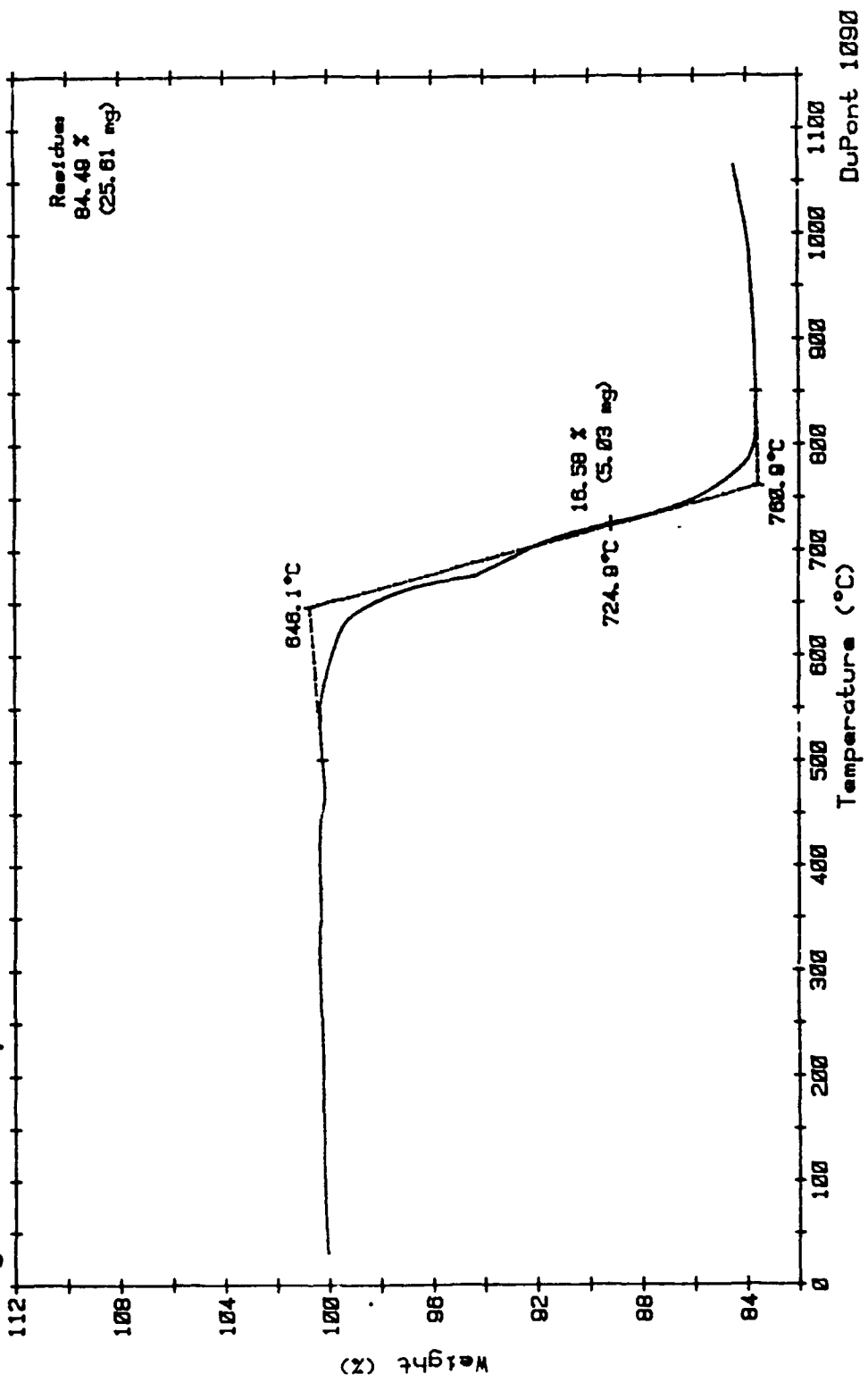
6.1.1. Preliminary Investigations

Commercially prepared ZnS (Alpha Chemicals) and NiS powders (Alpha Chemicals - found by XRD to be single phase α -NiS) were analyzed by DTA and TGA in air and in argon. The thermal stability of these materials in air is indicated by their TGA curves (Graphs 6 and 7.). Especially relevant is the decomposition of NiS, which begins at about 640°C when heated at 10°C/min.

An attempt was made to prepare a ZnS/NiS sample by a sintering route. Half inch compacts of ZnS with 13 wt % NiS powder mixtures and a small amount of organic binder were fired in evacuated quartz tubes at 750° C for one hour. Very little densification was observed for these samples.

Sample: NICKEL SULPHIDE
 Size: 30.31 mg
 Rate: 10C/M IN AIR
 Program: TGA Analysis V1.0
 Date: 1-Jun-90
 Time: 9:30:03
 File: NICKS.01
 Operator: ISAAC
 Plotted: 1-Jun-90 11:28:49

TGA

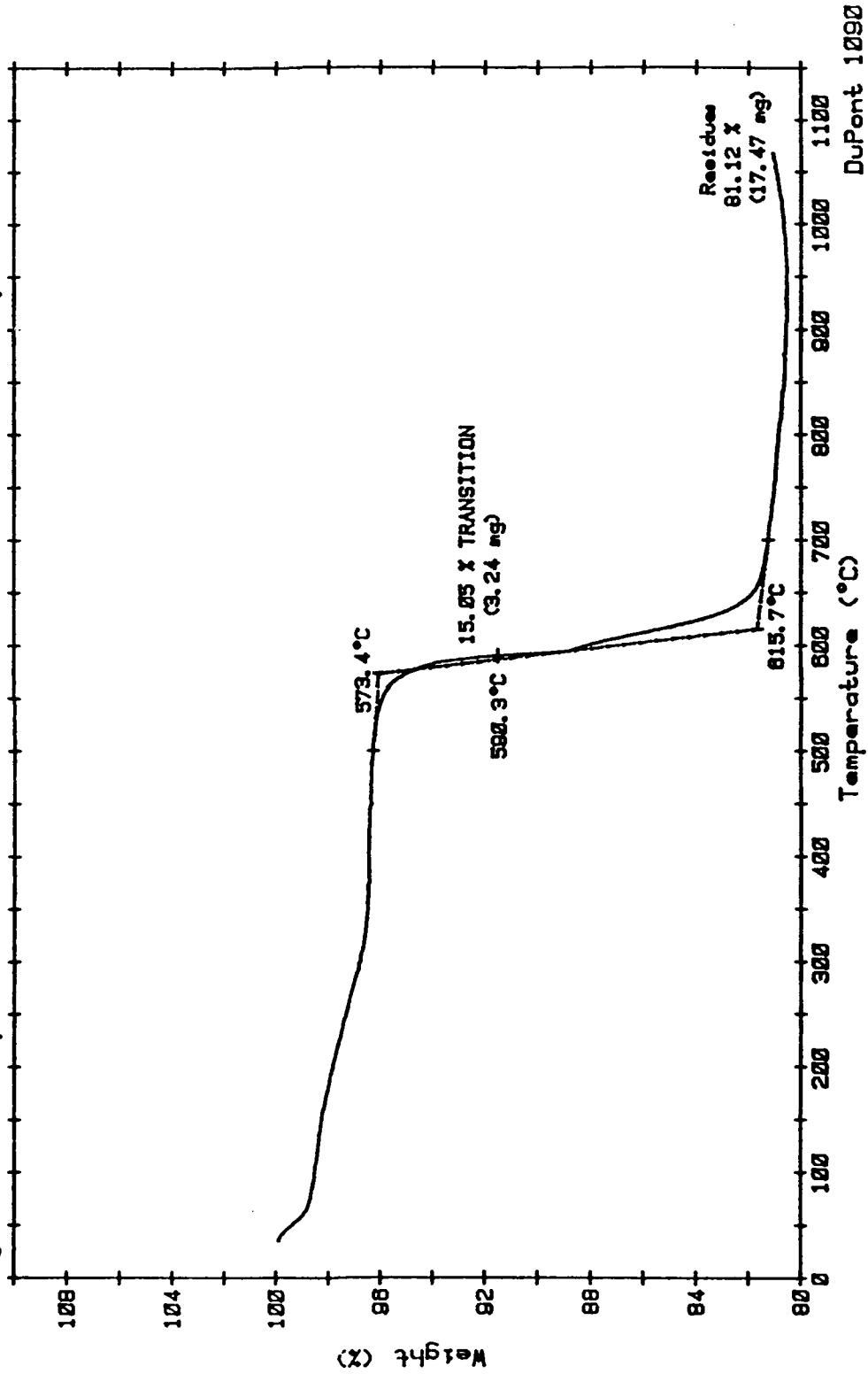


Graph 6. Thermogravimetric Analysis Trace for NiS Powder.

Sample: ZINC SULPHIDE
Size: 21.54 mg
Rate: 10C/M IN AIR
Program: TGA Analysis V1.0

TGA

Date: 28-May-90
Time: 9:51:15
File: ZINCS.01
Operator: ISAAC
Plotted: 28-May-90 12:43:29



Graph 7. Thermogravimetric Analysis Trace for ZnS Powder.

6.1.2. Conclusion

Preliminary investigations suggest that the thermal stability of NiS in air (< 640° C) is not compatible with the requirements for fabrication of a dense ZnS body (770 to 970° C, under 20000 psi pressure). The possibility of incorporating NiS into chemically-vapour-deposited ZnS has not been examined.

6.2. Glass matrices

Glass is a brittle material with a wide variety of applications. A number of different glasses would probably be equally suitable as a matrix material. Cordierite glass was initially chosen for study because of the possibility that the NiS-containing glass might subsequently be crystallized to produce a more conventional two phase ceramic system. Cordierite glass ceramics are used as high power loss electronic substrates because of their low dielectric constants and low thermal expansion coefficients. It has been shown that cordierite glass ceramics may be transformation toughened by ZrO₂ (23, 24). Fabrication of a cordierite/NiS composite was attempted by several methods. These are described below.

Silica glass is a simpler material, from which many glass compositions have been developed. In the interests of simplicity, it was decided to attempt the investigation of a silica glass/NiS composite also. Some success has been reported in the transformation toughening of a silica glass ceramic by ZrO₂ (25). Various methods are available for the production of silica glass, of which the sol-gel technique is particularly suited to our purposes, in light of the limited thermal stability of NiS and the volatility of sulphur. It is necessary to find a processing route which does not require temperatures in excess of 600-650°C, if special atmospheres are to be avoided. Some glasses have softening points below this range, and frits may be expected to sinter if processed by a normal powder processing route. This method was attempted using a commercial cordierite frit preparation.

Other low temperature glass fabrication methods are the molecular synthesis routes which use organic precursors to form polymeric gels which can be fired to yield dense glass bodies at substantially reduced temperatures compared to conventional techniques (26). The Pechini method is a versatile method for producing homogeneous powders of complex compositions, starting with cation salts solutions and a hydroxycarboxylic acid (27). A condensation reaction, followed by polyesterification and calcination yield fine crystallites of mixed cation oxides in the

desired proportions. This route was tried as a method of producing amorphous cordierite powder which could then be used as the basis for a NiS/cordierite glass composite.

A second method was based on the work of Nogami and Moriya (28) in preparing a silica glass by the hydrolysis of tetraethyl orthosilicate (TEOS). Recent developments by these workers (29, 30) have led to a novel technique for the in-situ formation of cadmium sulphide in a silica glass. Room temperature treatment of a CdO.SiO₂ glass precursor with hydrogen sulphide gas forms tiny crystals of CdS which have interesting optical properties. Attempts to adapt this method to the production of NiS particles in silica glass are underway.

6.2.1 Cordierite Glass by the Pechini Method

6.2.1.1. Experimental

Ludox, SM grade (17g) was brought to a pH of 1.4 by the addition of about 8 drops of nitric acid. A salt solution of 7g MgCl₂.6H₂O (Fisher Chemicals) and 16.5g AlCl₃.6H₂O (Mallinckrodt) was made up with about 15 ml of distilled water, stirred and warmed, then added to the Ludox. Resin (56.6g), prepared by mixing 60g of citric acid with 40 g of ethylene glycol and warming below 50° C whilst stirring until the acid was dissolved, was added to the Ludox mixture with stirring. The solution was gradually warmed and heated to ~115° C, until boiling. The mixture was dried until brittle and brown, then kept in an oven at 68° C for 3 days. The granular material was ground in a mortar and pestle to give a smooth powder which was calcined in two separate schedules: at 800° C for 1 hr, and at 1000° C for 1 hr. The powder was mixed with 2 wt % polyethylene glycol as a binding agent by dissolving in water and stirring over a hot plate until the powder was completely dried. This powder was die pressed at ~1250 psi and then isopressed at 15000 psi for 5 min. Pellets were fired on Pt foil in a Teresco furnace in air according to the following schedules:

300° C/hr to 1200° C; 1200° C for 1 hr;

300° C/hr to 1350° C; 1350° C for 1 hr;

300° C/hr to 1400° C; 1400° C for 1 hr.

The density of the fired pellets was estimated using Archimedes' principle. XRD was performed on both the calcined powders and the fired bodies using a Philips XRG 3100 instrument with a scanning rate of 0.1°/sec. DTA of the calcined powder was performed in air with a Dupont 1090 instrument at a heating rate of 10° C/min.

6.2.1.2. Results

XRD of the calcined powder indicates that the material was still amorphous after 800° C, and largely amorphous after 1000° C, with perhaps a small amount of Al₂O₃ formed. More crystallization occurred in the body fired at 1200° C, with SiO₂ being present in the XRD trace, but cordierite was not observed. After firing at 1350° C cordierite appeared in the XRD patterns. Comparison with the DTA results (Graph 8.) suggested that the crystallization of cordierite occurs between 1200° C and 1350° C. Each of the fired pellets shows some densification, and the 1400° C fired pellet was bloated. The pellet fired at 1350° C had a density of about 1.5 g/cc, but this was not pure cordierite.

6.2.1.3. Conclusion

The crystallization of cordierite derived from the Pechini process does not occur below 1200° C.

6.2.2. Cordierite Frit

6.2.2.1. Experimental

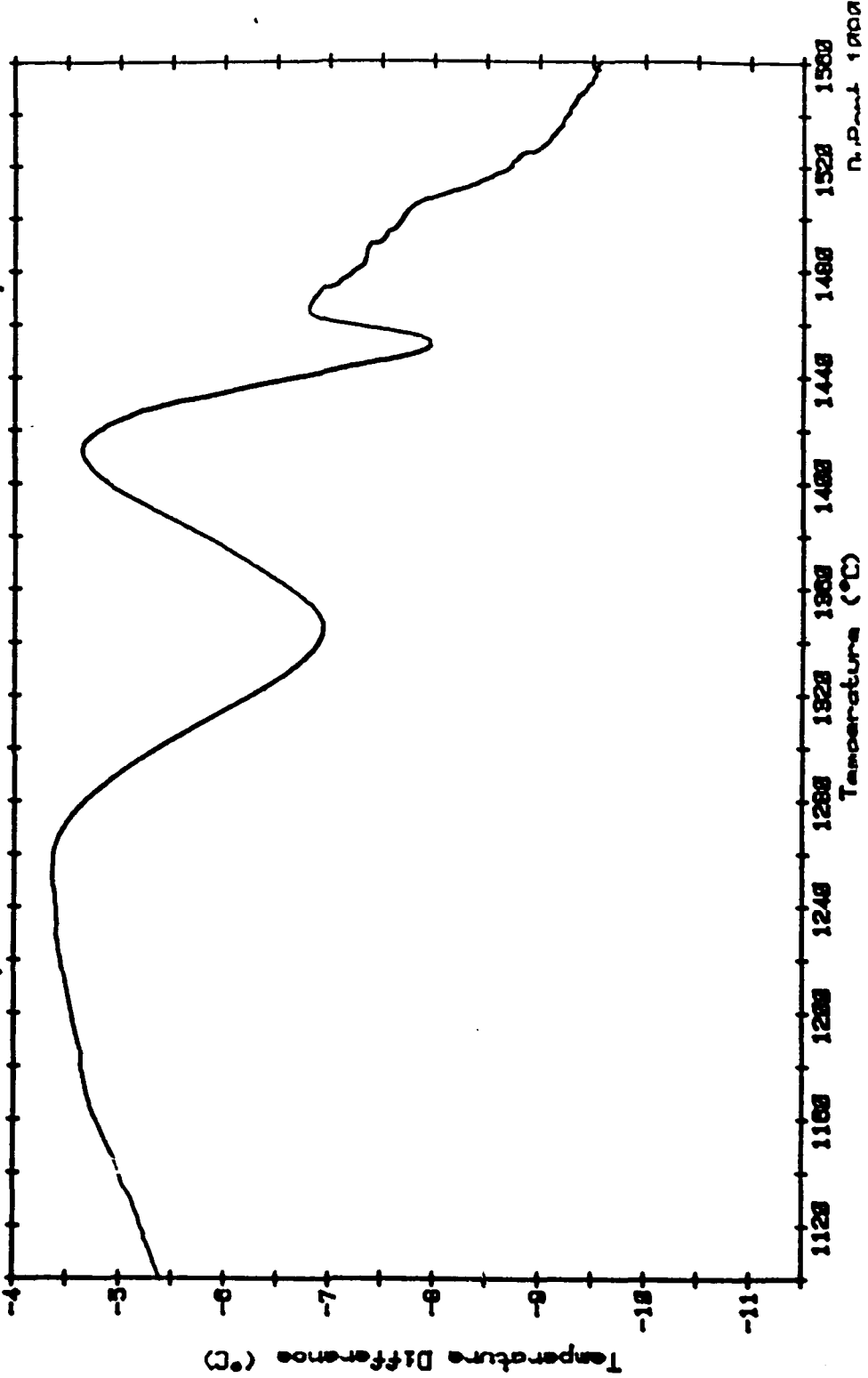
A powder of 5% by weight NiS (Alpha Chemicals) in a commercial debased cordierite frit (Ferro Corporation) was mixed with a small amount of organic binder. Pellets were die pressed at ~1250 psi and isopressed at 10 000 psi. These pellets were placed on Pt foil setters and fired in air for 1 hour at temperatures of 850°, 875° and 900° C, with a heating rate of 10° C/hr. XRD of the fired bodies was performed using a Philips XRG 3100 instrument at 40 kV and 10mA.

6.2.2.2. Results

The pellet fired at 850° C showed little densification, whereas the 900° C fired pellet was significantly more dense. XRD results from the pellet fired at 875° C showed the presence of NiO. This was consistent with the TGA results obtained for NiS in air.

Samples CORDIERITE
 Sizes 0.0316CM
 Rates 10C/M IN AIR
 Programs Extended Playback V2.0
 Dates 24-May-90 Times 10:14:12
 Files CORDI.01
 Operator: J COOPER
 Plotted 24-May-90 13:55:58

DTA



Graph 8. Differential Thermal Analysis of Cordierite Powder.

6.2.2.3. Conclusion

The densification of cordierite frit does not take place at sufficiently low temperatures to permit the retention of NiS without oxidation.

6.2.3. Silica Glass From TEOS

6.2.3.1. Experimental

300g of tetraethyl orthosilicate (TEOS; obtained from Aldrich Chemicals) was mixed with 240 ml of 0.15 mol/litre HCl solution to give a pH of 1.64. The solution was stirred vigorously for about 15 minutes, after which time mixing was complete. The solution was poured into small plastic trays and left to gel. One portion was refrigerated at about 7° C whilst the other was kept at room temperature. When the gel had become somewhat viscous, commercial NiS powder in small quantities was stirred into it. This powder remained suspended in the gel. After hardening (24 hrs for the room temperature gel; 2 weeks for the refrigerated gel) the gels were gently heated to 200° C over a period of 1 week. Despite this slow heating rate, severe cracking of the gels occurred, probably as a result of insufficient drying at the gelation temperature. Pieces of this gel were heated to 600° C and to 700° C at rates of 10° C/hr and 60° C/hr respectively.

Pieces of gel were hand ground on 600 mesh grit SiC paper to produce thin samples for TEM. Samples were then polished with successive grades of diamond paste. The small pieces were glued to copper grids with an epoxy and then dimpled on a Gatan Precision Dimple Grinder (Model 656/3) using 6 μ diamond paste.

6.2.3.1. Results

Cracking of samples at all stages of the drying and sample preparation process have prevented the preparation of a satisfactory specimen for TEM to date.

6.2.4. In-Situ Formation of NiS in Silica Glass from TEOS

6.2.4.1. Experimental

A two stage hydrolysis of TEOS was conducted. Firstly, 12g of acid catalyst solution (8.6g distilled water, 23g ethanol, 0.05g HCl) was added to 40g of TEOS and stirred for 1hr. To this was added 1.72g of nickel acetate dissolved in 5g methanol, with another hour of stirring. The final stage of the hydrolysis was carried out by adding 21.8g of base catalyst (23g distilled water, 15g ethanol, 0.08g NH_2OH) and stirring for 1 hr.

The solution was poured into plastic petri dishes, covered and left to dry at room temperature. One dish was dried at 68°C in an oven.

6.2.4.2. Results

The oven-dried solution gelled within 24 hours, whereas the room temperature solutions dried over a period of 1 week. Much shrinkage occurred, cracking the thinner films, although the thicker films suffered only minor cracking. Small fibrous crystals are present in the room-dried gel which could not be identified by XRD. Their presence may be due to insufficient mixing during the hydrolysis, since small fibres were observed to form on addition of the base catalyst to the TEOS. The pH of the TEOS solution also seems to be critical in preventing the gelation of the silica prior to hydrolysis.

7. Future Directions

Investigations to date have lead to a number of promising avenues for further work. Electron microscopy of the single phase materials produced by high temperature synthesis should continue to yield information about the crystallography of the transformation, and this will be facilitated by the production of single crystals of α and β -NiS in the near future. Alternative techniques of TEM sample preparation such as ultramicrotome and metallographic methods should give better quality samples for research.

Two methods of producing bulk samples for the future study of mechanical properties of NiS-containing systems are:

- 1) The in-situ formation of NiS in a sol-gel derived silica glass. This method has the advantage of allowing fine control of the size, size distribution and composition of the NiS particles as they are grown.
- 2) The production of single phase polycrystalline NiS thin films by metallorganic spin casting, a method which has been successfully used to prepare films of ZrO_2 (31).

Thin films samples will be important for characterizing the mechanical properties of NiS and in studying the toughening mechanism.

Acknowledgements

We are grateful to C. Suchicital for making the samples of single phase α and β NiS, and to M.Swain for providing the samples of fractured glass.

References

1. W.M. Kriven. 1988. "Possible Alternative Transformation Tougheners to Zirconia: Crystallographic Aspects" *J. Am. Ceram. Soc.* **71**. [12] pp 1021-1030
2. W.M. Kriven 1990. "Martensitic Toughening of Ceramics." *Mat. Sci. and Eng.* **A127**. pp 249-255.
3. E.R. Ballantyne. 1961. CSIRO Division of Building Research Report, Melbourne.
4. R.C. Bradt. 1986. "Macro- and Micro- Fracture Patterns of Thermally Tempered Plate Glass Failing From Nickel Sulphide Inclusions." Alfred University Fractography Conference, August 1986.
5. H. Tabuchi. 1974. "On the Study of Sulphide Inclusions in Plate Glasses." 10th International Congress on Glass, Ceram. Soc. of Japan. Kyoto, Japan, July 1974.
6. C.C.Hsiao. 1977. "Spontaneous Fracture of Tempered Glass." *Fracture 1977*, Volume 3, ICF4, Waterloo, Canada.
7. M.V. Swain. 1981. "Nickel Sulphide Inclusions in Glass: An Example of Microcracking Induced by a Volumetric Expanding Phase Change." *J. Mat. Sci.* **16**. pp 151-158.
8. St. Gobain Glass Industries, France. Internal Report.
9. V.Rajamani and C.T.Prewitt. 1974. "Thermal Expansion of the Pentlandite Structure." *Am. Mineral.* **60** pp 39-48.

10. F.F.Lange. 1982. "Transformation Toughening Part 1. Size Effect Associated with the Thermodynamics of Constrained Transformations." *J. Mater. Sci.* 17 pp 225-234.
11. A.G.Evans and R.M.Cannon. 1986. "Toughening of Brittle Solids by Martensitic Transformations." *Acta metall.* 34 pp 761-800.
12. G. Kullerud and R.A. Yund. 1962. "The NiS System and Related Minerals." *Journal of Petrology*, 3, Part 1, pp 126-175.
13. Wyckoff. 1963. Crystal Structures. Vol. 1. 2ed. Interscience Publishers.
14. W.A. Deer, R.A. Howie and J. Zussmann. 1962. Rock Forming Minerals. Vol.5, Non-Silicates. J. Wiley and Sons Inc. New York.
15. I.L.Aptekar', V.I.Ivanov, V.Sh.Shekhtman, and I.M.Shmyt'ko. 1982. "Transformation of the Real Structure of β -NiS during a Phase Transition." *Fiz. Tverd. Tela (Leningrad)* 24. pp 707-713.
16. J. Trahan and R.G.Goodrich. 1970. "X-Ray Diffraction Measurements on Metallic and Semiconducting Hexagonal NiS." *Phys. Review B.* 2 [8] pp 2859-2863.
17. D.B.McWhan, M.Marezio, J.P.Remeika and P.D. Dernier. 1972. "Pressure-Temperature Phase Diagram and Crystal Structure of NiS." *Phys Review B* 5 [7] pp 2552-2555.
18. L.Merker. 1974. "On the Behaviour of Nickel Sulphide in Glass." (in Ger), *Glastech. Ber.*, 47 pp 116-21.
19. Craig. 1984. in P.H.Ribbe (ed) Sulphide Mineralogy Vol 1. Mineralogical Society of America.
20. J.D.Grice and R.B.Ferguson. 1974. "Crystal Structure Refinement of Millerite (β -NiS)." *Canadian Mineralogist.* 12 pp 248-252.

21. Patent US 3131025.
22. H.P.Kirchner, J.A.Tiracorda and T.J.Larchuk. 1984. "Contact Damage in Hot-Pressed and Chemically-Vapor-Deposited Zinc Sulphide." *J. Am. Ceram. Soc.* 67 pp C-188 to C-190.
23. M.A.McCoy and A.H.Heuer. 1988. "Microstructural Characterization and Fracture Toughness of Cordierite-ZrO₂ Glass-Ceramics." *J. Am. Ceram. Soc.* 71 pp 673-77.
24. D.R.Clarke and B.Schwartz. 1987. "Transformation Toughening of Glass Ceramics." *J Mater. Res.* 2 pp 801-804.
25. M.Nogami and M.Tomozawa. 1986. "ZrO₂-Transformation-Toughened Glass-Ceramics Prepared by the Sol-Gel Process from Metal Alkoxides." *J. Am. Ceram. Soc.* 69 pp 99-102.
26. A.M.Kazakos, S.Komarneni and R.Roy. 1990. "Sol-gel Processing of Cordierite: Effect of Seeding and Optimization of Heat Treatment." *J. Mater. Res.* 5 pp 1095-1103.
27. P.A.Lessing. 1989. "Mixed-Cation Oxide Powders via Polymeric Precursors." *Ceram. Bull.* 68 pp 1002-7
28. M.Nogami and Y.Moriya. 1980. "Glass Formation Through Hydrolysis of Si(OC₂H₅)₄ with NH₄OH and HCl Solutions." *J. Non-Crystall. Solids* 37 pp 191-201.
29. M.Nogami, K.Nagasaka and E.Kato. 1990. "Preparation of Small-Particle-Size, Semiconductor CdS-Doped Silica Glasses by the Sol-Gel Process." *J.Am. Ceram. Soc.* 73 pp 2097-99.
30. M.Nogami and K.Nagasaka. 1990. "CdS Microcrystal-Doped Silica Glass Prepared by the Sol-Gel Process." *J. Non-Crystall. Solids.* 122 pp 101-106.

31. K.T.Miller and F.F.Lange. 1990. "The Instability of Polycrystalline Thin Films: Experiment and Theory." *J. Mater. Res.* 5 pp 151-160.

Section 2.5 Processing of Lutetium Borate Composites (Dr. Ian Nettleship)

1 Background

The polymorphism of lanthanide borates (LnBO_3) has been studied by Levin (1), but little attention has been paid to the crystalline forms of the lanthanide borates. These materials show CaCO_3 -type structures such as aragonite, calcite or vaterite. Lutetium borate has the smallest ionic radius and is the only borate to undergo the vaterite-calcite type transformation. This occurs at 1310°C and involves a volume increase of 8.1% on cooling that is reversible on heating. This was the basis on which the material was chosen as a possible transformation toughener(2), but nothing is known about the kinetics and the physical characteristics of the transformation.

Most borates are used in glass manufacture and the traditional mixed oxide route has been used for all the studies of borate material we are aware of. Levin et al (1) also used a mixed oxide route to prepare the materials for their study.

The objective of this work is to chemically prepare high vaterite phase that can be metastably retained at room temperature and to try to fabricate a LuBO_3 - Lu_2O_3 composite in order to study the transformation in LuBO_3 to see if it is a suitable toughener.

2 Experimental Procedure

A Pechini method (3) was used in an attempt to prepare LuBO_3 powder. This involves the formation of a chelate between a aqueous solution of mixed cations and a hydrocarboxylic acid such as citric acid. This is then mixed with a polyhydroxylalcohol such as ethylene glycol. When the mixture is heated there is a condensation/polyesterification reaction which forms a solid gel on drying that can be crushed and calcined to give the oxides.

In this case $\text{Lu}(\text{NO}_3)_3 \cdot 5\text{H}_2\text{O}$ and HBO_3 was dissolved in deionized water and a 60/40 wt% citric acid and ethylene glycol resin was added such that the weight of the final oxide divided by the weight of the resin is 0.3, i.e:

$$\frac{\text{weight of LuBO}_3}{\text{Weight of citric acid} + \text{weight of ethylene glycol}}$$

Then the mixture was heated on a hot plate and the water boiled off to give an expanded gel when dried. The gel was calcined at temperatures ranging from 800°C to 1200°C. Some of the powder calcined at 800°C was milled in alcohol and pressed into pellets and fired in air at 1500°C for 1 hour. The phase distribution was analysed by XRD and some SEM was done on the powders calcined at low temperature.

3 Preliminary Results and Discussion

Figure 1 shows the phase distribution in the powders calcined from 800°C to 1200°C and also of the pellets fired at 1500°C. This shows that the only crystalline phase present at 800°C is the cubic phase of Lu_2O_3 but when the calcination temperature is increased peaks of the high vaterite phase of LuBO_3 appear and the relative proportion of this phase increased. It seems that the high temperature vaterite phase can be formed at temperatures below the reported vaterite-calcite transformation at 1310°C and retained at room temperature. Figure 2 shows a micrograph of the powder calcined at 1000°C which shows the highly porous agglomerates of small crystallites that are typical of Pechini derived powders. The sample also contains some particles that are highly dense and some porous agglomerates are coated with a more dense material.

It is thought that boron is segregating either during the gelling reaction or during the pyrolysis of the gel. This would allow the observed crystallization of lutetium oxide during the low temperature calcinations. When the calcination temperature was increased the lutetium oxide appears to react with the segregated boron containing phase to give the high temperature vaterite form of lutetium borate even though some powders were calcined below the recognized transformation temperature. Hence this route is essentially a mixed oxide method.

To produce a high surface area powder of lutetium borate a low temperature chemical synthesis route must be developed in which the segregation of the boron is prevented. One possible solution to this problem is to prepare a chemical lutetium borate precursor and spin cast as a thin film on a suitable substrate such as sapphire. The thin films can then be flash pyrolysed at temperatures of 600°C or above to give lutetium borate. It is thought that flash pyrolysis should help to prevent the boron from segregating during calcination. The transformation could then be studied in the thin films using XRD and TEM (4).

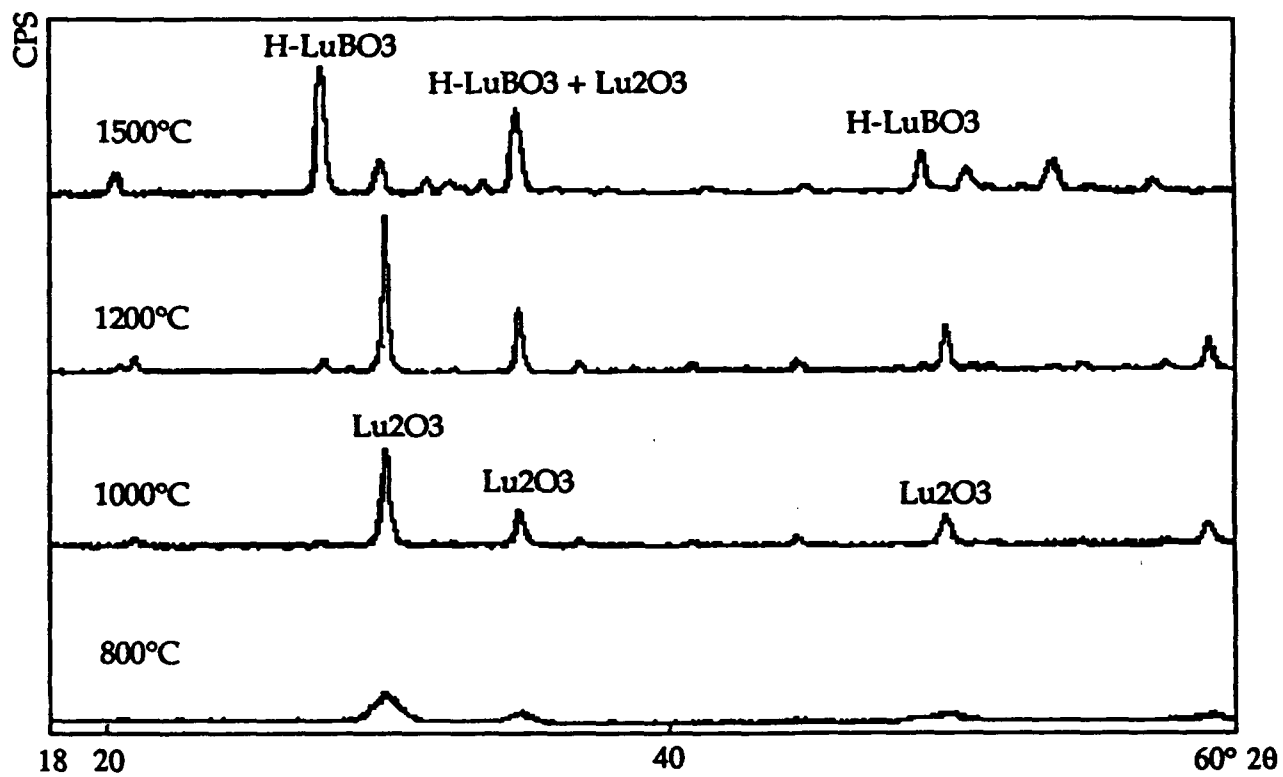


Figure 1: XRD plots of LuBO₃ powders calcined for 1 hour at temperatures between 800°C and 1500°C.

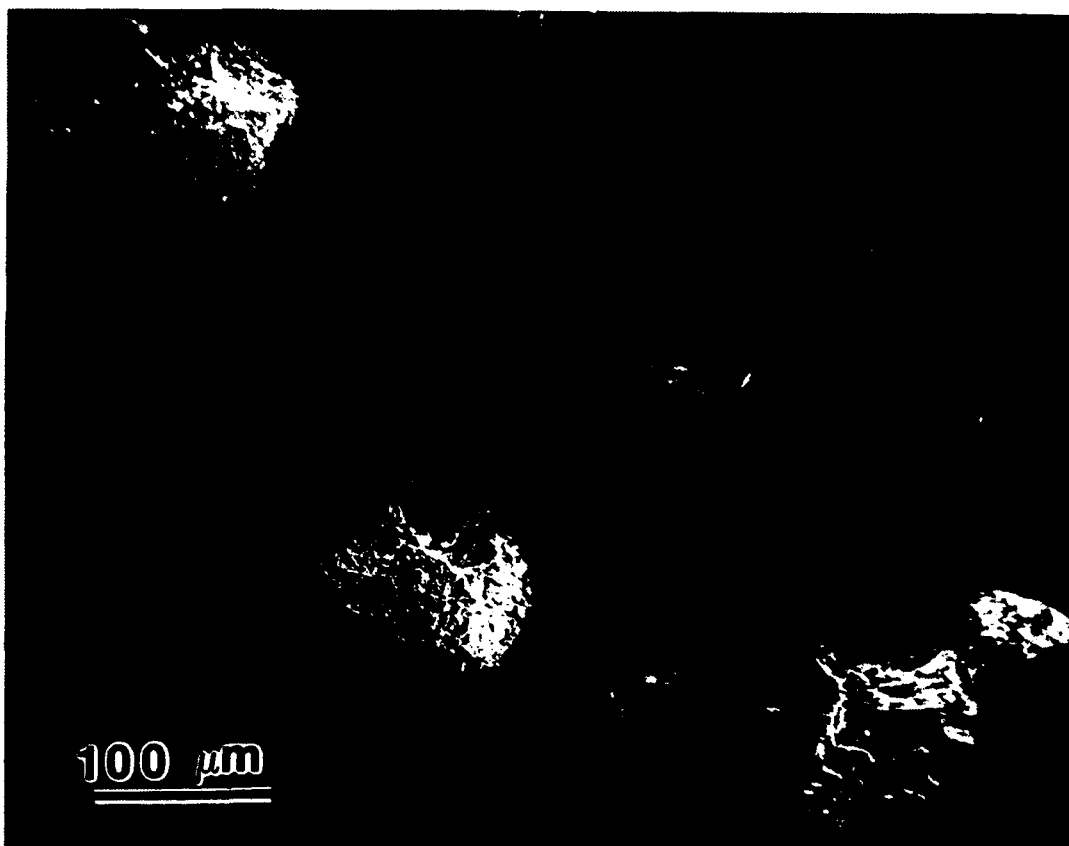


Figure 2: SEM micrograph of powder calcined at 1000°C for 1 hour.

4 Future Work

- (1) Synthesis of lutetium borate powder to characterize the unconstrained transformation by XRD.
- (2) Preparation of chemical precursors for lutetium borate and spin casting on to a suitable substrate in order to form lutetium borate at low temperature by metal-organic deposition. The resulting film will then be used to study the stress induced transformation by XRD and TEM.
- (3) Fabrication of Lu_2O_3 - LuBO_3 composites.

5 References

- (1) E.M. Levin, R.S. Roth, J.B. Martin, "Polymorphism of ABO_3 -Type Rare Earth Borates", *Am Mineral.*, **46** 1030-55 (1961).
- (2) W.M. Kriven, "Possible Alternative Transformation Tougheners to Zirconia: Crystallographic Aspects" *J Am Ceram Soc.*, **71** 1021 (1988).
- (3) P.A. Lessing, "Mixed-Cation Oxide Powders via Polymeric Precursors", *Ceram Bull.*, **68** 1002 (1989).
- (4) F.F. Lange, private communication at AFOSR Review, Dayton OH April (1990).

Section 2.6 Processing and Microstructure of SiC-Dy₂O₃ Composites (Mr. S. Kim)

2.6.1 Introduction

Continued research has been conducted in order to incorporate Dy₂O₃ into SiC matrix in such a way that a dense silicon carbide - B-dysprosia composite could be formed. Previous research has shown that oxygen that is present as impurities in SiC powders or from the atmosphere during densification is detrimental in retaining the B-Dy₂O₃ in the composite.

Recently, however, nearly ideal silicon carbide powders are produced by new synthesis methods such as laser synthesis or plasma synthesis. Attempts were made to combine these new powders with better processing methods. Complete outgassing of the powder mixtures, for example, is a way to minimize the oxygen during densification. Three different SiC powders were used and the important processing/microstructural parameters for the composites are studied.

2.6.2 Experimental Procedures

2.6.2.1 Starting Powders

Three different silicon carbide powders were investigated in this research. Very fine silicon carbide powders with low oxygen content were obtained from Aluminum Company of America. The powders were manufactured by the plasma process. This process yields powders with many desirable characteristics as a ceramic raw material. Submicron size, narrow size distribution, high purity and co-formed dopants and additives are some of the characteristics of the powder. Table 1 describes the characteristics of the powder as reported by the manufacturer. The plasma reactor used for fabrication of the powders is shown schematically in Fig. 1.

Table 1. Plasma SiC Powder Characteristics

Chemical Analysis

O	0.1 wt%
Cl	0.15 wt%
B	0.25 - 0.3 wt%
Free C	0.3 - 0.5 wt%
Free Si	< 0.1 wt%
Al, Fe, Mg	< 50 ppm each.
All Other Elements	Undetected

Surface Area 10 m²/g

Phase β

Particle Size Distribution

Median 0.5 μ m

D₉₀/D₁₀ 10

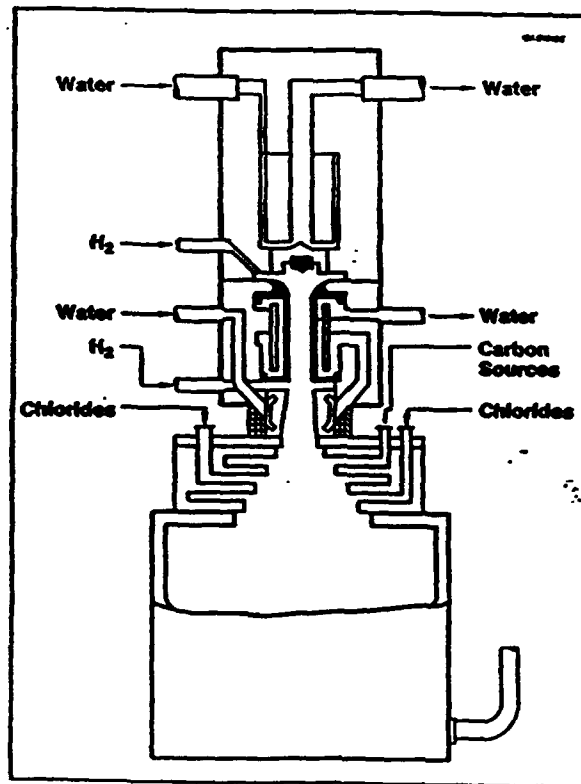


Fig. 1. Schematic of Plasma Reactor

Another SiC powder with intermediate oxygen content was purchased from Superior Graphite Co. Starck SiC powders doped with boron and carbon (Starck, AD 10) were also purchased. Table 2 shows the characteristics of these two powders. All SiC powders were analyzed for oxygen content by Leco oxygen analyzer.

Manufacturer	Superior Graphite	Starck (AD 10)
Oxygen Content (wt%)	0.5	0.76
BET surface area (m ² /g)	3.0	15
Particle size (Median, μm)	3.58	0.7
Phase (Major)	α	α and β
Boron Dopant (wt%)		0.6
Carbon Dopant (wt%)		4.0

2. 6. 2. 2 Powder Mixing

15 vol % of Dy₂O₃ was added to SiC powders. All SiC - Dy₂O₃ powders except doped powders (Starck) were attrition milled in methanol for 1 hour. Alcoa SiC - Dy₂O₃ powders were also attrition milled for 2 hours.

Starck doped powders were mixed using Spex mixer. After drying, the mixtures were passed through No. 40 sieves.

2. 6. 2. 3 Preparation of Pellets for Densification

For hot pressing, powder mixtures were poured directly into 2 inch diameter (ID) graphite die. The inside diameter of the die was wrapped with 0.01 inch thick graphite foil.

For hot isostatic pressing, pellets of 1 inch diameter were prepared by uniaxial steel die and consequently isostatically pressed to obtain densities near 58 % of theoretical density.

The pellets were outgassed in a vacuum furnace at 1000 °C for 5 hours. They were put in tantalum encapsulation can. In some specimens, graphite foil was placed between pellet and tantalum can. The assembly was placed in Pyrex ampules in a vacuum system and baked overnight at 400°C before sealing in helium gas. The ampules were then brought to an electron beam welding facility. Inside the electron beam welding chamber, the pellet/tantalum assembly was heated to red hot temperatures by using focused electron beam and outgassed overnight before vacuum sealing. They were tested for any leak using a helium leak detector before hipping.

2. 6. 2. 4 Densification

Hot pressing was conducted in a 2 inch ID graphite die at 2000°C for 1hr hold time. Applied pressure was 28 MPa. Argon atmosphere (50.5 KPa) was used.

Hot isostatic pressing was conducted at 2000°C with a pressure of 186 MPa for 1 hr hold. Tantalum can was used as encapsulation material. Fig. 2 summarizes the hipping process.

2. 6. 2. 5 Quenching heat treatment

Quenching heat treatment from the B-phase region was conducted in order to retain the B-phase at room temperature. Both hot pressed and hipped specimens were heated to 1950°C in a controlled atmosphere furnace in argon gas pressure of half an atmosphere. After a hold time of 15 min, the power was turned off. A very fast quench rate could be obtained. In 10 seconds, the temperature dropped from 1950°C to 1730°C.

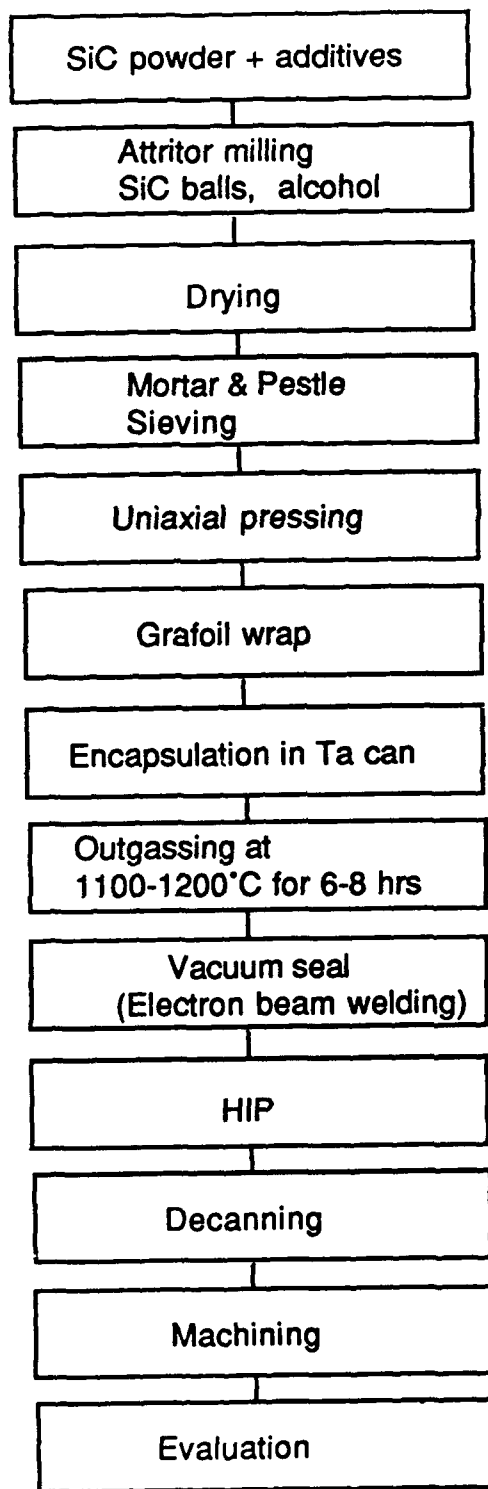


Fig. 2. Hot isostatic pressings flow diagram

2. 6. 3. Results and Discussion

2. 6. 3. 1 Oxygen Content of SiC Powders

Table 3 describes the analyzed oxygen content in each powder.

Table 3. oxygen content of SiC powders	
SiC Powder	Oxygen Content (wt%)
Alcoa SiC	0.146
Starck (AD 10)	0.85
Superior Graphite	0.501

2. 6. 3. 2 Density of Composites

Table 4 shows the densities of the composites after hot pressing or hipping.

Table 4. Densities of composites			
Specimen	Densification	Density	%TD
Alcoa SiC Only	hot pressing	3.16	98.4%
Alcoa15D	hot pressing	3.53	90.4%
SG A15D	hot pressing	3.36	86.1%
Alcoa 15D	1 hr attrition, hipping, grafoil	3.82	98.0%
Alcoa 15D	1 hr attrition, hipping, no grafoil	3.77	96.6%
Alcoa 15D	2 hr attrition, hipping, grafoil	3.83	98.1%
Starck 15D	Spex mixing, hipping, grafoil	3.81	97.7%

Notice the lower density (%TD) when Dy₂O₃ was added to SiC. An 8 % decrease in %TD was observed. Dy₂O₃ is thus acting as inhibitor for densification of the system. Superior Graphite powders did not densify readily. This is due to large particle size distribution of the powder. Large particles hinder densification of the powders. All hipped composites had densities higher than 97%.

2. 6. 3. 3 Phases and Microstructure

Fig. 3 compares X-ray diffraction patterns of hot pressed Alcoa 15D composites before and after quenching heat treatment. The as-hot pressed composite (bottom curve) shows C-Dy₂O₃ only. After quenching (top curve), B-Dy₂O₃ was clearly identified. X-ray diffraction patterns of Alcoa 15D composites after quenching are shown in Fig. 4 as a function of quenching temperatures. They show that the temperature ranges (1900 - 2000°C) for quenching have negligible effects on the retention of B-Dy₂O₃. The X-ray diffraction patterns of Superior Graphite (SG) A15D composites before and after quenching from various temperatures are shown in Fig. 5. The as-hot pressed composite (bottom curve) has C-Dy₂O₃ only. After quenching, most of the Dy₂O₃ was still in the C-form; i.e. it was not possible to retain the B-Dy₂O₃ by quenching in this composite. This behavior is due to the low density of this composite (86.1%). There is not sufficient matrix constraint effect at this low density to retain the B-Dy₂O₃.

Fig. 6 shows the X-ray diffraction patterns for hipped composites. As in hot pressed composites, as-hipped composites had C-Dy₂O₃ only. After quenching heat treatment, both C and B-Dy₂O₃ were present in the composites.

Typical microstructures are shown in Fig. 7. Attrition milling for 2 hours resulted in slightly smaller Dy₂O₃ grain size than for 1 hour attrition milling.

Bright field TEM observation (Fig. 8) shows that in the hipped composites, Dy₂O₃ grains were completely wetting SiC grains and were more interconnected to each other than in hot pressed composites. Thin Dy₂O₃ grain boundary phase between SiC grains and Dy₂O₃ phase at triple points of SiC grains were frequently observed (Fig. 9). This microstructure was unexpected, since great care has been taken to remove oxygen in the hip pellets before vacuum sealing. At present the reason for more liquid phase formation is not understood. However, more liquid phase during hipping accounts for the only partial retention of B-Dy₂O₃ after quenching. In the hot pressed composites, no C-phase was observed; i.e. complete retention of B-Dy₂O₃ after quenching was possible. Comparison of the two microstructures

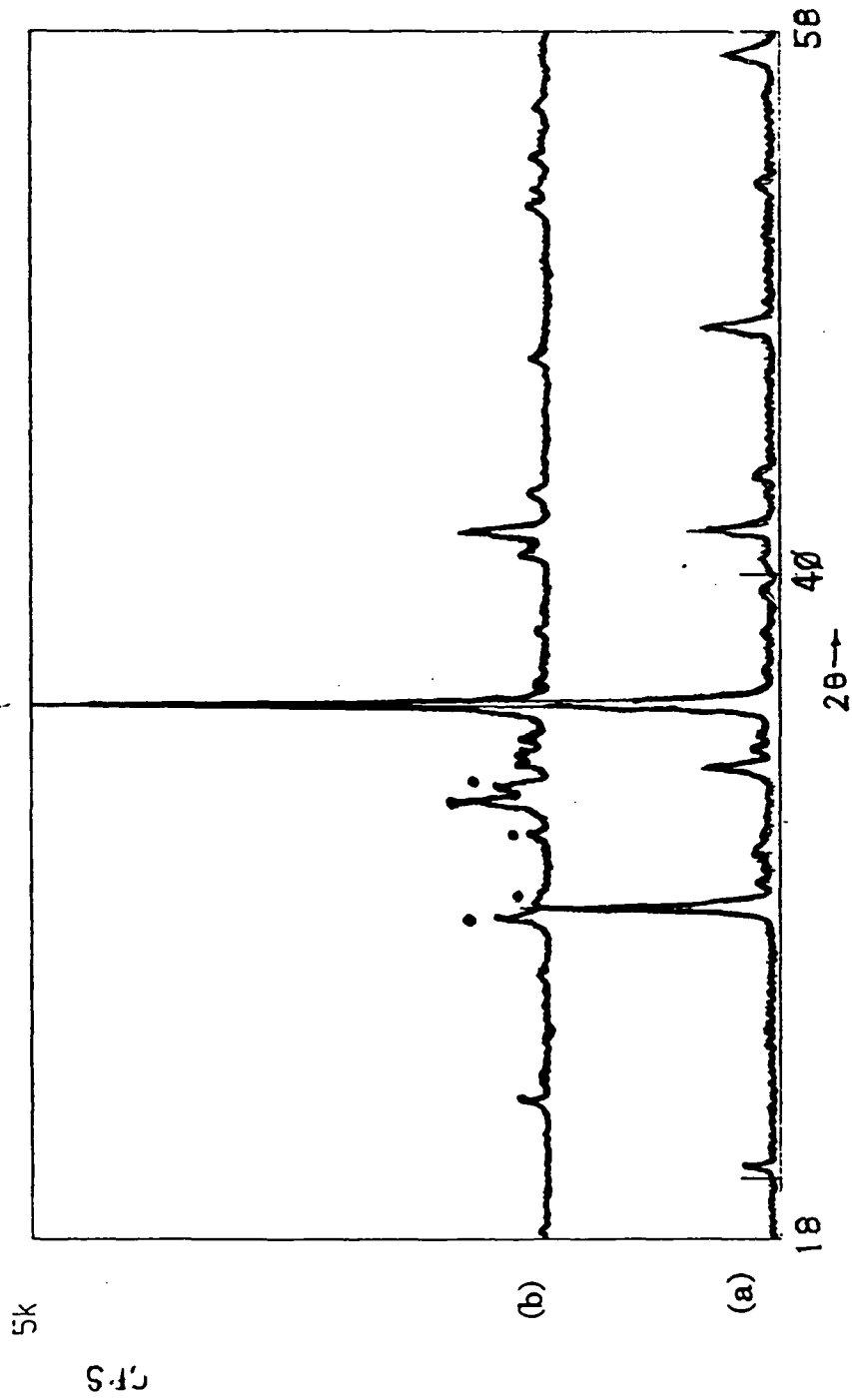


Fig. 3. X-ray diffraction patterns of hot pressed Alcoa 15D composites (a) before and (b) after quenching heat treatment. Small dots represent B-dysprosia.

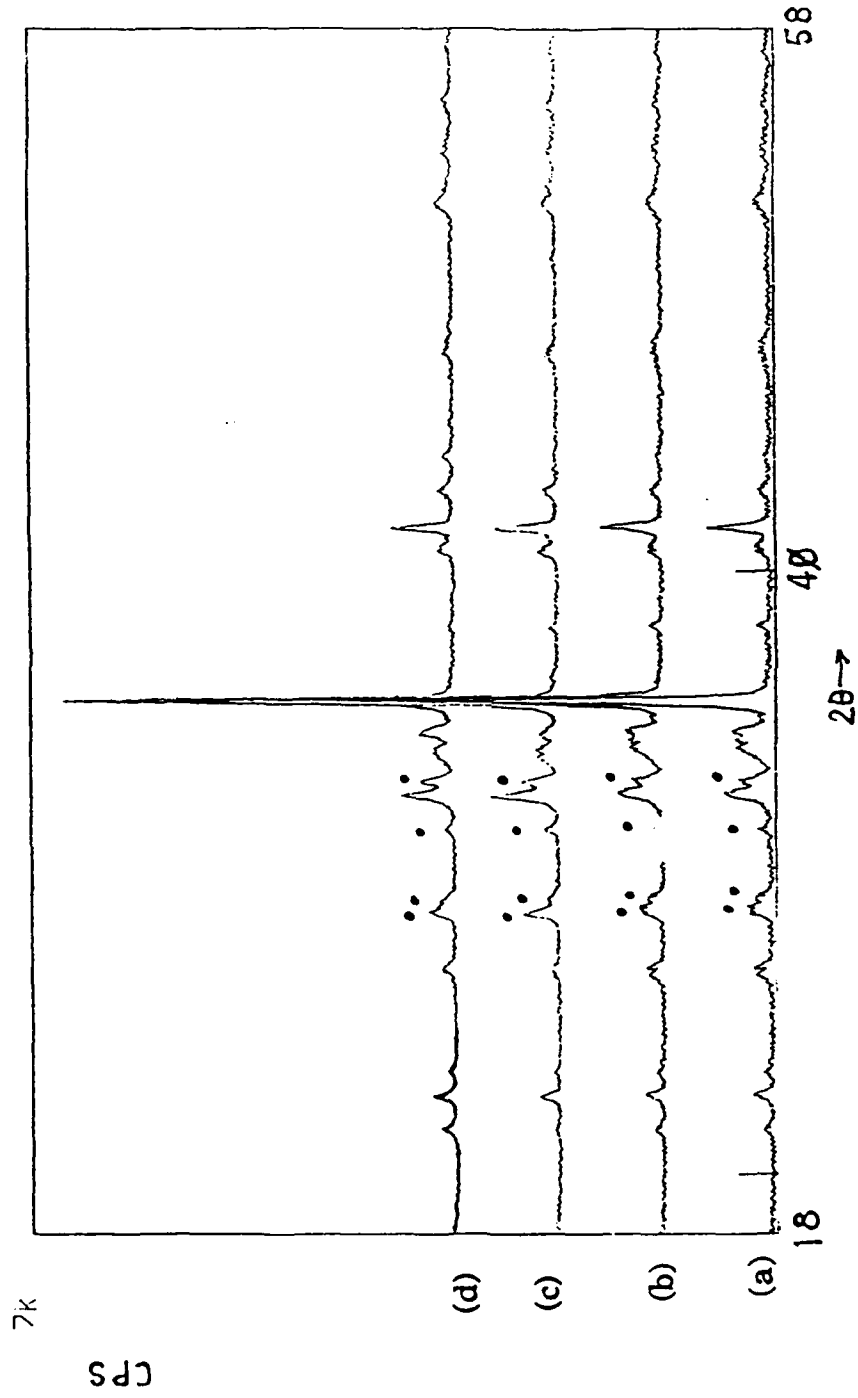


Fig. 4 X-ray diffraction patterns of Alcoa 15D composites after quenching from (a) 2050 °C; (b) 2000 °C; (c) 1950 °C; (d) 1900 °C.

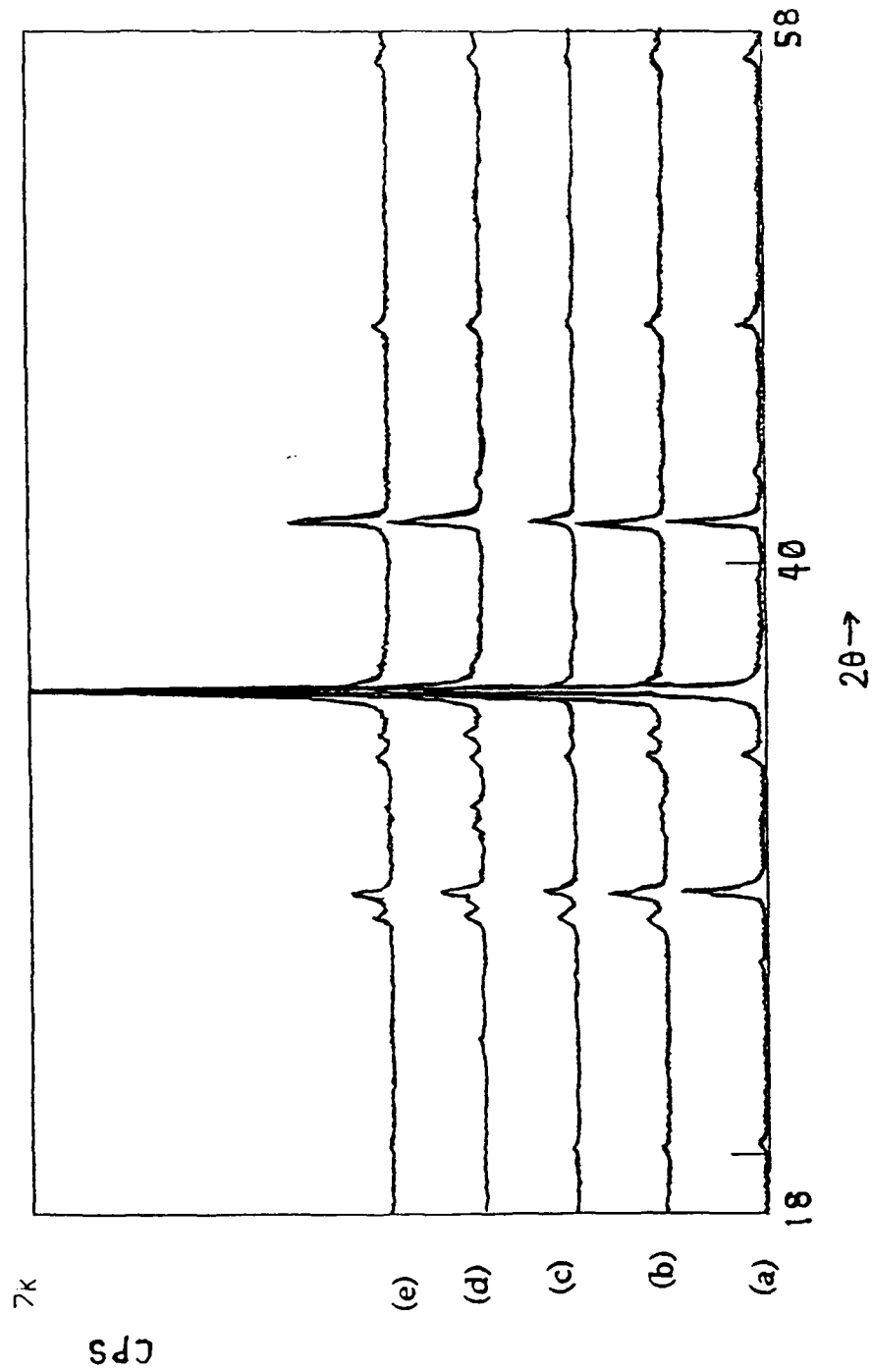


Fig. 5. X-ray diffraction patterns of Superior Graphite (SG) A15D composites before (a) and after quenching from (b) 2050 °C; (c) 2000 °C; (d) 1950 °C; (e) 1900 °C.

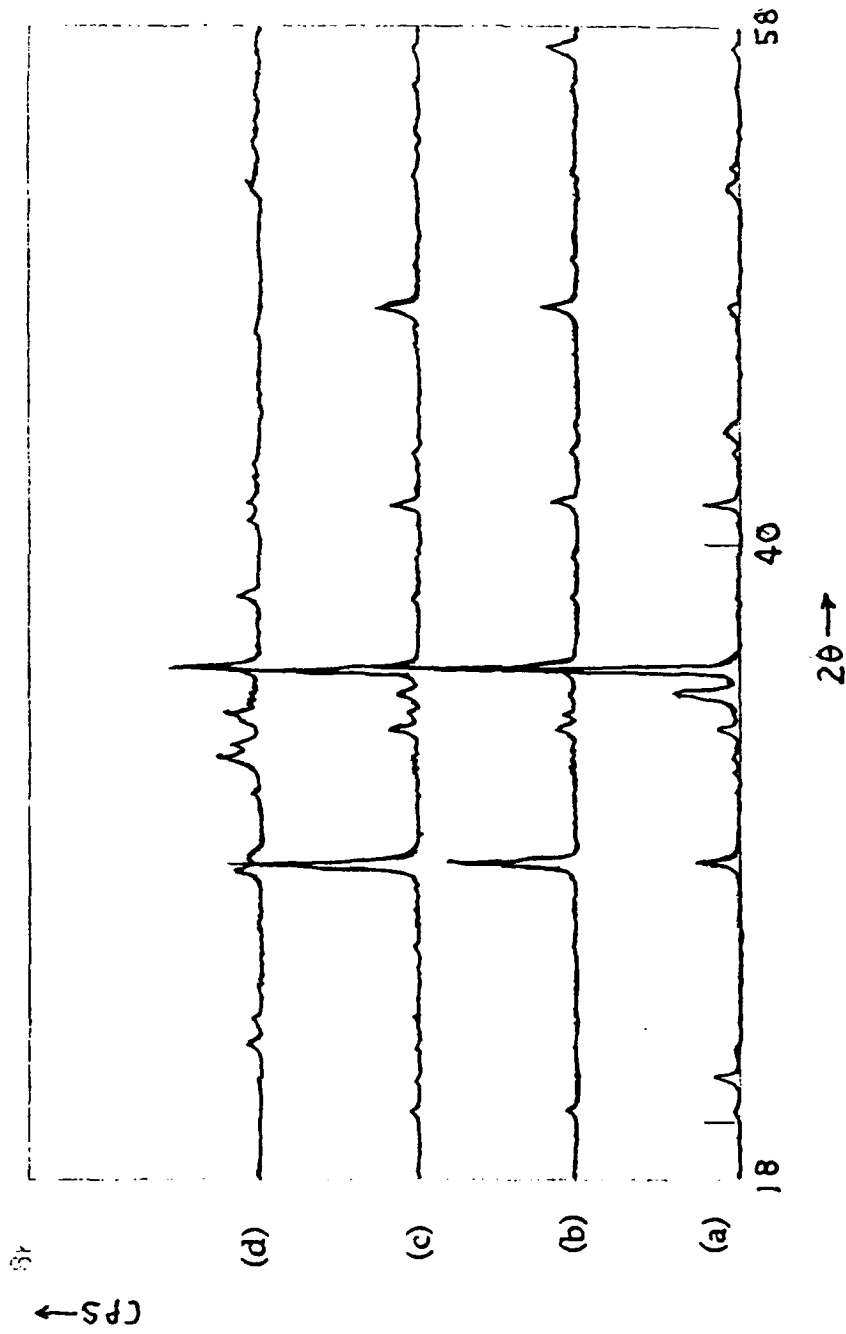
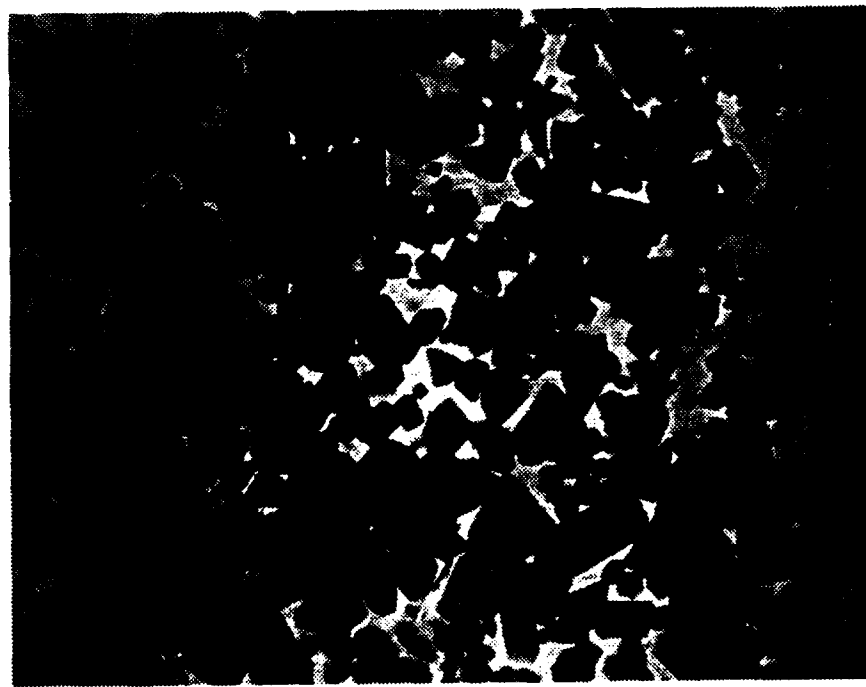
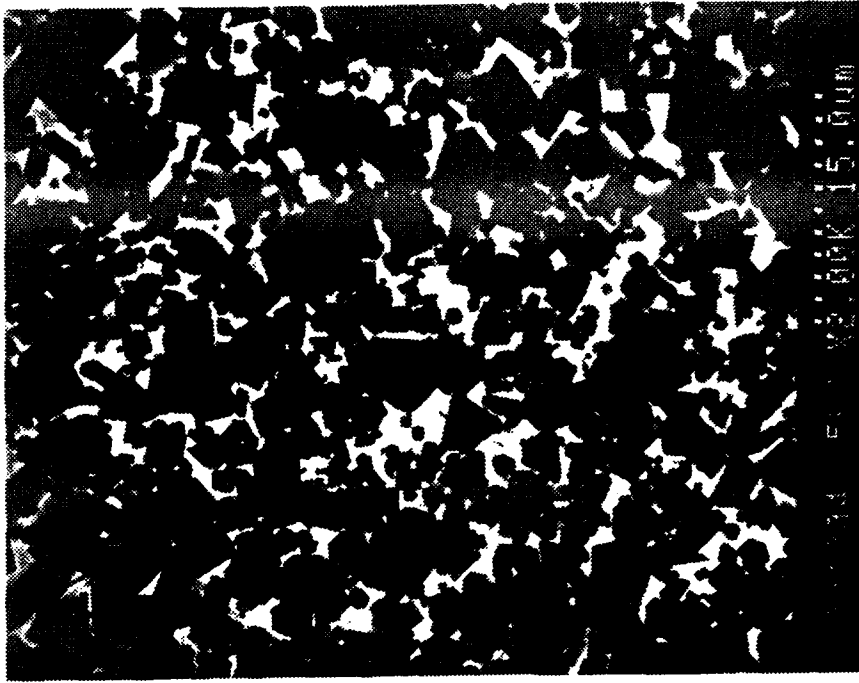


Fig. 6. X-ray diffraction patterns for hiped composites after quenching from 1950°C.
 (a) Alcoa 15D, grafoil wrap ; (b) Alcoa 15D, no grafoil;
 (c) Alcoa 15D, grafoil, 2 hr attrition; (d) Starck 15D

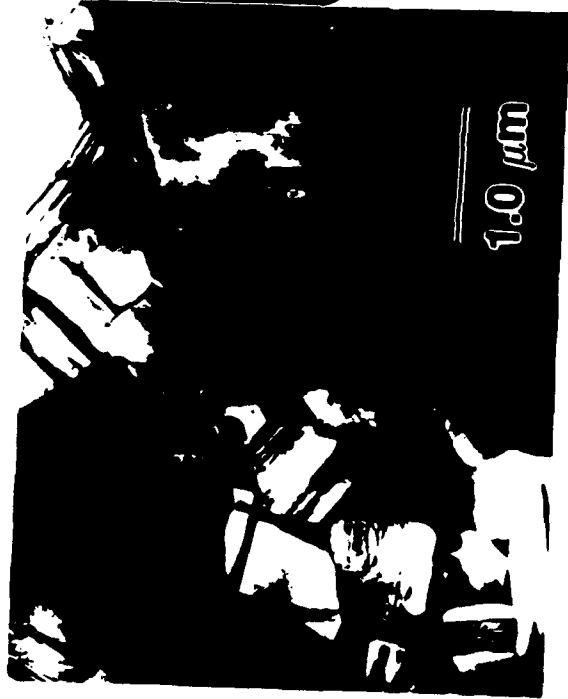


(a)



(b)

Fig. 7. SEM micrographs of hiped Alcoa 15D composites.
(a) attrition milled for 1 hr (b) attrition milled for 2 hrs.



(a)



(b)

Fig. 8 Bright field TEM micrographs of Alcoa 15D.
(a) hot pressed (b) hipped

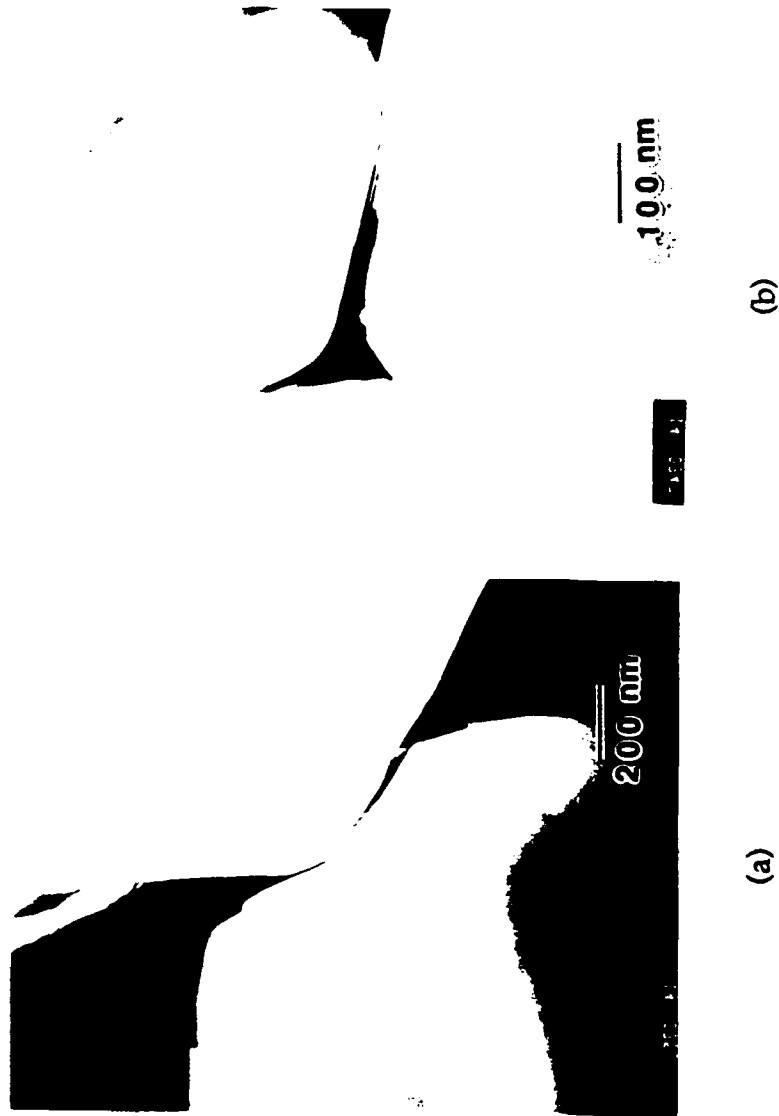


Fig. 9. Bright field TEM micrographs of hipped Alcoa 15D.
(a) grain boundary dysprosia phase (b) dysprosia at triple points of SiC grains.

shows that prevention or minimization of liquid phase is important for complete retention of the B-Dy₂O₃.

2. 6. 4 Conclusions

Dy₂O₃ incorporated into SiC matrix inhibits densification of the composites. As-hot pressed or as-hipped SiC - Dy₂O₃ composites contained C-Dy₂O₃ only. Precise microstructural control is essential in retention of the B-Dy₂O₃ in the composite; i.e. obtaining fully dense composite and minimization of liquid phase formation during densification. This can only be obtained by optimizing processing parameters.

Quenching from the B-phase region was required in order to retain B-Dy₂O₃ in the composite.

Section 2.7 Micromechanical Studies of β -Gadolinia (Gd_2O_3)

(Mr Kurt G. Slavick)

I. Introduction

Ln_2O_3 systems, otherwise known as rare earth oxides, have been suggested as candidates for high temperature transformation tougheners. [1,2,3] The phase equilibria of the rare earth oxides are shown in figure 1. [4] Phase A is hexagonal ($Z=1$), phase B is monoclinic ($Z=6$), and phase C is cubic and fluorite related ($Z=16$). The transformation from monoclinic (B) to cubic (C) is of special interest because it exhibits a 8%-10% volume increase on cooling [5] analogous to the 4.9% volume increase experienced by zirconia when transforming from the tetragonal (t) to monoclinic (m) phase.

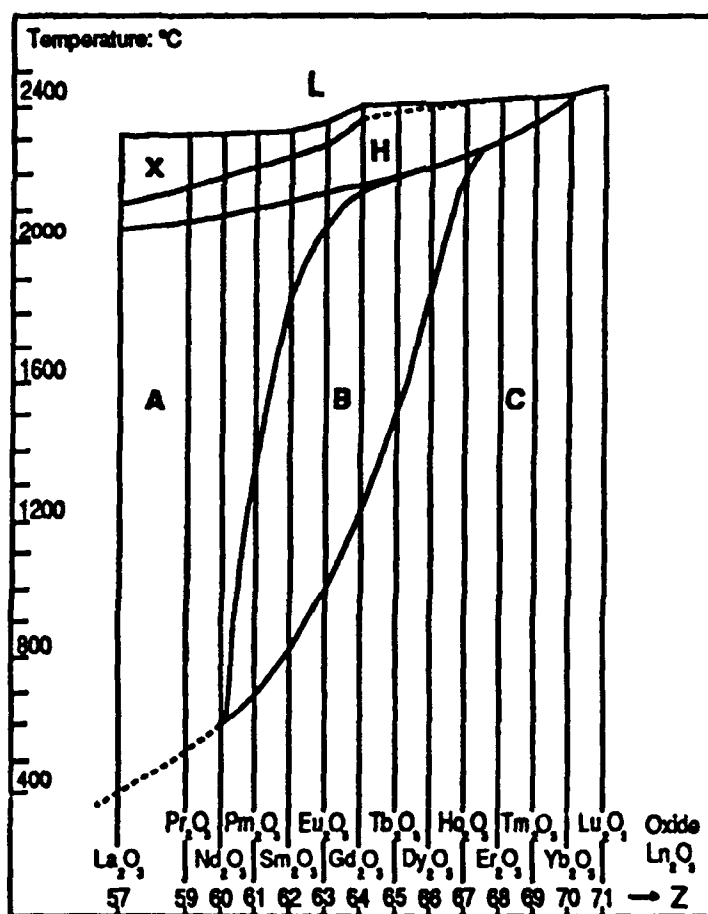


Figure 1. Polymorphic forms and transformation temperatures of the lanthanide sesquioxides. (After Foex and Traverse [4])

Jero [6] confirmed the possibility of applying Ln_2O_3 systems in transformation toughening in a composite of 20 vol.% B- Tb_2O_3 in 80 vol.% MgO matrix. The composite was sintered in an inert argon atmosphere at 1700°C . The microstructure was analogous to zirconia toughened alumina (ZTA). The toughness of the matrix and composite as measured in three-point bending, can be seen in Figure 2 as a function of the temperature.

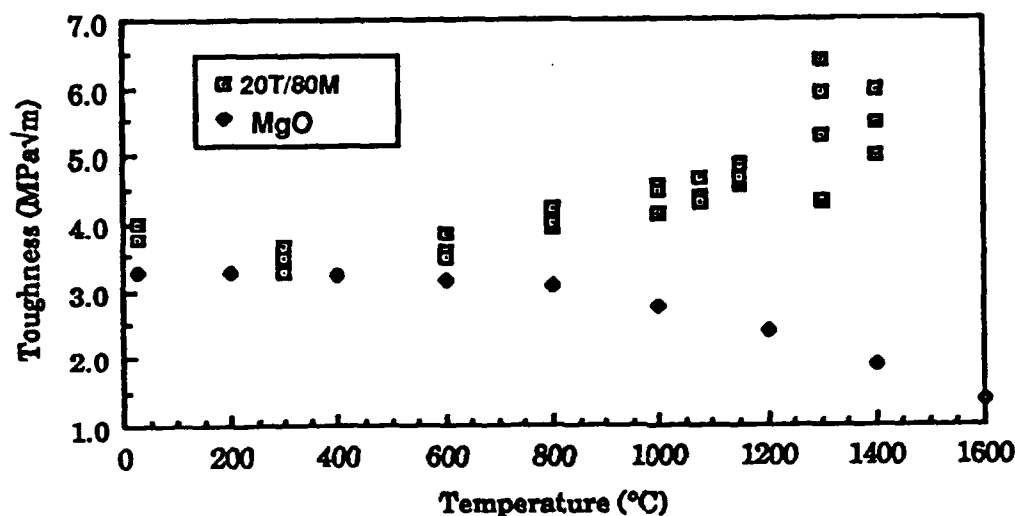


Figure 2. Plot of high temperature toughness values of MgO matrix and of composite of 20 vol.% B- Tb_2O_3 in 80 vol.% MgO vs. Temperature. After Jero [6]

Toughness can also be measured from radial cracks produced by Vickers indentation. Jero [6], however, observed that indents both at room temperature and up to 1000°C showed no radial cracks in B- Gd_2O_3 , B- Tb_2O_3 , B- Sm_2O_3 and B- Eu_2O_3 , and composites incorporating them (ie. Tb_2O_3 -MgO and Tb_2O_3 - Al_2O_3). The materials experienced chipping, pile-up and some limited microcracking around the indentations. The C-phase counterparts, however, exhibited classical radial cracking. X-ray analysis of the fracture surface of B- Gd_2O_3 (broken in single edge notch beam test) showed no C-phase.

It is generally considered that the B->C transformation exhibits displacive kinetics in compounds having atomic numbers equal to or greater than Tb_2O_3 , but reconstructive kinetics (replacive [2]) below Tb_2O_3 . This includes Gd_2O_3 , Eu_2O_3 and Sm_2O_3 . [7]

Vickers indentation experiments by Lejus et. al [8] showed "bundles" of parallel lines on either side of the indents in cleavage planes of the rare earths.

Observations of the parallel lines were made in all the rare earth oxides except Gd_2O_3 . The lines correspond to a relaxation of stress (by slipping or twinning) and are always in the same crystallographic direction. Stobierski and Lejus [9] observed that plasticity decreased in the series A->B->C by analyzing etch pit distributions around indents in Vickers microhardness experiments. Deformation occurred by slip, with the A type crystals exhibiting slip lines at room temperature and the B type at 800° C.

Case and Evans [10] reported 3x higher toughness values in B structures of a given Ln_2O_3 (Gd_2O_3 , Eu_2O_3 and Sm_2O_3) than in the C structure. Jero reported a factor of 1.4x. Evans and Case polished, indented and chemically etched polycrystalline specimens. They observed bands around the indents but could not unambiguously identify or differentiate slip, twin and shear bands by optical microscopy of surfaces.

B-phase Ln_2O_3 compounds have potential applications as flaw resistant tough coatings for sodium lamps made of dense transparent $Y_2O_3-La_2O_3$ materials. [11],[12]

The aim of this work was to use transmission electron microscopy (TEM) and high voltage electron microscopy (HVEM) on polycrystalline Gd_2O_3 and identify microstructural mechanisms eg. (i) slip, twinning (lattice deformational), (ii) microcracking, or (iii) transformation responsible for the lack of radial crack formation. This will be accomplished by indenting B-phase gadolinia and back thinning by argon ion bombardment such that the indent and its affected microstructure are in the area of the thin foil.

II. Experimental Procedure

Processing:

Molycorp[†] C-phase Gd_2O_3 powder was dispersed in isopropyl alcohol after ultrasonically the alcohol plus powder mixture to break up the soft agglomerates. The suspension was sedimented to <1 μm particle size. After allowing those particles > 1 μm to settle out over the requisite time (8.4 hours) the alcohol plus powder was drawn off and dried under a heat lamp. 1.5 w/o binder (poly-ethylene

[†] Molybdenum Corporation of America, Louviers, Colorado.

glycol, avg. M.W. 400) was added to the powder by dispersing the powder in again in alcohol and adding the correct amount of binder. After the powder was dried, it was broken up using a mortar and pestle and placed directly into the 1/2" cylindrical die. The powder was uniaxially pressed at 5 KPsi followed by a 25,000 KPsi cold isostatic press, with a 5 minute hold.

The dimensions of the green state pellet were taken and the pellet was fired at 1600° C for either 1 or 2 hours with both the heating and cooling rate being 5°C/min. The fired pellets experienced an average of 20% shrinkage in both height and diameter. The fired density exceeded 97% as measured by the Archimedes method in kerosene (kerosene was used to avoid contact with water as the Gd₂O₃ is hygroscopic).

X-ray diffraction revealed that the samples were entirely B phase. Figure 3 shows the B planes (401), (402) and (310) which, according to the JCPDS x-ray card, have relative intensities of 60, 100, 75% respectively. [13]

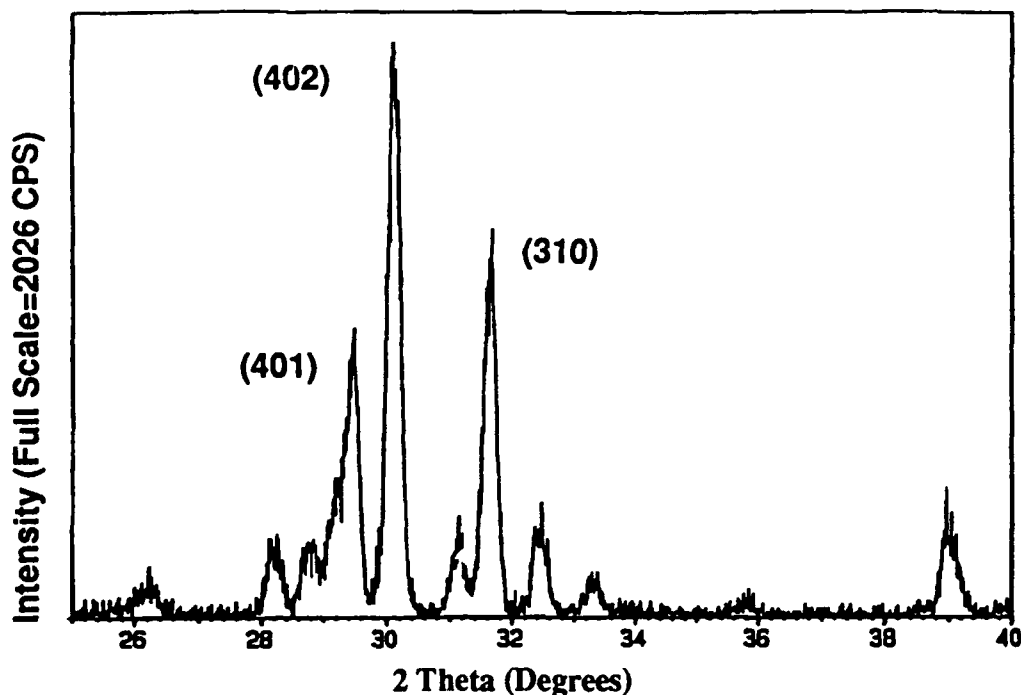


Figure 3. X-ray diffraction scan of polycrystalline Gd₂O₃ showing presence of major B phase peaks.

Scanning Electron Microscope Specimen Preparation:

The sintered samples were ground down at least 1 mm with a 30 μm diamond grinding plate to remove the surface reaction. The pellet was then polished using 6 μm diamond paste and finally 1 μm paste, until a mirror-like finish was obtained. The Gd_2O_3 was thermally etched at 1450°C for 30 minutes to enhance the visibility of the grains. Finally, the samples were carbon coated prior to observation in the ISI DS-130 SEM.

Transmission Electron Microscope Specimen Preparation:

Slices about 200 μm thick were cut from the polished surfaces of the SEM pellets using a slow speed diamond saw. 3 mm discs for the use in the TEM were cut from the thin slices using an ultrasonic disc cutter and 300 grit Boron Carbide powder. The discs were ground down to about 100 μm thickness using a 15 μm diamond impregnated metal platen on the precision thinning attachment to the Minimet polisher. Subsequent polishing and thinning was accomplished by 15 μm , 9 μm , 6 μm and finally 1 μm diamond polishing paste on the Minimet. For standard TEM specimens the 3 mm discs were then dimpled to a remaining thickness of approximately 40 μm and ion milled from both sides at 6 kV and 0.5 mA per Argon ion gun. Typically the milling was begun at 15° and the angle was decreased as the milling progressed. Figure 4 is a typical milling schedule for the cold stage on the ion mill. The cold stage was not used for any particular reason except availability.

Angle	Time
15°	6 hours
12°	2 hours
10°	2.5 hours

Figure 4. Typical ion milling time for Gd_2O_3 at 40 μm nominal thickness

Other samples were indented using either a Zwick or Tucon Vickers indenter with a load of 200 g, indenter velocity of 0.3 mm/sec and indentation duration of 20 seconds. This yielded a diagonal length D of 70 μm . A square array of indents was made by varying the number of indents per side and assuring that the indents were separated by at least the distance of $2D$. (This resulted in the center-to-center distance of $3D$). The seemingly large number of indents was necessary since the hole in the specimen after ion milling was not easily controlled. By having a large population of indents, the chances of the hole appearing near an indent was increased. The minimum separation was invoked in order to decrease the chances of the plastic deformation zones of multiple indents from overlapping. Thinning of the indented specimens had to be performed by ion milling from one side only (the unindented side) since milling from the indented side would eliminate the indents themselves. Milling time from one side without dimpling approached a total of 30 hours. Indented specimens may also be dimpled as long as the dimple was sufficiently far from the root of the plastic deformation zone. The milling time, of course, was the same as the unindented samples. SEM observations were made of the indented specimens and will be discussed in the Results section.

TEM of indented gadolinia was performed on the 1 MeV High Voltage Electron Microscope at Argonne National Laboratory and will be discussed forthwith.

III. Results

Experimental Difficulties:

TEM specimen preparation has proven to be the rate limiting step in this study. For samples with a high concentration of indents (50-80) the residual stress buckled the sample after a significant amount of thinning had occurred. Some samples have failed by cracks propagating from one indent area to another while others have had the middle area simply blown out when the foil became thin.

Preliminary Results: SEM

Dense, polycrystalline B-phase Gd_2O_3 has been fabricated. In figure 5 the general microstructure can be seen of a sample fired at 1600°C for 1 hour. The average grain size was approximately 10 μm . Longitudinal striations can be seen in

some of the grains (indicated by arrows) not due to polishing. This sample was not indented.

SEM micrographs of an indented sample is seen in figure 6. Notice the lack of normal radial cracks similar to that of Jero. [6] However, one can see a parallel band configuration (indicated by arrow) about 30 μm from the center of the indent.

Figure 7 shows a microcrack in indented B-Gd₂O₃ in Bright Field under 1 MeV. Possible twins are indicated by the two ended arrow; the large arrow delineates a highly strained region in the grain caused by the crack.

III. Discussion and Conclusions

Dense B-Gd₂O₃ has been fabricated and indented. The results replicate that of Jero [6] in so much as there are no classical radial cracks due to the indent. SEM results show some type of parallel banded configuration near the indents. This is unusual since Lejus [8] observed what they called bundles of parallel lines in all B phase rare earth oxides except B-Gd₂O₃. Their experiments were conducted on large single crystal cleavage planes and our study was conducted in polycrystalline materials. Stobierski and Lejus [9] only saw slip beginning at 800°C in B-phase rare earth oxides.

Clearly there is some mechanism ie. slip or twinning, microcracking, or transformation responsible for the lack of radial cracks at room temperature. Preliminary results from high voltage TEM shows possible twin formation around a microcrack formed by an indent.

IV. Future Work

More study needs to be done to identify the nature of the parallel banded configurations. By comparing traditional unindented TEM samples with indented specimens we will be able to discern the relative amount of microcracking occurring along with other microstructural phenomena.

An improved method of TEM specimen preparation must be developed. One must determine the minimum spacing of the indents in the array so that the strain fields do not overlap. The minimum spacing depends on the size of the plastic deformation zone which must be measured. As mentioned, the samples have ruptured while thinning, there being limited stress relaxation during ion milling due to the inability of dislocations to move to the surface of the sample.

V. REFERENCES

1. W.M. Kriven, "Possible Transformation Tougheners Alternative to Zirconia: Crystallographic Aspects," *J. Am. Ceram. Soc.*, **71** [12] 1021-1030 (1988).
2. W.M. Kriven, "Martensitic Toughening of Ceramics," *Materials Science and Engineering*, **A127** 249-255 (1990).
3. W.M. Kriven, Y.J. Kim, M.M. Flemming, "Phase Equilibria and Modulated Microstructures in the Calcia-Dysprosia System," Submitted to the *J. Am. Ceram. Soc.*
4. M. Foex, J.P. traverse, "A Study of the Polymorphism of the Rare Earth Sesquioxides at High Temperatures" (in French), *Bull. Soc. Fr. Mineral. Cristallogr.*, **89** 429-453 (1966).
5. H.R. Hoekstra, "Phase Relationships in the Rare-Earth Sesquioxides at High Pressure," *Inorg. Chem.*, **5** [5] 754-757 (1966).
6. P.D. Jero, "Investigation of the Lanthanide Sesquioxides as High Temperature Transformation Toughening Agents," Ph.D. Thesis, University of Illinois at Urbana-Champaign, to be published (1988).
7. O. Sudre, "Investigation of the Monoclinic (B) to Cubic (C) Transformation of Dysprosium Sesquioxide (Dy_2O_3)," Masters Thesis, University of Illinois at Urbana-Champaign, to be published (1988).
8. A.M. Lejus, R. Collongues, "Lanthanide Oxides, Structural Anisotropy, Physical and Mechanical Properties," Ch. 8 in *Current Topics in Mat. Sci.*, Vol. 4, ed. E. Kaldis, North Holland Publishing Co., Amsterdam, 481-577, (1980).
9. L. Stobierski, A.M. Lejus, "The Temperature Dependence of Microhardness of Lanthanide Sesquioxide Single Crystals with A, B, and C - Structure," *Rev. Int. Htes. Temp. Refract.*, **1**, 3-8 (in French) (1982)
10. E.D. Case, A.G. Evans, (Private Communication)
11. W.H. Rhodes, "Controlled Transient Solid-Second Phase Sintering of Yttria," *J. Am. Ceram. Soc.*, **64** [1] 13-19 (1981).
12. W.H. Rhodes, GTE Corporation, (Private Communication)
13. Joint Committee on Powder Diffraction Standards, B-phase (Monoclinic) card 12-474, C-phase (Cubic) card 12-797, A-phase (high temperature Hexagonal) card 24-430 (1974).

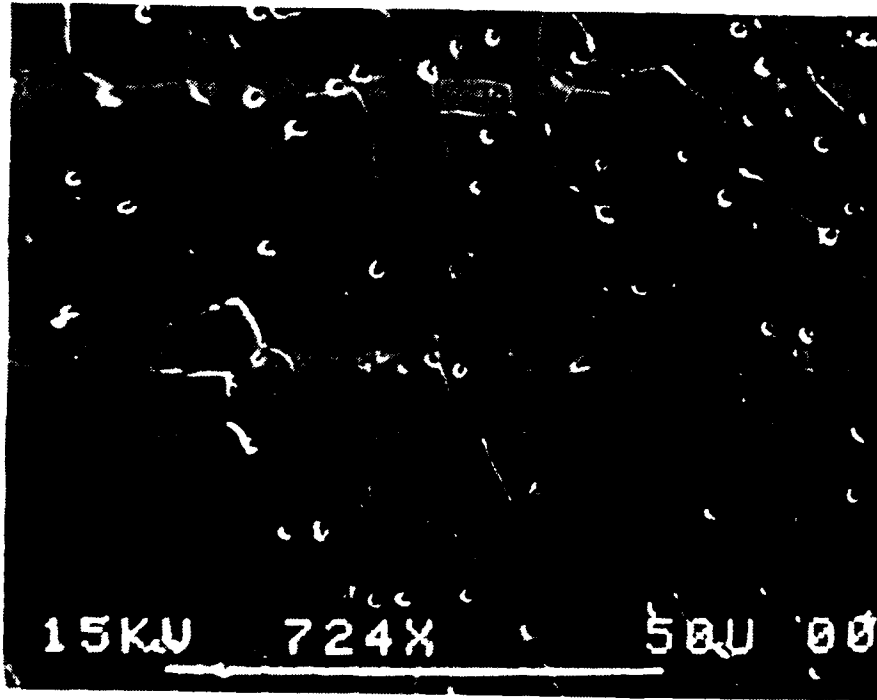


Figure 5. 97% Dense Polycrystalline B-Gd₂O₃ polished to 1 μm finish.

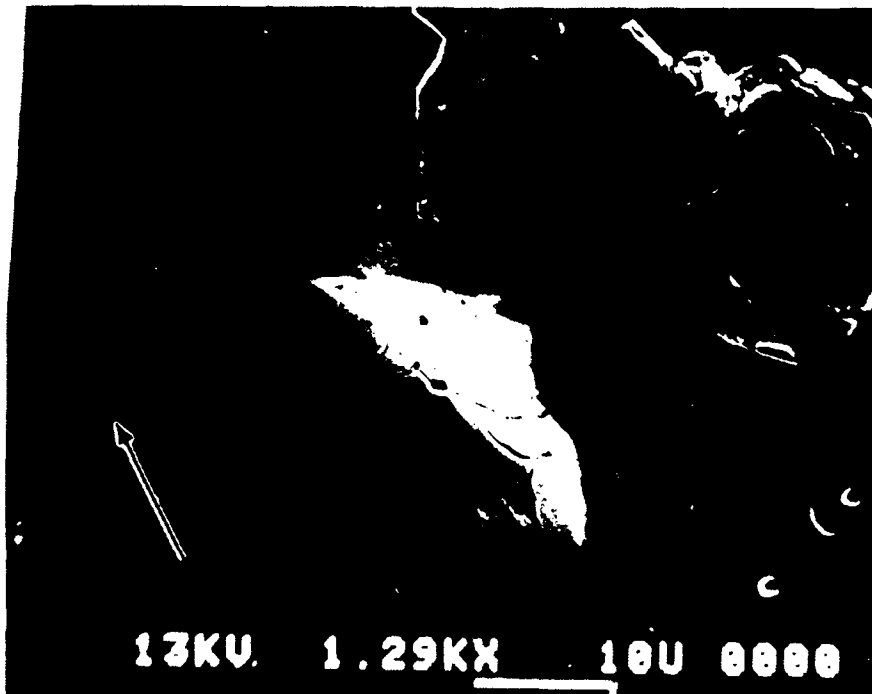


Figure 6. SEM micrograph of Vickers indented B-Gd₂O₃ at 200 g load. Parallel banded configuration is indicated by an arrow.

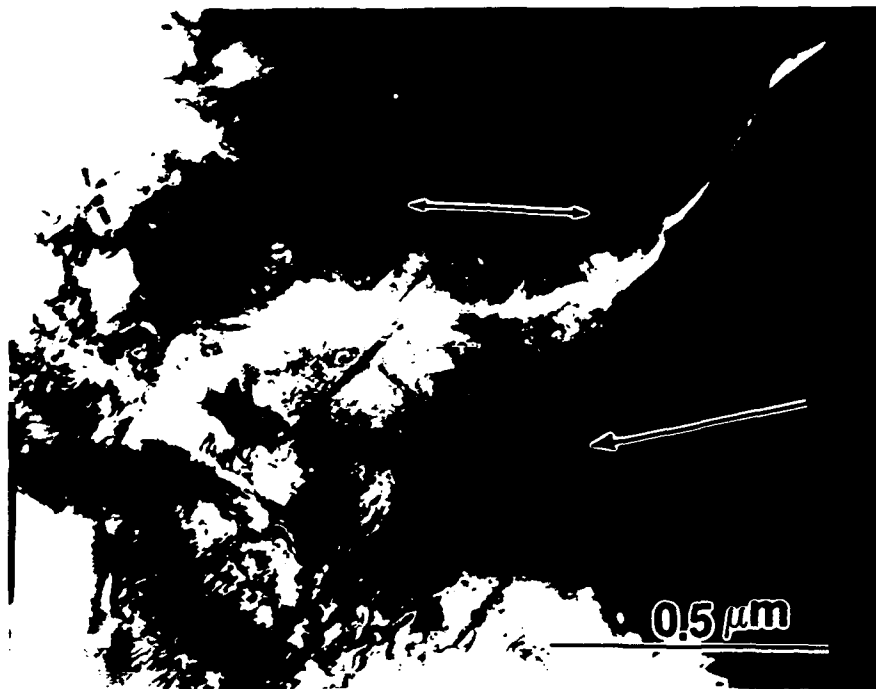


Figure 7. Indented B-Gd₂O₃ at 1 MeV, Bright Field.

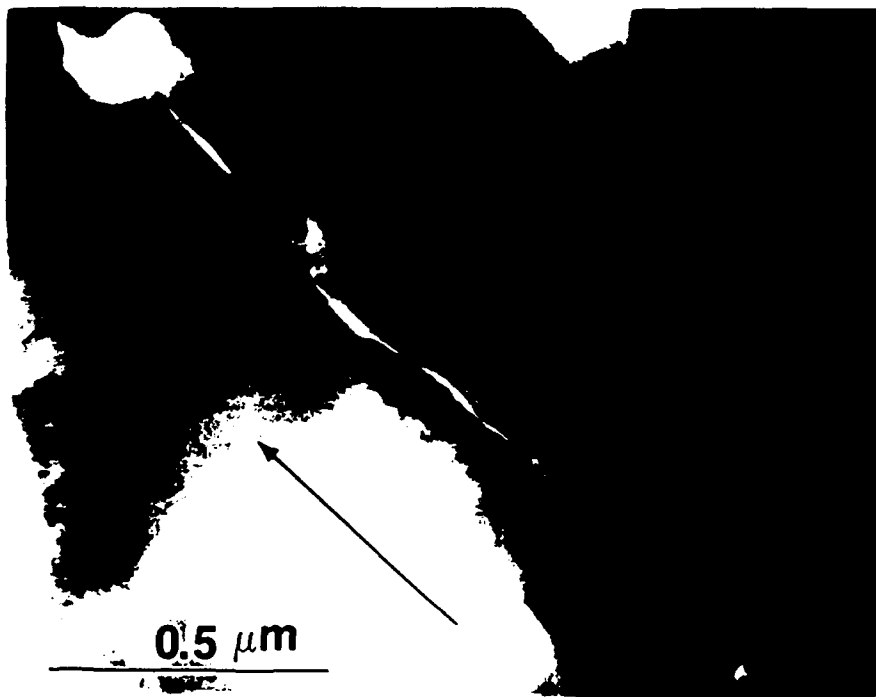


Figure 8. Microcrack and possible twins in a grain slightly removed from that in figure 7. Indented B-Gd₂O₃ at 1 MeV, bright field.

Section 3. Publications

- "Microstructural Characterization of Ca_2SiO_4 Particles in a CaZrO_3 and an MgO Matrix," by Y.J. Kim, E.S. Mast T.I Hou and W.M. Kriven. Proceedings of 12th International Congress for Electron Microscopy, pp 1050-1051, Washington, Seattle,(1990).
- "Physical Stabilization of the $\beta \rightarrow \gamma$ Transformation in Dicalcium Silicate," by C.J. Chan, W.M. Kriven and J.F. Young. Submitted to the Journal of the American Ceramic Society.

Publications Pending:

- "Development of $\beta\text{-Ca}_2\text{SiO}_4$ - MgO Composites by Mixing and by In-situ Reaction," by E.S. Mast, I. Nettleship and W.M. Kriven. In preparation for the Journal of the American Ceramic Society.
- "Fabrication and Mechanical Evaluation of $\beta\text{-Ca}_2\text{SiO}_4$ - CaZrO_3 Composites," by T.I. Hou and W.M. Kriven. In preparation for the Journal of the American Ceramic Society.
- "The Stress-induced Transformation in $\beta\text{-Ca}_2\text{SiO}_4$ Polycrystals," by I. Nettleship, Y.J. Kim and W.M. Kriven. In preparation for the Journal of the American Ceramic Society.
- "Transformation Toughening of Calcium Zirconate by Dicalcium Silicate," by E.A. Barinek and W.M. Kriven. In preparation for the Journal of the American Ceramic Society.
- "Kinetics and Crystallography of the Monoclinic (B) to (C) Transformation in Dysprosia," by O. Sudre, K.R. Venkatachari and W.M. Kriven. In preparation for the Journal of the American Ceramic Society.
- "Processing, Microstructure and High Temperature Chemical Stability Silicon Carbide - Dysprosia Composites," by S. Kim and W.M. Kriven. In preparation for the Journal of the American Ceramic Society.

Section 4. Professional Personnel

Professor Waltraud M. Kriven, Principal Investigator

Dr. Ian Nettleship, Post-doctoral Research Associate

Ph.D. Students:

Mr. Shin Kim.

Mr. Tien-I Hou, (with partial funding from the
Government of Taiwan).

Mr. Eric S. Mast.

Mr. Y.J. Kim. (partially funded by AFOSR URI)

M.S. Students:

Ms. Jemima J. Cooper

Mr. Kurt G. Slavick

Theses:

“Development and Possible Use of Dicalcium Silicate as a
Transformation Toughener of Magnesia”

M.S. thesis by Eric S. Mast, submitted in October 1990.

“Processing and Microstructure of Silicon Carbide - Dysprosia
Composites”

Ph. D. thesis by Mr. Shin Kim, writing is in progress.

Section 5. Interactions - Conference Presentations

Interactions

Dr. Mike Swain, CSIRO, Australia

- Supplied composites of NiS spheres in glass matrix.
- Anticipated interaction on fracture mechanics of NiS transformation in glass.

Dr. Adolf Micheli, General Motors, Warren, MI

- Production of NiS and NiS in ZnS thin films by spin casting of sol gel precursors.

Conference Presentations

1. "The monoclinic (B) to cubic (C) transformation mechanism in dysprosia," O. Sudre, K. R. Venkatachari and W. M. Kriven.* Abstract #[100-B-89]. Presented at the 91st Annual Meeting of the American Ceramic Society, Indianapolis, April 23-27, 1989.
2. "Processing and phase transformation of dysprosia in silicon carbide matrix," S. Kim* and W. M. Kriven. Abstract #[18-SI-89]. Presented at the 91st Annual Meeting of the American Ceramic Society, Indianapolis, April 23-27, 1989.
3. "Effect of microstructural engineering on stabilization of dicalcium silicate," C. J. Chan*, W. M. Kriven and J. F. Young. Abstract #[98-B-89]. Presented at the 91st Annual Meeting of the American Ceramic Society, Indianapolis, April 23-27, 1989.
4. "Sintering and microstructural development of dicalcium silicate in magnesia," E. S. Mast* and W. M. Kriven. Abstract #[7-SI-89]. Presented at the 91st Annual Meeting of the American Ceramic Society, Indianapolis, April 23-27, 1989.
5. "Eutectic sintering for formation of dicalcium silicate in magnesia," E. S. Mast*, R. Pilapil and W. M. Kriven. Abstract #[43-BP-89]. Presented at the 91st Annual Meeting of the American Ceramic Society, Indianapolis, April 23-27, 1989.
6. "Martensitic transformations in ceramics," W. M. Kriven.* Presented at the International Conference on Martensitic Transformations (ICOMAT-89), Sydney, Australia, July 3-7, (1989).

7. "Investigations of the monoclinic (B) to cubic (C) transformation in the lanthanide sesquioxides," W. M. Kriven*, P. D. Jero, O. Sudre, and K. R. Venkatachari. Presented at the International Conference on Martensitic Transformations (ICOMAT89), Sydney, Australia, July 3-7, (1989).
8. "Martensitic nucleation and transformation in β dicalcium silicate," W. M. Kriven*, C. J. Chan and E. A. Barinek. Presented at the International Conference on Martensitic Transformations (ICOMAT-89), Sydney, Australia, July 3-7, (1989).
9. "Preparation and Microstructure of Dispersed Dysprosia in Silicon Carbide Matrix," S. Kim* and W.M. Kriven, Abstract # [72-SIV-90]. Presented at the Annual Meeting of the American Ceramic Society, Dallas, Texas, April 22nd -26th 1990.
10. "The Development of Dicalcium Silicate as a Transformation Toughener," W.M. Kriven* and E.A. Barinek, Abstract # [7-SVI-90]. Presented at the Annual Meeting of the American Ceramic Society, Dallas, Texas, April 22nd -26th 1990.
11. "Processing and Mechanical Evaluation of Ca_2SiO_4 -Transformation Toughened CaZrO_3 Composites," T.I. Hou * and W.M. Kriven, Abstract # [8-SVI-90]. Presented at the Annual Meeting of the American Ceramic Society, Dallas, Texas, April 22nd -26th 1990.
12. "Retention of β Dicalcium-Silicate in a Magnesia Matrix," E.S. Mast*, I. Nettleship and W.M. Kriven, Abstract # [9-SVI-90]. Presented at the Annual Meeting of the American Ceramic Society, Dallas, Texas, April 22nd -26th 1990.
13. "Microstructural Characterization of Ca_2SiO_4 Particles in a CaZrO_3 and an MgO Matrix," Y.J. Kim*, E.S. Mast, T.I. Hou, and W. M. Kriven. Presented at the Proc.12th Int. Congr. for Electron Microscopy, Washington, Seattle, Aug, (1990).